

ABSTRACT

Title of Document: CONCRETE SHRINKAGE PREDICTION USING
MATURITY AND ACTIVATION ENERGY

Christopher Clarke
Master of Science, 2009

Directed By: Professor Dimitrios G. Goulias
Department of Civil and Environmental Engineering

Shrinkage is a complex material response that often affects concrete in an adverse manner. The characteristics of the natural environment in which concrete is placed and the rate of strength development have been used to model the rate of shrinkage development. Furthermore, concrete maturity has been used to predict the rate of strength development of concrete cured at different temperatures. This study sought to find a correlation between activation energy based concrete maturity and concrete shrinkage. A single concrete mixture was tested to determine the apparent activation energy of the mixture and the shrinkage under varying environmental conditions. A shrinkage model incorporating relative humidity and temperature was developed to predict the shrinkage of the concrete mixture. A relationship between concrete shrinkage and activation energy based maturity was investigated.

CONCRETE SHRINKAGE PREDICTION USING MATURITY AND
ACTIVATION ENERGY

By

Christopher Clarke

Thesis submitted to the Faculty of the Graduate School of the
University of Maryland, College Park, in partial fulfillment
of the requirements for the degree of
Master of Science
2009

Advisory Committee:
Dr. Dimitrios G. Goulias, Chair
Dr. Chung C. Fu
Dr. M. Sherrif Aggour

© Copyright by
Christopher Clarke
2009

Acknowledgements

I would like to thank the following individuals for their support and assistance while I completed this thesis study:

- Dr. Dimitrios G. Goulias, thank you for your instruction, advice, and patience while I completed this thesis. You have helped me grow intellectually and professionally as your teaching assistant, student, and advisee.
- Dr. M. Sherif Aggour and Dr. Chung C. Fu, thank you for the time and effort you have provided as part of my thesis committee.
- Dr. Sushant Upadhyaya, thank you for providing me with your knowledge of concrete maturity and your assistance during my laboratory testing.
- Thank you to my wife, parents, and family for your continued support and unconditional love.

Table of Contents

Acknowledgements.....	ii
Table of Contents	iii
List of Tables	v
List of Figures	vi
Chapter 1: Introduction	1
1.1 Introduction.....	1
1.2 Background.....	2
1.3 Research Objectives.....	3
1.4 Report Organization.....	4
Chapter 2: Literature Review.....	5
2.1 Introduction.....	5
2.2 Properties of Concrete Shrinkage	6
2.2.1 Plastic Shrinkage.....	6
2.2.2 Carbonation Shrinkage.....	8
2.2.3 Thermal Shrinkage.....	9
2.2.4 Autogenous Shrinkage	9
2.2.5 Drying Shrinkage	12
2.3 Concrete Maturity	16
2.3.1 Nurse-Saul Method	17
2.3.2 Arrhenius Based Method	20
2.4 Maturity and Shrinkage.....	23
2.5 Shrinkage Prediction Models.....	27
2.5.1 ACI 209.....	28
2.5.2 CEB-FIP 90.....	30
2.5.3 B3 Model	32
2.5.4 GL2000	34
2.6 Performance of Shrinkage Prediction Models	35
Chapter 3: Materials and Testing Plan.....	39
3.1 Materials and Mixture Design	39
3.2 Testing Plan	42
Chapter 4: Experimental Results	45
4.1 Penetration Testing	45
4.2 Fresh Concrete Properties	46
4.3 Compressive Strength for Activation Energy Calculations.....	47
4.4 Monitoring of Temperatures	49
4.5 Shrinkage Testing	50
4.6 Compressive Strength Results at Isothermal Conditions.....	52
Chapter 5: Discussion of Results	55
5.1 Determination of Activation Energy.....	55
5.1.1 Penetration Data and Activation Energy Determination	55
5.1.3 Analysis of Calculated Activation Energies	62
5.1.4 Conclusions.....	72

5.2 Maturity and Shrinkage.....	73
5.2.1 Direct Application of Maturity Concept.....	73
5.2.2 Maturity Approach as a Function of Ultimate Shrinkage.....	77
5.2.3 Derivative Approach to Relate Shrinkage to Activation Energy.....	80
5.2.4 Compressive Strength under Shrinkage Curing Conditions.....	83
5.2.5 Conclusions.....	88
5.3 Shrinkage Modeling.....	88
5.3.1 Analysis of Existing Shrinkage Models.....	88
5.3.2 Development of a Shrinkage Time Function.....	90
5.3.3 Development of Humidity and Temperature Functions.....	91
5.3.4 Validation of the Shrinkage Models.....	93
5.3.5 Temperature and Humidity Response of Models.....	96
5.3.6 Conclusions.....	99
5.4 Comparison of Model 1 and Model 2 to Existing Models.....	99
Chapter 6: Conclusions.....	105
6.1 Conclusions.....	106
6.2 Recommendations.....	107
Appendix A.....	109
References.....	114

List of Tables

Table 2.1: Correction Factor for Moist Curing Duration (ACI 209).....	29
Table 2.2: Error Percentages and Chi Square Error Percentages for Shrinkage Models (Mokarem et. al., 2003).....	36
Table 3.1: Mixture Design and Aggregate Properties.....	40
Table 3.2: Type I/II Portland Cement Physical and Chemical Properties.....	42
Table 4.1: Setting Times for 4 °C, 23 °C, and 38 °C.....	46
Table 4.2: Concrete Properties.....	47
Table 4.3: Compressive Strength for 4 °C.....	48
Table 4.4: Compressive Strength for 23 °C.....	48
Table 4.5: Compressive Strength for 38 °C.....	48
Table 4.6: Shrinkage Measurements.....	51
Table 4.7: Compressive Strength Results for Shrinkage Conditioned Samples.....	52
Table 5.1: Calculated Activation Energy Values.....	62
Table 5.2: Chi-squared Error Analysis of Activation Energy.....	71
Table 5.3: Summary of Activation Energy Values.....	72
Table 5.4: Time Function Error Measurements.....	91
Table 5.5: Chi-Squared Analysis Results.....	95
Table 5.6: Chi-Squared Values for Existing and Developed Models.....	102
Table A.1: Mixture Proportions.....	109
Table A.2: Consistency data for concrete.....	109
Table A.3: Concrete Materials.....	110
Table A.4: Activation Energy-UMD Study (Upadhyaya 2008)	110

List of Figures

Figure 2.1: Plastic Shrinkage Crack Formation (Soroushian and Ravanbakhsh, 1998)	8
Figure 2.2: Chemical and autogenous shrinkage behavior (Holt 2001).....	12
Figure 2.3: Shrinkage versus Water Content (Videla and Aguilar, 2006).....	15
Figure 2.4: Maturity Crossover Effect (Carrino 2003)	19
Figure 2.5: Relative Strength versus Equivalent Age (Carrino 2003).....	23
Figure 2.6: Autogenous Shrinkage versus Concrete Age (Mounanga et. al., 2004)	24
Figure 2.7: Degree of Hydration versus $\text{Ca}(\text{OH})_2$ Content (Mounanga et. al., 2004)	25
Figure 2.8: Volumetric Shrinkage versus Equivalent Age (Mounanga et. al., 2004)	27
Figure 2.9: Shrinkage versus age (Goel et. al., 2007).....	38
Figure 3.1: Coarse Aggregate Gradation.....	41
Figure 3.2: Fine Aggregate Gradation.....	41
Figure 3.3: Aggregate Blend Gradation.....	42
Figure 4.1: Penetration Testing Results	46
Figure 4.2: Activation Energy Compressive Strength Testing Results.....	49

Figure 4.3: Monitoring of Isothermal Conditions.....	50
Figure 4.4: Shrinkage Results.....	52
Figure 4.5: Compressive Strength -Conditioned Samples.....	53
Figure 4.6: Compressive Strength-Conditioned Samples at Early Ages.....	53
Figure 5.1: AE Determination Based Upon Penetration Data-Mixing to Initial Set.....	56
Figure 5.2 AE Determination Based Upon Penetration Data-Mixing to Final Set.....	57
Figure 5.3: AE Determination Based Upon Penetration Data-Initial Set to Final Set.....	57
Figure 5.4: S vs. Equivalent Age-Control (Upadhyaya 2008).....	63
Figure 5.5: S/S _u versus Equivalent Age-Control (Upadhyaya 2008)	64
Figure 5.6: S vs. Equivalent Age-ASTM 1074-A1.1.8.....	65
Figure 5.7: S/S _u versus Equivalent Age-ASTM 1074-A1.1.8.....	65
Figure 5.8: S vs. Equivalent Age-All Data with t ₀ = final setting time.....	66
Figure 5.9: S/S _u versus Equivalent Age-All Data with t ₀ = final setting time.....	66
Figure 5.10: S vs. Equivalent Age-Six data points and t ₀ = final setting time.....	67

Figure 5.11: S/S_u versus Equivalent Age-Six data points and $t_0 =$ final setting time.....	67
Figure 5.12: S vs. Equivalent Age-All data with $t_0 =$ final setting for 38 °C data.....	68
Figure 5.13: S/S_u versus Equivalent Age-All data with $t_0 =$ final setting for 38 °C data.....	68
Figure 5.14: S vs. Equivalent Age-Six data points and $t_0=$ final setting time for 38 °C data.....	69
Figure 5.15: S/S_u versus Equivalent Age-Six data points and $t_0=$ final setting time for 38 °C data.....	69
Figure 5.16: Shrinkage versus Actual Concrete Age.....	74
Figure 5.17: Shrinkage versus Equivalent Age.....	75
Figure 5.18: Shrinkage versus Age Divided by the Age Conversion Factor.....	76
Figure 5.19: e/e_u versus Equivalent Age	78
Figure 5.20: e/e_u versus Age Divided by Age Conversion Factor.....	79
Figure 5.21: e/e_u versus Age.....	80
Figure 5.22: Derivative of the Shrinkage Polynomial versus Time	82
Figure 5.23: Earlier age Compressive Strength Development versus Time.....	84
Figure 5.24: Compressive Strength of Conditioned Samples versus Equivalent Age.....	85
Figure 5.25: Shrinkage versus Compressive Strength-50% RH.....	86

Figure 5.26: Shrinkage versus Compressive Strength -90% RH.....	86
Figure 5.27: Model 1 Predicted Shrinkage and Experimental Shrinkage.....	94
Figure 5.28: Model 2 Predicted Shrinkage and Experimental Shrinkage.....	94
Figure 5.29: Humidity Response of Model 1.....	97
Figure 5.30: Temperature Response of Model 1.....	97
Figure 5.31: Humidity Response of Model 2.....	98
Figure 5.32: Temperature Response of Model 2.....	98
Figure 5.33: Shrinkage Data (50% RH at 23°C) and Existing and Developed Models.....	100
Figure 5.34: Shrinkage Data (90% RH at 23°C) and Existing and Developed Models.....	101
Figure 5.35: Percentage Residual Error-50% RH at 23°C.....	103
Figure 5.36: Percentage Residual Error-90% RH at 23°C.....	103
Figure 5.37: Percentage Residual Error-50% RH at 38 °C.....	104
Figure 5.38: Percentage Residual Error-90% RH at 38 °C.....	104

Chapter 1: Introduction

1.1 Introduction

Many materials used for civil engineering applications are impacted by changes in environmental factors, manufacturing practices, and composition characteristics. Asphalt, for instance, changes its stiffness characteristics as its temperature increases or decreases. Furthermore, a seemingly uniform material such as steel can possess a wide array of characteristics by varying elements such as carbon content or by applying different heat treatments during manufacturing. Even natural products such as timber can possess different strength characteristics if kept moist rather than dry. Portland cement concrete is also impacted by similar characteristics. Environmental factors, mixture design, placement, and curing characteristics significantly affect the rate and degree of strength development, as well as the durability, of concrete. Achieving an understanding of these characteristics and how they affect concrete is a significantly challenging and fulfilling task.

Concrete shrinkage is a physical response that concrete displays due to many different parameters. These include water-to-cement ratio, coarse and fine aggregate proportions, percentage of exposed surface area, cement type, compressive strength, curing temperature and humidity, and exposure time. Since the beginning of the twentieth century, engineers and scientists have attempted to identify the variables that cause shrinkage and to develop a methodology to predict shrinkage. Shrinkage

prediction has proven to be difficult to accurately assess because many of the variables that affect concrete shrinkage are complexly related to one another.

The fundamental problem with shrinkage is that it can cause undesirable stress development in concrete which can lead to cracking. Cracking, in turn, will lead to a reduction in strength and durability. If the degree of strain developed by concrete shrinkage could be accurately predicted, then it is possible that the detrimental effects of strength and durability reduction could be minimized and accounted for with better designs.

1.2 Background

As previously stated, concrete shrinkage is a difficult material behavior to predict because of the many factors affecting this property. In general, however, concrete shrinkage is a result of the development of negative pore pressures within concrete. Since the development of negative pore pressure can occur in several different ways and at different concrete ages, engineers have characterized concrete shrinkage by five different types: plastic shrinkage, autogenous shrinkage, thermal shrinkage, carbonation shrinkage, and drying shrinkage. The sum of these five types of shrinkage equals total shrinkage. It is common for drying shrinkage to simply be referred to as shrinkage because the majority of the measurable volumetric change, when compared to the other forms, is due to drying.

Furthermore, concrete shrinkage has been found to be related to the magnitude of developed concrete strength as well as the rate at which concrete strength develops. In fact, several researchers have looked at both autogenous and chemical shrinkage and found that they are proportional to the rate at which concrete strength develops

through hydration (Mounanga et. al 2004). In turn, they have utilized activation energy based concrete maturity to build this relationship for chemical and autogenous shrinkage. The maturity function relates how rapidly concrete gains strength at different temperatures in relation to the chemical reaction known as hydration. This maturity relationship can then be applied to various temperatures to accurately predict concrete strength with age. Using this existing knowledge, it seems plausible that total shrinkage could be better predicted by incorporating concrete maturity into shrinkage modeling.

1.3 Research Objectives

The primary objective of this investigation was to determine whether a link between the total amount of concrete shrinkage (experienced at different temperatures) and concrete maturity (based upon activation energy) existed. French cement researchers have demonstrated a relationship between chemical and autogenous shrinkage during the early ages of concrete strength development while concrete is still semi-rigid. It would be a valuable improvement to show that concrete maturity can be related to the total amount of shrinkage, rather than simply to some components of shrinkage such as chemical shrinkage.

To achieve this objective, this research investigation was broken into several different objectives which are listed as follows:

1. to determine the setting times of concrete and use this information to calculate activation energies for time periods at early ages, prior to final setting time;

2. to determine the activation energy at later ages using strength data from different temperature exposures;
3. to measure and compare shrinkage at different temperatures and relative humidity levels;
4. to establish a relationship between concrete maturity (based upon activation energy) and concrete shrinkage;
5. to develop a model that predicts the concrete shrinkage as a function of the temperature and humidity levels;
6. to compare existing shrinkage prediction models to the model developed by this study to assess its validity.

1.4 Report Organization

The first chapter of this thesis contains the introduction, research objectives, a brief description of the background, and the organization of the report. The following chapter reviews the existing literature to comprehensively summarize the state of knowledge on concrete shrinkage and concrete maturity. The third chapter presents the testing plan and the materials used. Next, the fourth chapter presents the experimental results from the laboratory testing. The fifth chapter presents the analysis of the data including results of the activation energy calculations, shrinkage and maturity correlation, shrinkage modeling, and model comparison. The sixth and final chapter summarizes the research work, draws conclusions based upon this work, and provides recommendations for further improving concrete shrinkage predictions.

Chapter 2: Literature Review

2.1 Introduction

It is well known that concrete is a heterogeneous material composed of various sized aggregates, cementitious materials, water, and a multitude of admixtures and additives. Understandably, it is difficult to completely predict and model the long term behavior of concrete with such non-uniformity found in its components. As concrete ages it tends to reduce in volume. This phenomenon is known as shrinkage, and is typically related to a loss of water from concrete over time, but can also be associated with environmental exposure and temperature. Researchers have attempted to model the behavior of shrinkage and concrete creep, but as described by Bazant, "...shrinkage is still far from being fully understood, even though it has occupied some of the best minds in the field on cement and concrete research and materials science (Bazant 2001)." However, researchers do seem to have a good grasp of the mechanisms driving the volume change of concrete.

Each of these mechanisms has been defined as its own type of shrinkage and broken into components of a complete volume change known as total shrinkage. These various components include plastic shrinkage, drying shrinkage, autogenous shrinkage, thermal shrinkage, and carbonation shrinkage. One of the difficulties in predicting total shrinkage is that each of these components of concrete shrinkage has its own driving factors which can create an immense number of variables to

incorporate into prediction models. Therefore, many researchers attempt to simplify their calculations by only observing autogenous shrinkage and drying shrinkage as substitute for total shrinkage because their magnitudes will be greater than other types of shrinkage. Thermal shrinkage is accurately described as thermal expansion and contraction of concrete due to temperature change, and can be reversed upon heating; therefore, it will not be discussed as a contributing shrinkage mechanism.

It is important to understand and to be able to predict the amount of shrinkage, because the strain that occurs will translate into stress development and cracking within a concrete section. The degree of shrinkage will be much greater at early ages. It has been shown from research that concrete sections will typically display approximately 50% of its total shrinkage within the first 28 days of drying and 80% within the first 90 days of drying (Altoubat and Lange, 2001). The problem with significant early shrinkage is that concrete at early ages may not have developed sufficient rigidity and strength to resist the tensile stresses developed by shrinkage. Properly predicting these stresses could lead engineers to better predict whether or not cracking will be acceptable, what mixture components can be modified to account for shrinkage, and what curing techniques could be used to minimize shrinkage.

2.2 Properties of Concrete Shrinkage

2.2.1 Plastic Shrinkage

Chronologically, plastic shrinkage occurs before all other types of shrinkage, and therefore, it will be discussed first. Plastic shrinkage is defined as the volume change of concrete associated with water lost while concrete is still in a plastic state (Aitcin et. al., 1997). When water is removed from concrete paste while still in a

plastic state, a series of menisci are formed which generate negative capillary pressures that cause volume contraction of the paste. These pressures will continue to rise until enough pressure is reached that the water will begin to rearrange within the paste such that it pools and forms voids. This process can be attributed to the loss of water from the surface or subgrade of concrete. Often, the surface of the concrete will begin to dry and attain some initial rigidity before any other portion of the concrete structure and will no longer undergo plastic flow. This proves to be problematic, because it leads to the formation of plastic shrinkage cracking, which typically act as pathways for moisture to exit the concrete system. Figure 2.1 demonstrates the mechanisms driving the formation of plastic shrinkage cracks. Notice that the surface is dry while the base is moist, which is integral to forming shrinkage cracks; clearly if it was still somewhat fluid the shrinkage cracks would not form. Plastic shrinkage cracking can be significantly reduced, if not completely eliminated, simply by providing adequate moisture to the concrete through good curing practices.

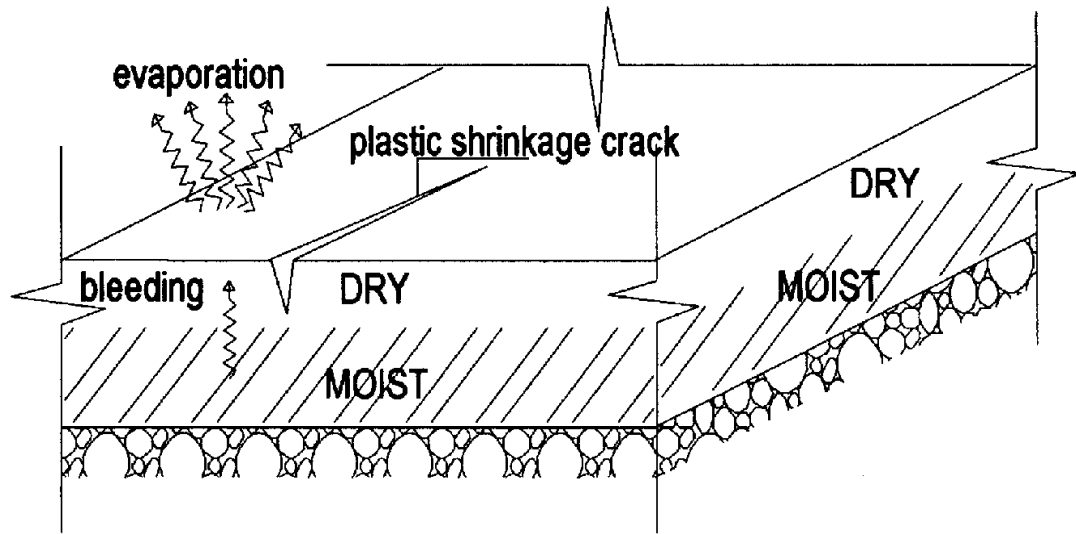


Figure 2.1: Plastic Shrinkage Crack Formation (Soroushian and Ravanbakhsh, 1998).

2.2.2 Carbonation Shrinkage

Another form of shrinkage, which occurs after the final setting of concrete, is carbonation shrinkage. By definition, carbonation shrinkage is caused by a chemical reaction between the hydrated cement paste and carbon dioxide found in air (Aitcin et. al., 1997). The carbonation reaction occurs between the calcium hydroxide molecules ($\text{Ca}(\text{OH})_2$) and Carbon Dioxide (CO_2) found in air under the presence of moisture. Clearly, the degree of carbonation shrinkage is dependent upon how permeable to air is the concrete specimen. This in turn means that concrete that is well cured and has a low water-to-cementitious material ratio will undergo less carbonation shrinkage as it ages.

The amount of carbonation shrinkage that occurs is typically at a maximum at relative humidity around 50%, while its amount is negligible at relative humidity below 25% or above 100%. It has been stated by Powers that carbonation shrinkage results from the dissolution of calcium hydroxide crystals which are under

compression due to the drying shrinkage, leading to the formation of stress-free calcium carbonate in the pores (Powers 1962). This means that the effects of drying shrinkage and carbonation shrinkage are correlated. Once the carbonation process begins, it causes the pore voids to densify and realign to a lower stress state. This helps explain why drying shrinkage specimens, when rewetted, may not return to the original volume prior to drying. The carbonation shrinkage reduces the amount of water that can be reabsorbed.

2.2.3 Thermal Shrinkage

Thermal shrinkage is a reaction by the concrete to a reduction of temperature shortly after the formation of a rigid concrete structure. During the chemical hydration reaction there is an inevitable increase in the temperature of concrete because the reaction itself is an exothermic reaction. Following the peak of this reaction, heat is dissipated causing a cooling of the concrete structure and a volume reduction as a result of this cooling. Some researchers believe that this cooling behavior would be more accurately described as thermal contraction rather than thermal shrinkage (Aitcin et. al., 1997). Thermal shrinkage is due solely to the thermal expansion and contraction coefficients rather than the buildup of negative pore pressures, as in the four other types of shrinkage. However, like the other types of shrinkage formation the concurrent volume reduction can lead to cracking and other problems. Thermal shrinkage would be most pronounced in large concrete mass structures that can generate a significant amount of heat during hydration.

2.2.4 Autogenous Shrinkage

Autogenous shrinkage is a phenomenon that is almost mysterious when producing concrete. This is because there can be a volume change found in concrete even

within sealed specimens free of environmental effects. Autogenous shrinkage is defined as the macroscopic volume reduction of cementitious materials when cement hydrates after initial setting. This type of shrinkage can also be referred to as self-desiccation shrinkage, because within the concrete macroscopic pore structure as water hydrates with cement particles to produce hydrated cement paste, the water and cement reduce in volume. This reduction in volume develops negative pressures within the capillary pores. The major problem is that concrete at an early age has minimal strength; in fact, autogenous shrinkage tends to plateau as the degree of concrete hydration reduces typically after 24 hours (Mounanga et. al., 2004). This means while capillary pressures developed due to cement hydration may be small, these pressures can still produce measurable shrinkage values.

Furthermore, autogenous shrinkage can often be confused with what is called chemical shrinkage. To clarify the variation, chemical shrinkage is a result of the reaction occurring between water and cement causing a reduction in the volume of the hydrated byproduct. Chemical shrinkage is often measured by sealing a cement paste specimen in an impermeable membrane and placing it in a water bath under a weigh below scale to see what the reduction in the upward buoyancy force is over time. As the sealed mass would remain constant, any reduction in volume would cause an increase in measured mass because the cement paste would have less displaced volume of water. This means that chemical shrinkage is a measured total volume change which may prove to cause no measurable external dimensional change.

Autogenous shrinkage, however, is the externally measurable reduction in volume. In fact, researchers have explained that autogenous shrinkage has three different phases of formation (Holt 2001). First is the liquid stage where the material is still highly fluid and has not formed its structure. Autogenous shrinkage during this phase is the same as the measured chemical shrinkage. Second is the skeleton formation phase, where the concrete is semi-rigid and autogenous shrinkage is a function of both self desiccation as well as chemical shrinkage. During this phase the measured autogenous shrinkage will begin to diverge from the measured chemical shrinkage, as shown in Figure 2.2. Finally, autogenous shrinkage reaches the hardened phase, when the concrete is rigid and chemical shrinkage will have little to no effect on the measured autogenous shrinkage but rather the self desiccation of the internal relative humidity within the concrete will cause the measurable volume change.

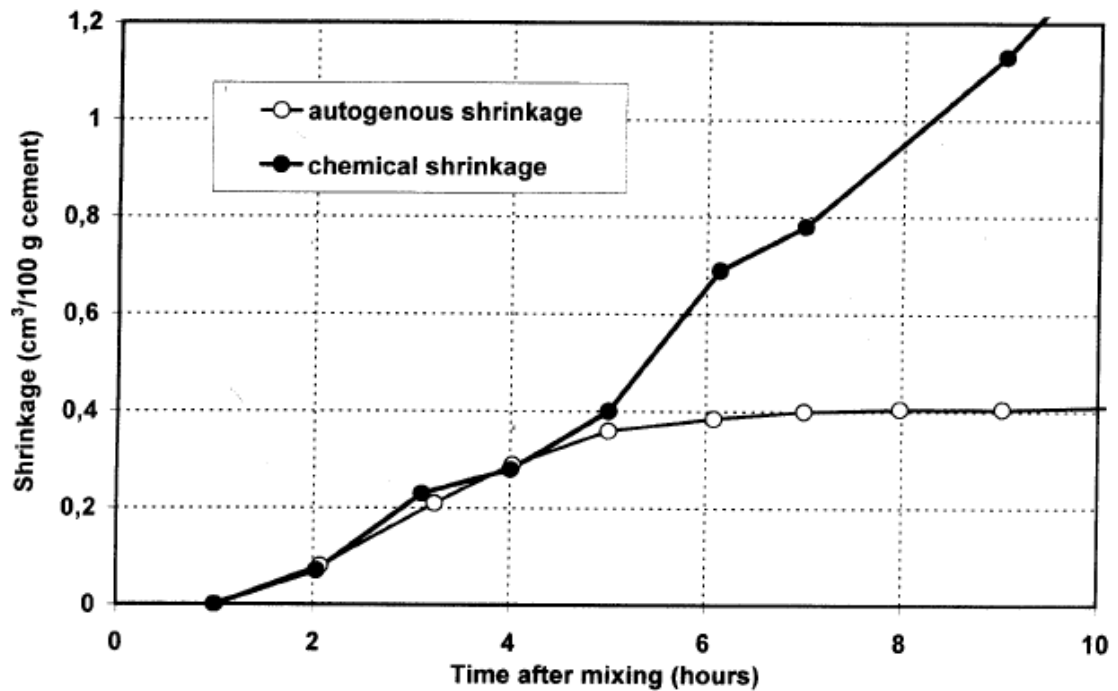


Figure 2.2: Chemical and autogenous shrinkage behavior over time.

Note: Notice that at early ages the two shrinkages are proportional, but at later ages they diverge significantly (Holt 2001).

Traditionally, autogenous shrinkage has been neglected from consideration in measurements of total shrinkage. This is because at normal range water-to-cement ratios, the magnitude of autogenous shrinkage is very small in comparison to drying shrinkage measurements. However, with the advent of high-performance concrete (HPC), which has low water-to-cement ratios, autogenous shrinkage strains are as or more significant than drying shrinkage strains (Aitcin 1999). It has been shown that water-to-cement ratios below 0.33 typically will produce significant amounts of autogenous shrinkage strains.

2.2.5 Drying Shrinkage

Drying shrinkage is the most commonly recognized form of shrinkage.

Drying shrinkage is caused by the development of capillary tension, solid surface

tension, and withdrawal of hindered absorbed and interlayer water from cement gel (Bazant 2001). The definition for drying shrinkage is the reduction in volume due to the effect of moisture loss from environmental exposure after concrete has set. Effectively, this is the drying of the moisture found in the pores on the surface of the exposed concrete. Clearly, this means that concrete dimensions can play a large roll in the degree of drying shrinkage that occurs; more exposed surface area will lead to a greater amount of shrinkage.

Due to the significant effect that concrete drying shrinkage has on the total shrinkage concrete will experience, Chilean researchers Videla and Aguilar looked at the drying shrinkage of blended and normal Portland cement concretes. They developed a comprehensive study where they sought to minimize the amount of drying shrinkage by optimizing the mixture design components. Their study effectively broke down testing into two phases. The first phase looked at the effects of the mixture design variables on drying shrinkage by varying the type of aggregate, the nominal maximum aggregate size, the slump achieved, and the type and blend of cement with varying finenesses. The second phase of the study was designed to isolate the effects of cement on drying shrinkage by varying the type of cement and cement content. In turn, the aggregate type, slump, and nominal maximum aggregate size were kept constant (Videla and Aguilar, 2006). It is important to note that they used their national naming system for describing the types of cement used. These included Portland cement (P similar to Type III), coarse Portland pozzolan cement (PPC, a slow hardening cement), and fine Portland Pozzolan Cement (PPF, a fast hardening cement).

In discussion of the results it was shown through an analysis of variance test (ANOVA) that the researchers attempted to identify significant independent variables affecting drying shrinkage. It was shown that for concretes with equal compressive strength, the relevance of the independent variables on drying shrinkage in order of importance is: drying time, volume-to-surface ratio, cement type, aggregate maximum size, aggregate type, cement type to aggregate type, and aggregate type to volume-to-surface ratio (Videla and Aguilar, 2006). Furthermore, Figure 2.3 shows that with increasing water content the magnitude of drying shrinkage experienced also increases. This proves to be constant for various drying times. This can be explained by the fact that concrete with a lower water-cement ratio will produce concrete with lower permeability and therefore less ability for capillary pores to dry over time.

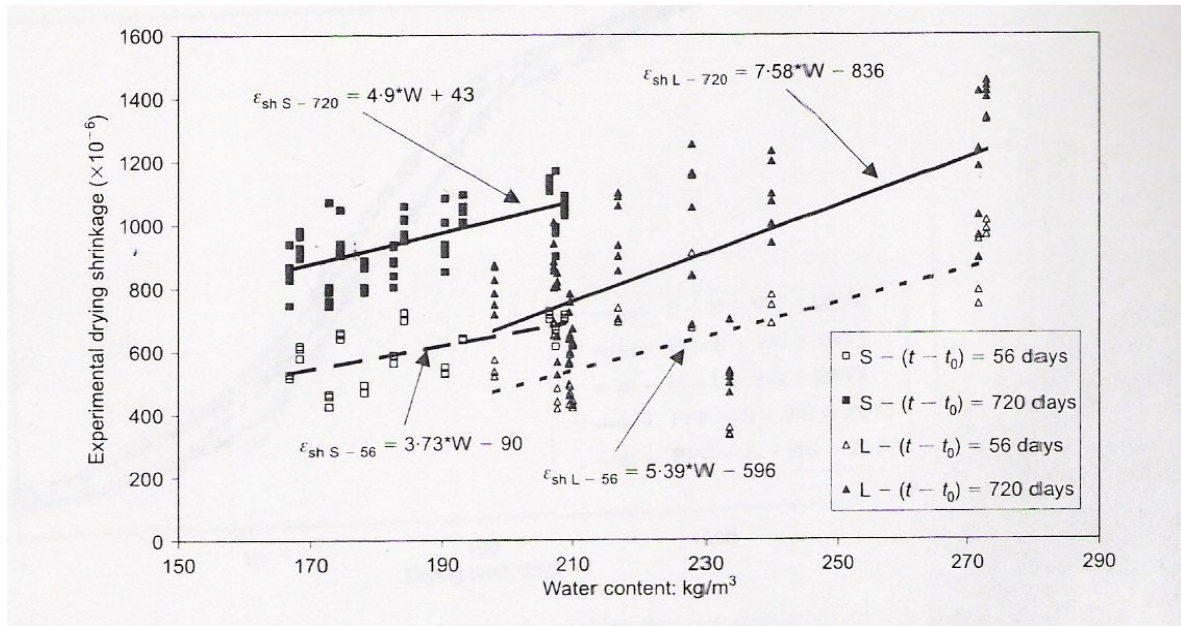


Figure 2.3: Observed drying shrinkage versus the water content for two different time periods, 56 days and 720 days.

Note: *S* corresponds to siliceous aggregate and *L* corresponds to limestone aggregate. Notice that as water content is increasing amount of drying shrinkage appears to increase (Videla and Aguilar, 2006).

Interestingly, it was shown that even though limestone aggregate requires more water content to achieve a desired slump than siliceous aggregates, it displays less drying shrinkage over time. Videla and Aguilar propose that this is because the limestone aggregate used has a higher modulus of elasticity than the siliceous aggregate used (Videla and Aguilar, 2006). Moreover, it has been suggested that the amount of drying shrinkage that occurs is influenced by the aggregate content in concrete, meaning that more or less aggregate by volume of a cubic yard of concrete will effect drying shrinkage. This was proven by the results from Videla and Aguilar and led them to conclude that the amount of drying shrinkage can be reduced by using an aggregate with a high elastic modulus and in large amounts (Videla and Aguilar, 2006).

The results of the second portion of their study looked at the effects of various types of Portland cement on drying shrinkage. However, the results of their analysis prove to be difficult to interpret since the cement types used do not follow standard ASTM nomenclature. What was uncovered was that the cement type that had the highest degree of shrinkage was the coarse grained Portland pozzolan cement (PPC). The fine grained Portland pozzolan cement (PPF) had less drying shrinkage than type PPC but more than the Portland cement (P) (Videla and Aguilar, 2006). What this can be interpreted as meaning is that the coarse grained cements, PPC, should hydrate more slowly and be more susceptible to volume changes than the faster hydrating type PPF and P cements. This makes sense, if one considers that the PPC concrete should have a slower strength gain over time versus the other types, which in turn means that its elastic modulus will be lower.

2.3 Concrete Maturity

Concrete exhibits a relationship between strength development and temperature. As the temperature of concrete increases, its rate of strength gain increases and vice versa. This can prove to be problematic when trying to predict whether or not a certain sample of concrete has achieved adequate strength development for the loading it will endure. A standard relationship needed to be developed so that the daily variation in temperature could be accounted for in predicting strength development. Therefore, a concept known as maturity was developed where a type of concrete is related to an index value that either increases faster for higher temperatures or slower for lower temperatures.

2.3.1 Nurse-Saul Method

In 1949, research by McIntosh dealing with accelerated curing found that the relationship between strength development and temperature may be explained by a product of the time a sample of concrete was exposed to a certain temperature. He theorized that this product could then be related to a set of samples cured above a datum temperature to generate a relatively accurate prediction of the strength of the concrete. However, his formulation did not discover a unique relationship between temperature and strength (Carrino 2003).

Shortly after the work by McIntosh, Nurse also looked at the product of time and temperature to relate the rate of strength of development. He did not utilize a datum temperature as McIntosh did but found that as the product of time and temperature was plotted versus relative strength for concrete samples cured at different ambient temperatures, a single nonlinear curve appeared to form (Carrino 2003). Further, research conducted by Saul expanded upon what Nurse had found and related it to a datum temperature. It was during Saul's research in 1951 that the term "maturity" was first used to describe the relationship between concrete strength development and temperature and an equation to relate the rate of strength development was formulated.

The equation created is shown below in Equation 1 and it has become commonly known as the Nurse-Saul function.

Equation 2.1: The Nurse-Saul maturity function (Carrino 2003).

$$M = \sum_0^t (T - T_0) \Delta t$$

Where:

M=maturity at age t

T=average temperature of concrete during time interval Δt

T_0 =datum temperature

Interestingly, the calculation is simply finding the area under the curve of a plot of time versus temperature above a datum temperature. Due to the sheer simplicity of the formulation of the Nurse-Saul equation it has been widely adopted by the concrete community.

By finding the strength versus age of concrete cured at a reference temperature, the concrete cured at other temperatures can be related to the reference temperature. With knowledge of what the maturity index would be for the referenced concrete and for the concrete cured at various temperatures, the strength of concrete can be predicted (Carrino 2003).

There is a fundamental flaw with using the Nurse-Saul function to relate the rate of concrete strength development to shrinkage. As further research was conducted in the 1960's, it was found that a "crossover effect" occurs when concrete is cured at lower temperatures versus higher temperatures. This crossover effect can be shown in Figure 2.4.

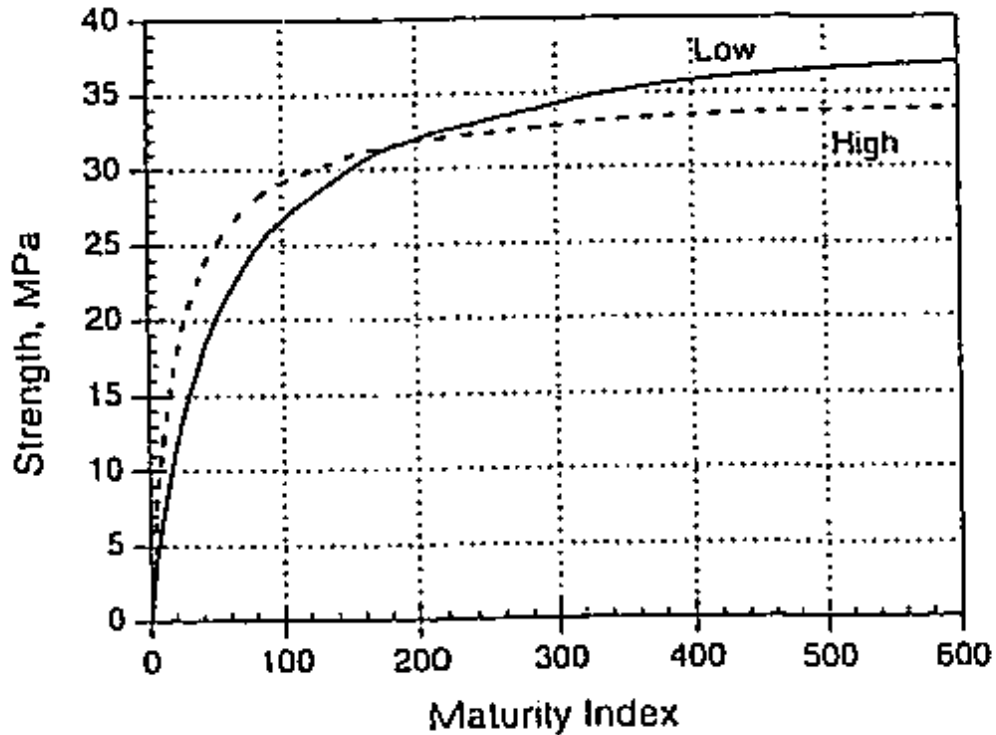


Figure 2.4: The “crossover effect” with strength and maturity at high and low temperatures (Carrino 2003).

The crossover effect occurs because at lower temperatures the hydration reaction occurs at a slower rate and the hydrated cement grains form in a more uniform manner when compared to concrete cured at higher temperatures. The primary problem with the Nurse-Saul function is that it assumes that the product relationship between time and temperature above a datum temperature is linear which would be the case if the crossover effect did not exist (Carrino 2003). Therefore, it has been found that the Nurse-Saul function does an acceptable job at predicting the longer term strengths but is not as accurate as other function in the earlier ages.

2.3.2 Arrhenius Based Method

The advancement of the maturity concept led towards the development of an Arrhenius based maturity function. In 1977, Freiesleben, Hansen, and Pedersen developed an equation to describe the equivalent age of concrete to the rate at which a chemical reaction occurs as defined by the Arrhenius Equation. The Arrhenius Equation is a fundamental part of physical chemistry that quantifies the amount of energy required to initiate a chemical reaction. The maturity concept developed by Freiesleben, Hansen, and Pedersen is often referred to as an activation energy maturity function and sometimes referred to as an Arrhenius based maturity function. The format of this equation is shown below in Equation 2.2.

Equation 2.2: Equivalent age function based upon activation energy (Carrino 2003).

$$t_e = \sum_0^t e^{\frac{-E}{R} \left[\frac{1}{273+T} - \frac{1}{273+T_r} \right]} \cdot \Delta t$$

Where:

t_e = equivalent age at the reference curing temperature

T = average temperature of concrete during the time interval Δt , °C

E = activation energy, J/mol

R = universal gas constant, 8.3144 J/(mol K)

This function, shown in Equation 2.2, provides not only a chemistry based relation to strength development, but it also provides a better approximation of the early age strength development of concrete (Carrino 2003). However, its complexity is much greater than that of the Nurse-Saul function which has led to a slow adoption by engineers working with concrete.

The strength-maturity relationship using the activation energy based maturity function is determined by first finding the activation energy of concrete for a specific mixture design. This is done by casting compressive strength specimens and wet curing them at various temperatures. At time intervals that increase as a function of the final setting time of the mixture, compressive strength tests are performed and the stress at failure is determined. While there are several methods to approximate the activation energy based upon strength data, the recommended method is to fit Equation 2.3, shown below, to the compressive strength values found at certain time intervals using a computer that can perform regression analysis.

Equation 2.3: Strength-age relationship based upon activation energy based maturity (Carrino 2003).

$$S = S_{\infty} \frac{k_t(t - t_o)}{1 + k_t(t - t_o)}$$

Where:

S = compressive strength

S_{∞} = limiting strength at infinite age

k_t = a rate constant

t = age of concrete

t_o = age at which strength development begins

The above equation relates three constant terms (k_t , t_o , and S_{∞}) that are calculated to relate the independent variable (t) to the dependent variable (S). To calculate activation energy, Equation 2.3 is used to fit sets of compressive strength data for at least three different temperatures. The calculated values of k_t are then used to determine the activation energy by finding the slope of the best-fit line of

reciprocal of k_t versus the reciprocal of temperature in degrees Kelvin. The slope of this line is multiplied by the universal gas constant, R , and the resulting value is the activation energy for the concrete mixture.

Once the activation energy of a concrete mixture has been determined, the function previously shown in Equation 2.2 can be used to calculate the equivalent age of that concrete mixture. The equivalent age then can be used to relate the strength of concrete cured at a different temperature to concrete cured under isothermal conditions at a datum temperature (usually 23 °C). In theory, the strength of concrete at an equivalent age should be equal to the strength of concrete at a datum temperature for a value of actual concrete age equal to the calculated equivalent age.

As previously stated, the maturity method that uses activation energy improves upon the method proposed by the Nurse-Saul function because it explains the rate of strength development based upon physical chemistry. To prove that the rate of strength development is related to the Arrhenius equation, as shown in Equation 2, researchers have shown that the relative strength of concrete can be summarized by a single curve (Carrino 2003). Relative strength is the ratio of concrete strength at age t divided by the calculated limiting strength (S/S_∞). Essentially, this means that the percentage or proportion of strength development should be the same for all curing temperatures at the same equivalent age. Figure 2.5 shown below demonstrates an example of relative strength plotted versus equivalent age. Notice that the experimental data points group well into a single curve which means that the equivalent age does an excellent job of explaining the rate of strength development. This gives credence to the belief that the activation energy based

maturity function does a better job of summarizing the strength development of concrete than the Nurse-Saul maturity method because the relative strength data would not plot to a uniform curve for the Nurse-Saul method.

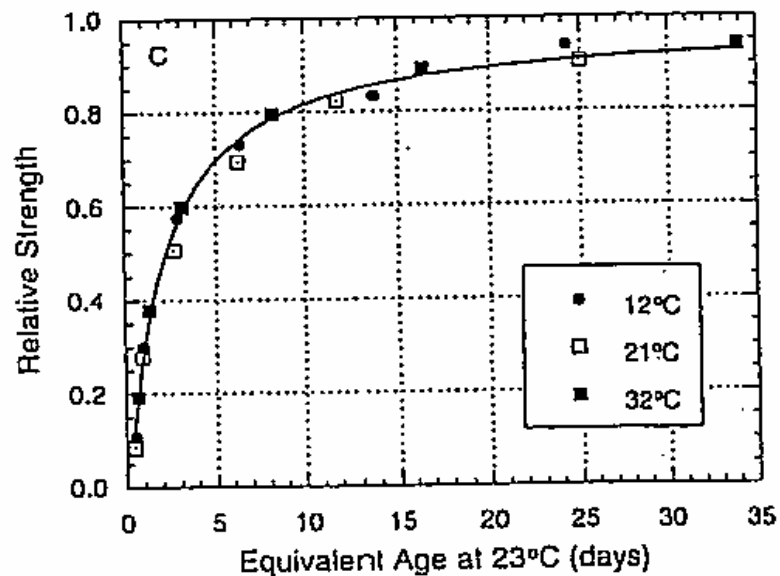


Figure 2.5: Relative strength versus the equivalent age of concrete cured at various temperatures (Carrino 2003).

2.4 Maturity and Shrinkage

If concrete shrinkage can be related to the amount of developed strength and the rate of strength development, then possibly concrete shrinkage can be summarized by a maturity concept. Mounanga et. al. have shown that with increasing temperature the amount of autogenous shrinkage will also increase (Mounanga et. al., 2004). These effects can be shown in Figure 2.6 where amount of volumetric autogenous shrinkage is plotted against concrete age.

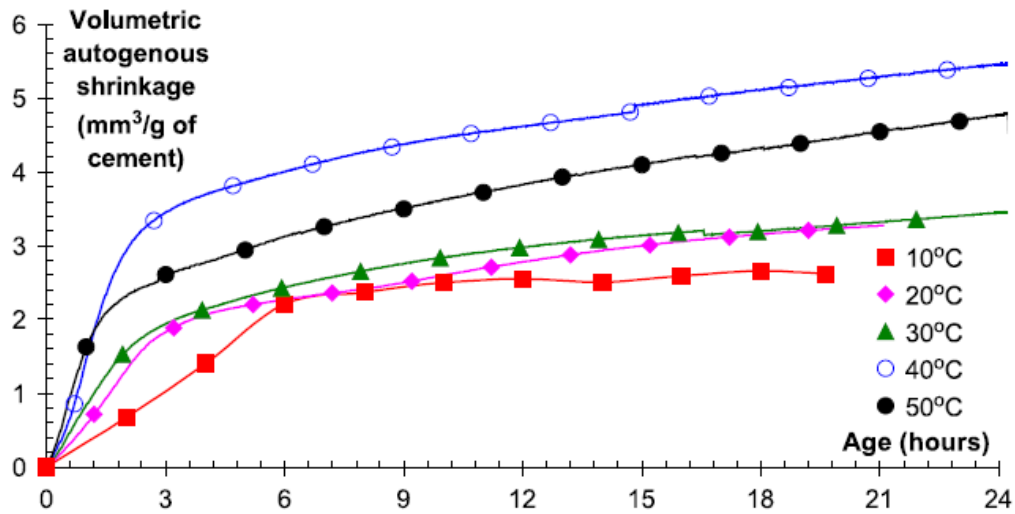


Figure 2.6: Autogenous Shrinkage versus Concrete Age (Mounanga et. al., 2004).

Their research has looked at the temperature effects on autogenous deformations in cement pastes. The research attempted to better understand the mechanisms associated with the development of autogenous shrinkage deformations and to investigate the usage of the maturity concept to describe these deformations.

The first significant finding was that the standard methods for measuring shrinkage typically do not incorporate the full amount of autogenous shrinkage (Mounanga et. al., 2004). As shown in Figure 2.7, the degree of hydration plotted against the Ca(OH)_2 content produces a noticeable bend that the authors identify as the Ca(OH)_2 content threshold. This threshold is an assumed point where autogenous stresses would begin to develop as concrete is no longer plastic. From other research, it was shown that for most water-to-cement ratios the Ca(OH)_2 threshold is reached at a point between the initial and final setting times of concrete identified by Vicat testing. In concrete hydration, there is a significant acceleration of the chemical reaction at seven to eight hours after mixing, then clearly there should also be a significantly high amount of chemical shrinkage and by relation autogenous

shrinkage occurring at this time as well. Standard testing requires shrinkage measurements to begin after 24 hours of placement, which would undoubtedly lead to an inaccuracy in the amount of measured autogenous shrinkage.

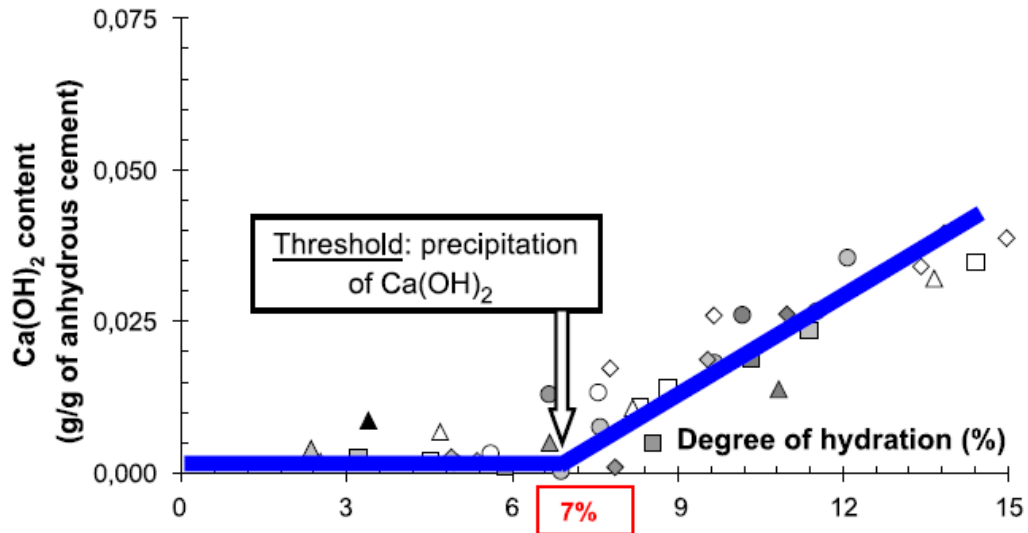


Figure 2.7: Degree of hydration versus Ca(OH)_2 content. Notice the threshold point at 7% hydration (Mounanga et. al., 2004).

As has been described earlier, the degree of hydration and temperature have an effect on the rate of autogenous shrinkage deformation. The authors attempted to employ a maturity model to autogenous shrinkage to account for the variations in degree of hydration and temperature. The most recent model of concrete maturity relates the temperature-time history of a concrete to the activation energy concept based upon Arrhenius law. Fundamentally, each type of cement should hydrate at different rates in accordance to their chemical composition and the temperature history of the sample. These various properties are then related to a standardized sample history at a controlled temperature. A modified equation for equivalent age is shown on the following page as Equation 2.4.

Equation 2.4: Modified Equivalent Age Equation (Mounanga et. al., 2004).

$$t_e = \int_0^t \exp\left(\frac{E_a}{R} \cdot \left(\frac{1}{(273 + T_{ref})} - \frac{1}{(273 + T(t))}\right)\right) dt$$

Where:

E_a = apparent activation energy

R = universal gas constant

T = the actual temperature

T_{ref} = reference temperature typically 20 °C

Mounanga et. al. utilized this equation to relate the equivalent age of concrete specimens to the total autogenous shrinkage with moderate success. One difficulty is that the authors identified that the apparent activation energy value needs to be separated into two portions. Referring back to Figure 2.6, if one looks at the beginning of autogenous shrinkage measurements it clear that there are two portions of the plots with different magnitudes of shrinkage change over time. This led the researchers to believe that multiple activation energies need to be summarized for various time steps rather than taking one average that summarizes the entire life of the concrete (Mounanga et. al., 2004). Figure 2.8, demonstrates the results using activation energy to model shrinkage at various temperatures. The specimens are initialized at 6 hours of equivalent age, which corresponds to an activation energy value from concrete that has reached its threshold of 7% hydration. It is evident from the graph that the model gives a close grouping for values between 20 °C and 50 °C. At low temperatures of 10 °C the maturity concept does not sufficiently normalize the predicted autogenous shrinkage strain. This research proves that while it may be

difficult, it should be possible to incorporate a maturity model into better predicting shrinkage.

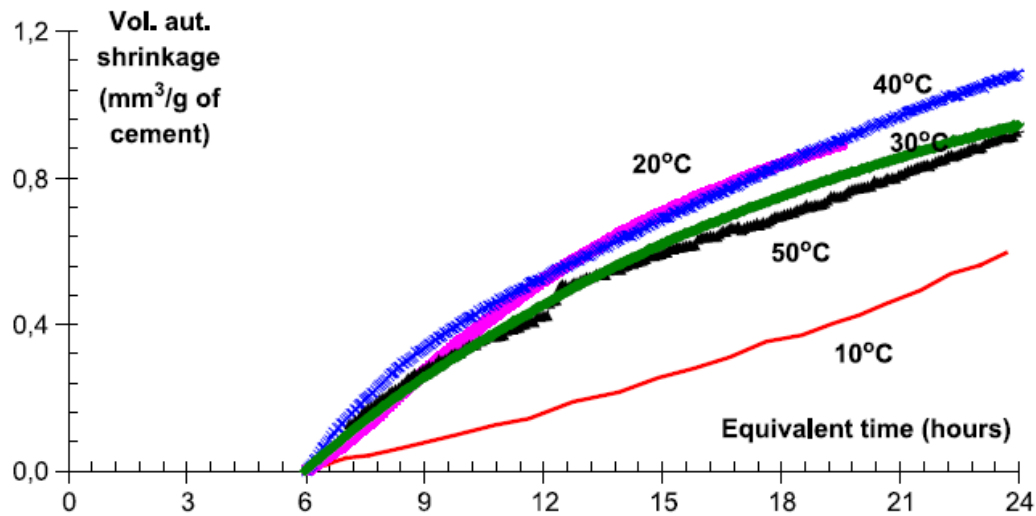


Figure 2.8: Volumetric shrinkage versus equivalent age in hours (Mounanga et. al., 2004).

2.5 Shrinkage Prediction Models

Various shrinkage prediction models have been developed to predict the total amount of shrinkage concrete will experience at any concrete age. The main problem with these prediction models is that they quite often produce large overestimations of the total amount of concrete shrinkage. However, due to the complex nature of modeling shrinkage, they are widely viewed as acceptable. In fact, one prominent researcher in the area of concrete shrinkage, Zdenek P. Bazant, has produced one of the most complex models of shrinkage, yet it still has a coefficient of variation of 34% (Bazant, 2001). The problem is that concrete shrinkage is complex and can be related to diffusion theory, activation energy, residual stress development, solidification theory, and microstress (Bazant 2001).

There are multiple shrinkage prediction models; however, the most accurate and most recently developed models are Bazant's B3 model and Gardner and Lockman's GL2000 model. All of shrinkage predicting models currently utilize similar formulas that are bounded by an ultimate shrinkage value. These models also include measurements of concrete strength, curing conditions, and time drying in their calculations. These models have been empirically developed from a database of shrinkage data incorporating a vast array of data points.

2.5.1 ACI 209

The ACI 209 shrinkage prediction model is one of the oldest equation sets still used to predict concrete shrinkage. Its composition is based upon a time function that relates the rate of strength development to an ultimate shrinkage value and a set of correction factors for characteristics like relative humidity, curing time, cement content, etc. The format of ACI 209 can be shown below in Equation 2.5 through Equation 2.12.

Equation 2.5: ACI 209 Shrinkage versus time (ACI 209).

$$\epsilon_{sh}(t, t_{sh,0}) = \frac{t - t_{sh,0}}{35 + (t - t_{sh,0})} \cdot \epsilon_{sh\infty}$$

Equation 2.6: ACI 209 Shrinkage Corrections (ACI 209)

$$\epsilon_{sh\infty} = \gamma_{\lambda} \cdot \gamma_{VS} \cdot \gamma_{cp} \cdot \gamma_S \cdot \gamma_{\psi} \cdot \gamma_c \cdot \gamma_{\alpha} \cdot 780 \times 10^{-6}$$

Equation 2.7: Correction Factor for Relative Humidity (ACI 209).

$$\gamma_{\lambda} = 1.40 - 0.010\lambda \quad \text{for } 40\% \leq \lambda \leq 80\%$$

$$\gamma_{\lambda} = 3.00 - 0.030\lambda \quad \text{for } 80\% < \lambda \leq 100\%$$

Equation 2.8: Correction Factor for Specimen Size (ACI 209).

$$\gamma_{VS} = 1.2e^{-0.12V/S}$$

Table 2.1: Correction Factor for Moist Curing Duration (ACI 209).

Moist Curing Duration	Shrinkage γ_{cp}
1	1.2
3	1.1
7	1.0
14	0.93
28	0.86
90	0.75

Equation 2.9: Correction Factor for Concrete Slump (ACI 209).

$$\gamma_s = 0.89 + 0.041 \cdot S$$

Equation 2.10: Correction Factor For Fine Aggregate Percentage (ACI 209).

$$\gamma_\psi = 0.30 + 0.014\psi \quad \text{for } \psi \leq 50\%$$

$$\gamma_\psi = 0.90 + 0.002\psi \quad \text{for } \psi > 50\%$$

Equation 2.11: Correction Factor for Cement Content (ACI 209).

$$\gamma_c = 0.75 + 0.00036c$$

Equation 2.12: Correction Factor for Air Content (ACI 209).

$$\gamma_\alpha = 0.95 + 0.008\alpha$$

Where:

- $\epsilon_{sh}(t, t_0)$ = predicted shrinkage
- $\epsilon_{sh\infty}$ = ultimate shrinkage for the concrete
- t = age of concrete (days)
- $t_{sh,0}$ = age at which concrete stopped moist curing (days)
- γ_λ = relative humidity correction
- λ = relative humidity
- γ_{vs} = volume to surface area correction
- V/S = ratio of volume to surface area (in^3/in^2)
- γ_{cp} = moist curing duration correction
- γ_s = slump correction
- S = slump (in)
- γ_ψ = fine aggregate percentage correction
- ψ = fine aggregate percentage

γ_c	= cement content correction
c	= cement content
γ_a	= air content correction
α	= air content

One benefit of the ACI 209 code model is that it has a wide range of correction factors that can easily be applied to the prediction equations. This means that the limitations of the equations are not as restricted as some of the other prediction equations which will be presented. The standard parameters that the ACI 209 model was developed for include a cement content between 279 and 446 lb/yd³, relative humidity between 40% and 100%, type I or III cement, at least 1 day of moist curing, and at least 7 days before exposure to drying conditions (ACI 209, 2008). However, the correction factors listed above do provide for analysis of conditions other than standard.

2.5.2 CEB-FIP 90

While ACI 209 is the American code model for shrinkage and creep prediction, the CEB-FIP 90 model is a European code model for concrete shrinkage and creep prediction. The CEB-FIP 90 model was developed by Muller and Hildorf and released in 1990. It has a wide range of applicability and is notably useful to many practicing engineers because it does not require the input of curing duration or type of curing to predict shrinkage (ACI 209, 2008).

Equation 2.13: CEB-FIP 90 Shrinkage versus Time (CEB-FIP 90).

$$\epsilon_{cs}(t, t_s) = \epsilon_{cso} \beta_s(t - t_s)$$

Equation 2.14: Ultimate Concrete Shrinkage (CEB-FIP 90).

$$\epsilon_{cso} = \epsilon_s(f_{cm}) \cdot \beta_{RH}$$

Equation 2.15: Shrinkage Relation to Compressive Strength (CEB-FIP 90).

$$\varepsilon_s(f_{cm}) = \left[160 + 10 \cdot \beta_{sc} \left(9 - \frac{f_{cm}}{f_{cmo}} \right) \right] \cdot 10^{-6}$$

Equation 2.16: Shrinkage Conversion for Relative Humidity (CEB-FIP 90).

$$\beta_{SRH} = 1 - \left(\frac{RH}{RH_0} \right)^3$$

Equation 2.17: Shrinkage Conversion for Relative Humidity (CEB-FIP 90).

$$\beta_{RH} = -1.55 \beta_{SRH} \quad \text{for } 40\% \leq RH < 99\%$$

$$\beta_{RH} = 0.25 \quad \text{for } RH \geq 99\%$$

Equation 2.18: Shrinkage in function of time (CEB-FIP 90).

$$\beta_s = \left[\frac{t - t_s}{350 \cdot \left(\frac{2A_c}{\mu} \right)^2 + (t - t_s)} \right]^{0.5}$$

Where:

ε_{cs} = concrete shrinkage at time “t”

ε_{cso} = notional shrinkage coefficient

β_s = shrinkage as a function of time

β_{RH} = relative humidity correction

β_{SRH} = relative humidity correction function

t = age of concrete (days)

t_s = age at which concrete began drying (days)

$\varepsilon_s(f_{cm})$ = shrinkage as a function of compressive strength

β_{sc} = coefficient for cement type (5 for Type I cement)

f_{cm} = mean compressive strength at 28 days

f_{cmo} = 10 MPa or 1450 psi

RH = relative humidity of the ambient atmosphere

RH_0 = 100%

A_c = cross-sectional area section

M = perimeter of section

The CEB-FIP model is limited to a 28 day mean compressive strength between 2,500 and 10,000 psi, a water-to-cement ratio of between 0.35 and 0.85, a relative humidity between 40% and 100%, type I, II, or III cement, at least one day of moist curing, and between 5° and 30° C temperatures (ACI 209, 2008). Like the ACI 209 model the range of applicability is quite significant. There is, however, a larger and more complex set of equations to predict shrinkage which could be justifiable if the predicted shrinkage is more accurate than the existing older shrinkage prediction models.

2.5.3 B3 Model

The B3 model is easily the most complex of all the current prediction models. This model has developed from Bazant's previous work and has evolved chronologically from the BP model to the BPKX model and finally to the B3 model (Bazant 2001). The incorporates variables such as humidity, specimen size, time dependence, elastic modulus, cement type, and curing conditions. This model is summarized in the set of Equations 2.19 through 2.25, shown below.

Equation 2.19: Shrinkage Calculated at Time 't' (Bazant 1995).

$$\varepsilon_{sh}(t, t_o) = -\varepsilon_{sh\infty} k_h S(t)$$

Equation 2.20: Shrinkage as a Function of Time (Bazant 1995).

$$\varepsilon_{sh\infty} = \varepsilon_{s\infty} \frac{E(7 + 600)}{E(t_o + \tau_{sh})}$$

Equation 2.21: Shrinkage as a Hyperbolic Function of Time (Bazant 1995).

$$S(t) = \tanh\left(\frac{t - t_o}{\tau_{sh}}\right)^{1/2}$$

Equation 2.22: Shrinkage Half-Time Function (Bazant 1995).

$$\tau_{sh} = k_t (k_s D)^2$$

where

$$k_s = \begin{cases} 1.00 & \text{for an infinite slab} \\ 1.00 & \text{for an infinite cylinder} \\ 1.00 & \text{for an infinite square prism} \\ 1.00 & \text{for a sphere} \\ 1.00 & \text{for a cube} \end{cases}$$

Equation 2.23: Constant Relation to Initial Time and Compressive Strength (Bazant 1995)

$$k_t = 190.8 t_0^{-0.08} f'_c$$

Equation 2.24: Ultimate Shrinkage Calculation (Bazant 1995).

$$\varepsilon_{s\infty} = \alpha_1 \alpha_2 \left[26 w^{2.1} (f'_c)^{-0.28} + 270 \right] \cdot 10^{-6}$$

where

$$\alpha_1 = \begin{cases} 1.0 & \text{for type I cement} \\ 0.85 & \text{for type II cement} \\ 1.1 & \text{for type III cement} \end{cases}$$

and

$$\alpha_2 = \begin{cases} 0.75 & \text{for steam cured specimens} \\ 1.0 & \text{for specimens moist cured} \\ 1.2 & \text{for specimens sealed during curing} \end{cases}$$

Equation 2.25: Humidity Relationship to Shrinkage (Bazant 1995).

$$k_h = \begin{cases} 1 - h^3 & \text{for } h \leq 0.98 \\ -0.2 & \text{for } h = 1 \text{ (swelling in water)} \end{cases}$$

Where:

$\varepsilon_{sh}(t, t_0)$ = shrinkage strain at time "t"

k_h = humidity dependence factor

τ_{sh} = shrinkage half-time (days)

$D = 2V/S$ = effective cross-section in inches

k_s = size dependence factor

w = water content

α_1 = factor for cement time

$\varepsilon_{sh\infty}$ = ultimate shrinkage strain

$s(t)$ = time function for shrinkage

h = relative humidity of the environment

V/S = volume to surface ratio

E = 28 day Elastic Modulus

f'_c = 28 day compressive strength

α_2 = factor for type of curing

Several simplifications for this model exist, for instance, $\varepsilon_{sh\infty}$ can be assumed equal to ε_{sh} , which will remove one equation from calculations. Also, many coefficients go to 1. There are restrictions to the models however. The B3 model can only work for cylinder strengths between 17 and 70 MPa, w/c ratios between 0.30-0.85, aggregate to cement ratios of 2.5-13.5, and cement contents between 160-720 kg/m³. Using values that deviate to these ranges should only be based upon tested results.

2.5.4 GL2000

The model proposed by Gardner and Lockman, GL2000, is a model that is much simpler in its usage. It is an advancement of the model proposed by Gardner and Zhao, the GZ model (Goel 2007). As evident by the equation set it is much simpler to use when predicting shrinkage strains. Similar to the B3 model, it utilizes an ultimate shrinkage value, a relative humidity function, and a time dependent function to estimate shrinkage. It also looks at variables such as the drying time, 28 day compressive strength, cement type, and volume to surface area ratio. The model is summarized in the Equation 2.26 through 2.29, shown below.

Equation 2.26: Shrinkage Calculated at Time 't' (Gardner and Lockman 2001).

$$\varepsilon_{sh} = \varepsilon_{shu} \beta(h) \beta(t)$$

Equation 2.27: Humidity Dependence of Concrete (Gardner and Lockman 2001).

$$\beta(h) = (1 - 1.18h^4)$$

Equation 2.28: Ultimate Shrinkage in Function of Compressive Strength (Gardner and Lockman 2001).

$$\varepsilon_{shu} = 1000 \cdot K \cdot \left(\frac{4350}{f_{cm28}} \right)^{1/2} \cdot 10^{-6}$$

Equation 2.29: Shrinkage as a Function of Drying Time (Gardner and Lockman 2001).

$$\beta(t) = \left(\frac{t - t_c}{t - t_c + 97 \cdot (V/S)^2} \right)^{0.5}$$

Where:

- h = humidity expressed as a decimal
- t = age of concrete (days)
- t_c = age drying commenced, end of moist curing (days)
- K = 1.0 for Type I cement
- V/s = volume-surface ratio, mm
- f_{cm28} = concrete mean compressive strength at 28 days, MPa

Similar to the B3 model, certain restrictions exist. The GL2000 model is acceptable for 28 day compressive strengths less than 70 MPa, and w/c ratios between 0.40 and 0.60. As will be demonstrated in the next section, the GL2000 model does an excellent job of modeling shrinkage strains for concrete structures. Unlike the B3 model, due to its inherent simplicity, the GL2000 model does not have the same simplifications to the equation.

2.6 Performance of Shrinkage Prediction Models

Analysis has been conducted to examine the various concrete shrinkage prediction models and to interpret which performs the best. Mokarem et. al. performed testing to develop a concrete shrinkage performance specification for the state of Virginia. The testing plan utilized various aggregates from throughout Virginia to prepare concrete samples from mixture designs regularly used by the Virginia Department of Transportation. The testing involved performing compressive strength testing, elastic modulus testing, restrained shrinkage testing, and free

shrinkage testing at various ages. Once completed the shrinkage results were compared to predicted results from the various shrinkage models in order to identify which mixture appears to model the entire data set most correctly (Mokarem et. al., 2003).

Values of free shrinkage were taken at 7, 28, 56, 90, 120, 150, and 180 days after drying had begun; which is a relatively short age compared to some shrinkage measurements taken at 5 and 10 years. Similarly, shrinkage values for each day were predicted using code models for those same days. To determine the best model, an error percentage analysis and a Chi Square Test were performed and analyzed. The results showed that regardless of the aggregate type, the CEB-FIP 90 Model predicted shrinkage best, followed by the Gardner/Lockman and Bazant models, followed by the ACI 209 and Sakata Models (Mokarem et. al., 2003). These results are summarized in Table 2.2 shown below. The researchers noted that all of the models overestimated shrinkage for the 180 day period (Mokarem et. al., 2003).

Table 2.2: Error Percentages and Chi Square Error Percentages for all Models (Mokarem et. al., 2003).

Model	Test	Limestone	Gravel	Diabase
ACI 209	Error %	42	40	25
	Chi Square	4,550,038	4,230,628	1,861,072
Bazant	Error %	25	17	11
	Chi Square	1,360,508	835,433	529,537
CEB90	Error %	22	17	10
	Chi Square	961,924	714,085	378,416
Gardner/Lockman	Error %	26	19	12
	Chi Square	1,224,848	797,398	528,312
Sakata	Error %	80	72	57
	Chi Square	13,501,862	12,505,781	8,859,553

However, Mokarem et. al. takes a simplified approach when analyzing the shrinkage values of concrete. Several factors, especially within the B3 model, are not correctly labeled from the original models such as the k_h factor is listed as a cross-sectional shape factor when it is really a relative humidity correction factor. Also, the effect of volume to surface area appears to be ignored in several of the calculations. While this data was specifically tailored for use in Virginia, it doesn't seem expansive enough to incorporate a large array of concrete shrinkage data.

A more recent analysis of the various prediction models yielded different results. Goel et. al. analyzed a large data bank of shrinkage results to seek which model best predicted the behavior of concrete. As suggested by Zdenek P. Bazant, the variations of shrinkage were analyzed for various age categories: up to 365 days, 365 days to 5,000 days, and 28 days to 5,000 days (Goel et. al., 2007). This allows the performance of the models to be analyzed at various phases, so that if a model better predicts long term shrinkage versus early age shrinkage, it can be identified. This was completed by taking a standard of deviation (SD) and a mean ratio (R) to compare the models to the actual data. From the results it is shown that the shrinkage prediction model that works the best is the GL 2000 model. This is demonstrated in Figure 2.9, which represents a standard plot of shrinkage versus age showing the experimental results as the line "Russell and Larson" and the various predicted shrinkage values. The results have shown that the GL2000 model is the best model for shrinkage prediction (Goel et. al., 2007). Furthermore, the researchers noted that all of the models appear to underestimate the shrinkage results.

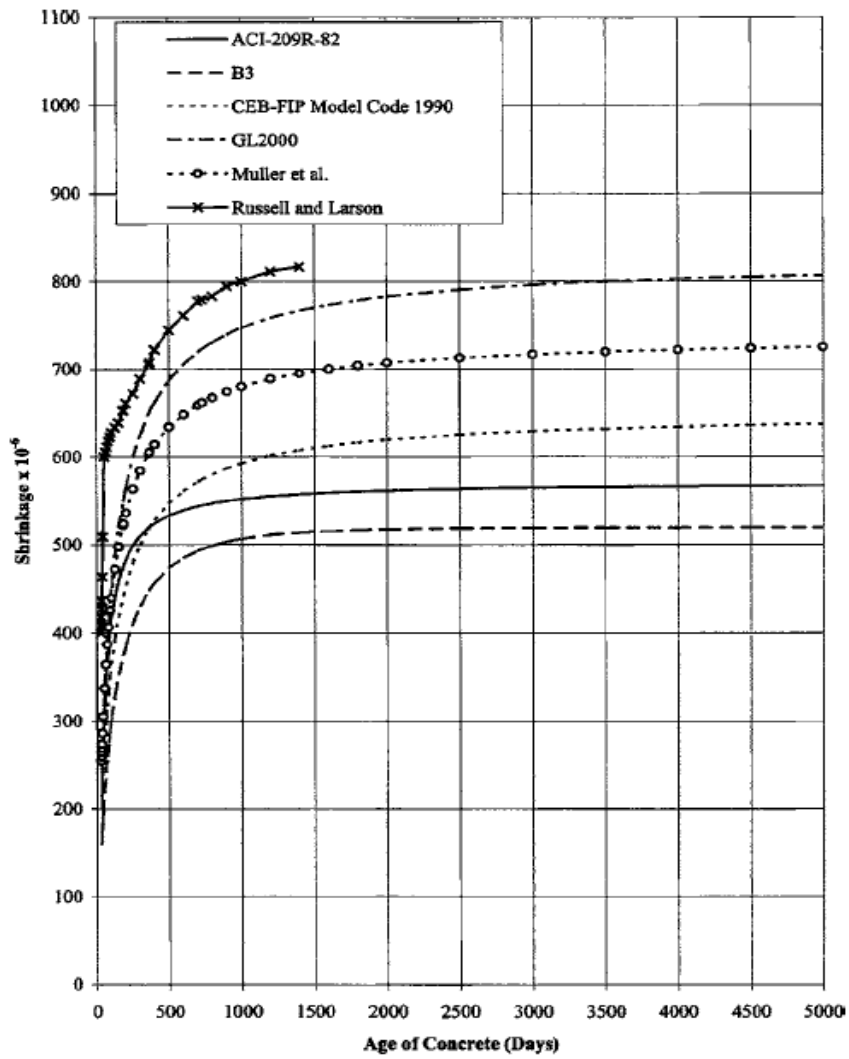


Figure 2.9: Shrinkage versus age.

Note: Russell and Larson are experimental results while other values are predicted shrinkage values (Goel et. al., 2007).

Chapter 3: Materials and Testing Plan

3.1 Materials and Mixture Design

For this study, materials were collected from the Aggregate Industries batch mixing plant located in Crofton, Maryland. A conventional Portland Cement Concrete mixture design was selected consisting of cement, #57 crushed coarse aggregate, fine aggregate meeting ASTM C 33 specifications, water, and high range water reducing admixture. The mixture had a water-to-cement ratio of 0.56.

The fine aggregate used was originally sourced from Aggregate Industries Accokeek Quarry in Brandywine, Maryland. The coarse aggregate came from the Aggregate Industries Millville Quarry in Harpers Ferry, West Virginia. The physical properties of both coarse and fine aggregate, as well as the concrete mixture design, are displayed in Table 3.1. The gradations for coarse aggregate and fine aggregate are displayed in Figure 3.1 and 3.2 respectively, and the gradation for the aggregate blend as found in the concrete batch mixture is displayed in Figure 3.3.

The Portland Cement that was used was manufactured by Lehigh Cement Company in Union Bridge, Maryland. The cement was classified as Type I/II cement that met ASTM and AASHTO specifications. Chemical and physical properties of the cement are displayed in Table 3.2.

The mixture design used a high range water reducing admixture known as VisoCrete® 2100 produced by Sika®. This high range water reducing admixture is a

polycarboxylate based admixture that appears light blue and meets the requirements set forth in ASTM C-494 for Types A and F water reducing admixtures.

Table 3.1: Mixture Design and Aggregate Properties

Type I/II cement (kg/m ³)	302.4
Coarse Aggregate (kg/m ³)	1150.4
Fine Aggregate (kg/m ³)	769.7
Water (kg/m ³)	169.6
Water-to-Cement Ratio	0.56
Type F HRWR (ml/cwt)	88.7 ml
Gs of Coarse Aggregate (#57)	2.84
Gs of Fine Aggregate	2.58
Gs of Cement	3.15
Absorption of Fine Aggregate	0.99%
Absorption of Coarse Aggregate	0.40%
Fineness Modulus	2.74

*1 kg/m³ = 1.686 lb/yd³

Gs = Bulk Specific Gravity

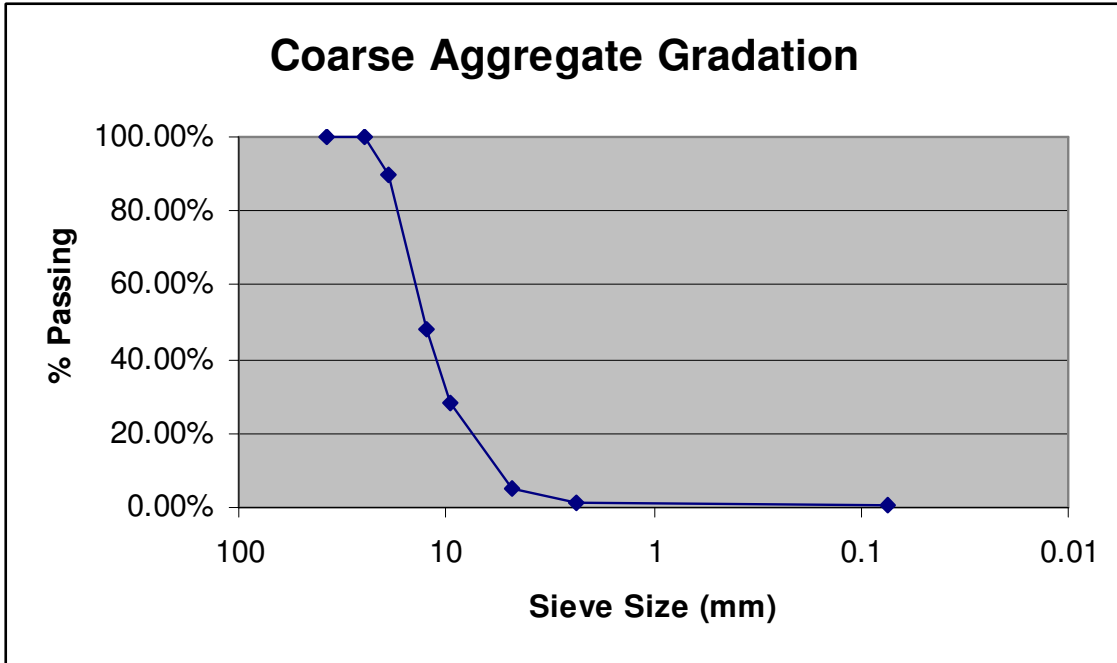


Figure 3.1: #57 Coarse Aggregate Gradation.

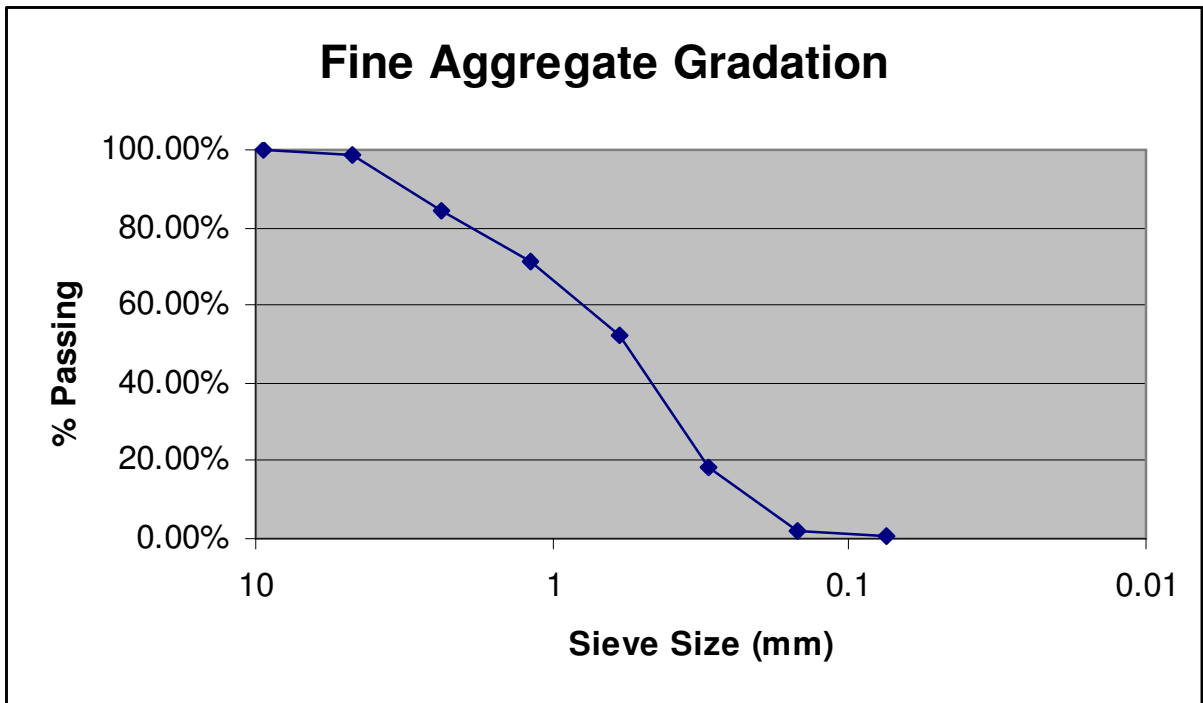


Figure 3.2: Fine Aggregate Gradation.

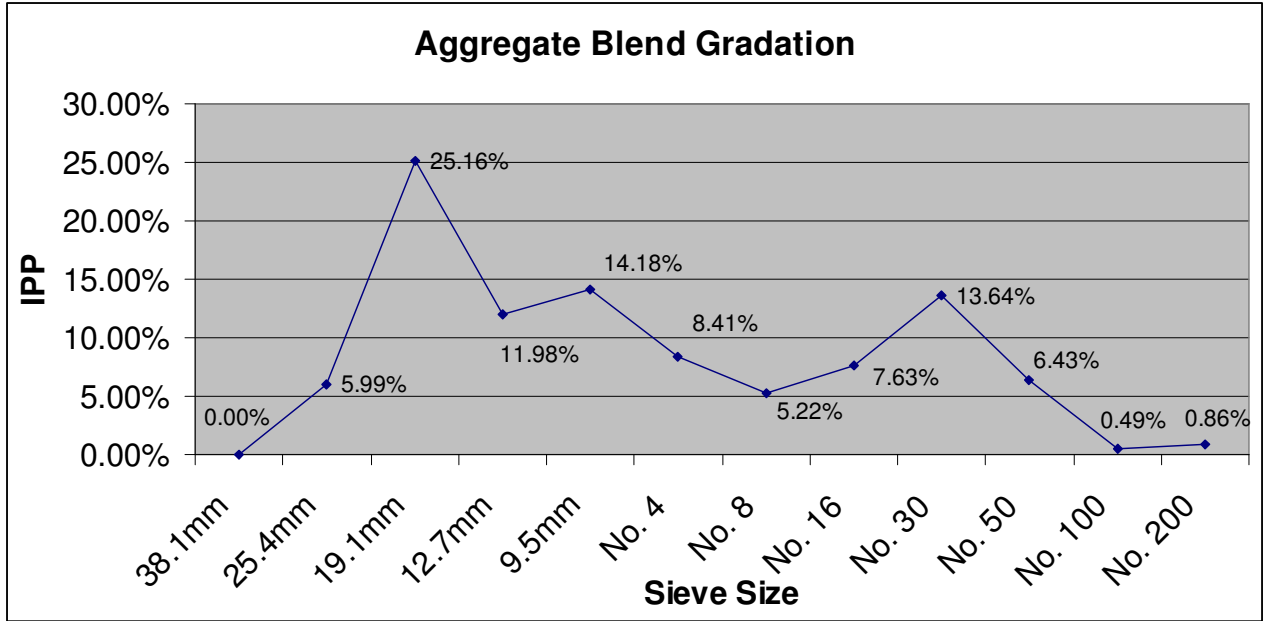


Figure 3.3: Mixture Design Aggregate Blend Gradation.

Table 3.2: Type I/II Portland Cement Physical and Chemical Properties

C ₃ S	55.30%
C ₂ S	15.30%
C ₃ A	6.90%
C ₄ AF	10.10%
Blaine Fineness (m ² /kg)	373
Autoclave Expansion	0.11%

3.2 Testing Plan

The testing plan, which is included in Appendix A, was prepared in order to develop a relationship between maturity and the rate at which concrete shrinkage occurs. To achieve this goal specific attention had to be paid to time and temperature, as these are two very important components in concrete maturity.

The first phase of testing attempted to determine the activation energy at early age through the determination of the setting times of the concrete mixture. To

achieve this, penetration testing was conducted according to ASTM C403. A total of four 15.24x15.24 centimeter (6x6 inch) cylinders of mortar were cast for each of three different curing temperatures of 4 °C, 23 °C, and 38 °C. One of each set of four cylinders contained an “i-button,” which is a temperature monitoring device that can be programmed to record temperature over a certain time interval within the concrete specimens. The specimens were sealed with a plastic cylinder cap and the penetration resistance was measured at various times.

The second phase of testing sought to calculate the activation energy of the concrete mixture at ages past final setting time. This was done by following the procedures laid forth in ASTM C1074 for estimating concrete compressive strength through the maturity method. A total of 60 10.2x20.4 centimeter (4x8 inch) cylinders were prepared. For each temperature (4 °C, 23 °C, and 38 °C), twenty cylinders were cast and two of these twenty were embedded with an i-button. The samples were then moist cured in water baths kept constant at each temperature. Compressive strength testing was conducted at time intervals that were based on the final setting time of the mixture. Time intervals were calculated by doubling the final setting time 7 times for each controlled temperature (4 °C, 23 °C, and 38 °C). Equation 3.1, shown below, demonstrates how time intervals were calculated.

$$t_n = t_{final\ set} \cdot 2^n \qquad \text{Equation 3.1}$$

The third phase of testing was to measure the free shrinkage of concrete over time at various temperature and relative humidity conditions. Length change

measurements were conducted based upon ASTM C157, the standard specification for measuring the length change of concrete. Five 7.62x7.62x28.58 centimeter (3x3x11.25 inch) concrete length change samples were prepared for each of the four different exposure conditions. These exposure conditions were 38 °C at 50% relative humidity (RH), 38 °C at 90% RH, 23 °C at 50% RH, and 23 °C at 90% RH. Each of these conditions was kept constant for the span of testing. The measurement of free shrinkage was conducted at final setting time and at 1, 2, 4, 7, 14, 21, and 28 days from mixing. The shrinkage specimens began exposure to temperature and humidity conditions at the final setting time that corresponded to either temperature.

The fourth phase was to evaluate the compressive strength of concrete at different ages and curing conditions. These curing conditions coincided with the shrinkage conditions outlined above in the third phase of testing (38 °C at 50% RH, 38 °C at 90% RH, 23 °C at 50% RH, and 23 °C at 90% RH). A total of 72 compressive strength cylinders were cast from the concrete mixture and exposed to the four different exposure conditions at final setting time. At ages of 1, 2, 4, 7, 14, and 28 days three of these specimens were tested for compressive strength using ASTM C39. This testing attempted to relate strength development and the amount of free shrinkage of concrete under the various exposure conditions.

Chapter 4: Experimental Results

4.1 Penetration Testing

The following results were obtained from the penetration testing at 4 °C, 23 °C, and 38 °C. Figure 4.1 presents a plot of the penetration resistance versus time for the various temperatures. Presented in Table 4.1 is the calculated setting times for each temperature, which were found by fitting a power curve to the penetration resistance versus time data and solving for the time it takes for concrete to develop 3.5 MPa (500 psi) of strength for initial set and 27.6 MPa (4000 psi) of strength for final set. As would be expected, based upon the maturity concept, the time it takes to achieve final setting time is longer for lower temperatures than for higher temperatures. This is because the rate of chemical reaction for the hydration reaction that causes concrete strength to develop is accelerated by an increase in temperature.

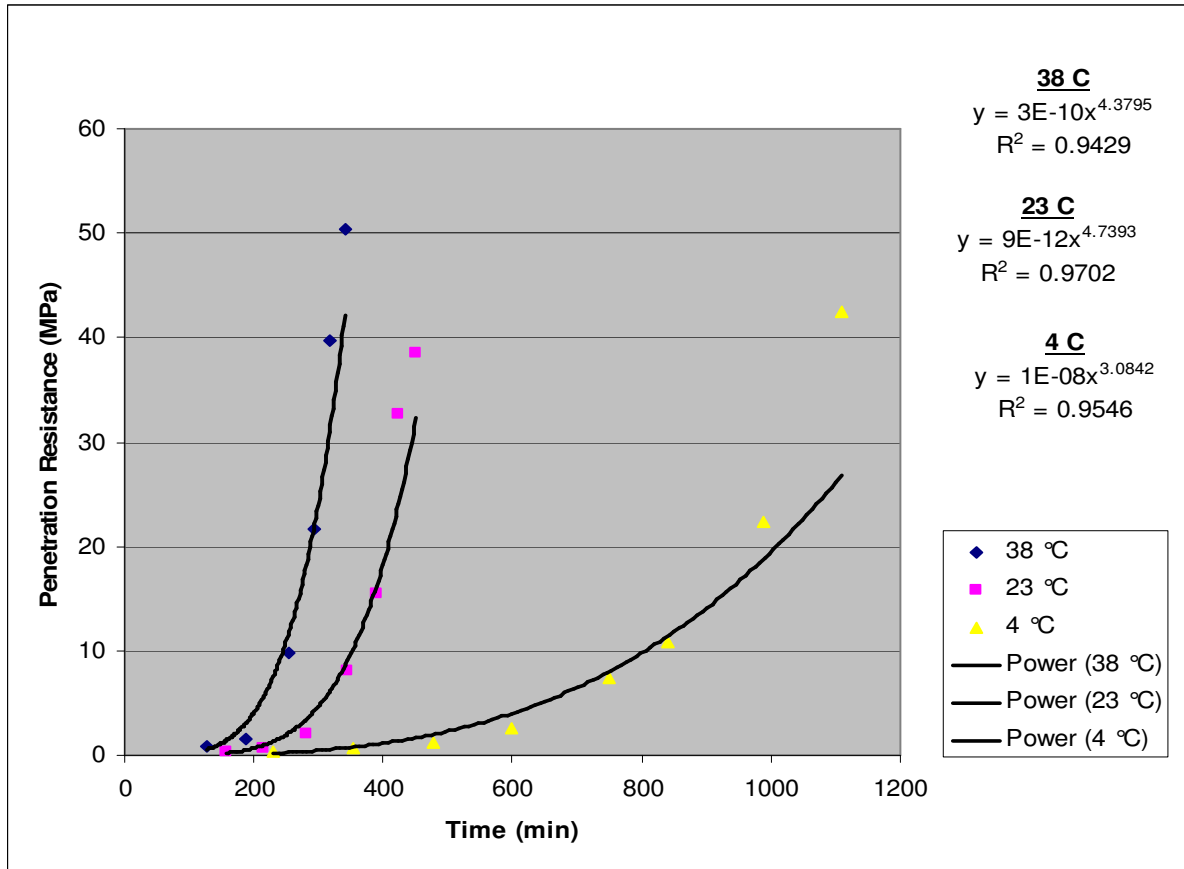


Figure 4.1: Penetration testing results for 4 °C, 23 °C, and 38 °C

Table 4.1: Setting times for 4 °C, 23 °C, and 38 °C

	Time (min)	
	Initial Set	Final Set
4 °C	570.17	1118.96
23 °C	281.15	436.00
38 °C	192.20	309.00

4.2 Fresh Concrete Properties

The fresh properties of the concrete are listed below in Table 4.2. These properties include air content, slump, and unit weight. The ambient air temperature

and the fresh concrete temperature during mixing are also included. The batch mixtures prepared during this investigation showed relatively good uniformity with only minimal fluctuations in fresh mixed properties.

Table 4.2: Concrete properties

Testing Exposure		Unit Weight (kg/m ³)	Air Content (%)	Slump (cm)	Temperature (°C)	
					Air	Concrete
Shrinkage Testing	23 °C and 50% RH	2418.06	2.9%	17.15	23	24
	23 °C and 90% RH	2433.51	2.7%	17.15	22	19
	38 °F and 50% RH	2426.99	2.4%	16.51	22	23
	38 °F and 90% RH	2412.54	2.9%	16.51	27	27
Activation Energy Testing	4 °C	2434.50	2.6%	16.51	24	26
	23 °C	2441.01	2.4%	17.78	24	21
	38 °C	2436.20	2.4%	17.15	26	28
Average		2428.97	2.6%	16.96	24	24

4.3 Compressive Strength for Activation Energy Calculations

To examine the impact of temperature on the rate of strength development for this concrete mixture, concrete samples were cast and kept under isothermal curing conditions at 4°C, 23°C, and 38°C. The final setting time relative to curing temperature was used to determine time intervals at which the concrete compressive strength would be measured. As mentioned previously in Chapter 3, these time intervals were determined by doubling the final setting time a total of seven times for each isothermal curing temperature. Because the rate of strength development is slowed by lower temperatures and accelerated by higher temperatures, using time intervals based upon final setting time ensures that strength samples cured at lower temperatures are allowed to develop a comparable percentage of strength as samples cured at higher temperatures. Tables 4.3, 4.4, and 4.5 show the average compressive strength with concrete age for 4°C, 23°C, and 38°C isothermal curing conditions,

respectively. Figure 4.2 demonstrates the plotted compressive strength versus concrete age as a function of time.

Table 4.3 Compressive strength for 4 °C

Age(Days)	Strength (MPa)
1.55	2.65
3.11	9.40
6.22	18.20
12.43	25.63
24.87	29.99
49.73	35.84
83.79	40.40

Table 4.4 Compressive strength for 23 °C

Age(Days)	Strength (MPa)
0.61	4.07
1.21	11.17
2.42	18.66
4.84	22.76
9.69	26.81
19.38	31.63
34.11	37.01

Table 4.5 Compressive strength for 38 °C

Age(Days)	Strength (MPa)
0.43	7.01
0.86	12.42
1.72	16.74
3.43	21.80
6.87	26.15
13.73	31.05
27.02	35.00

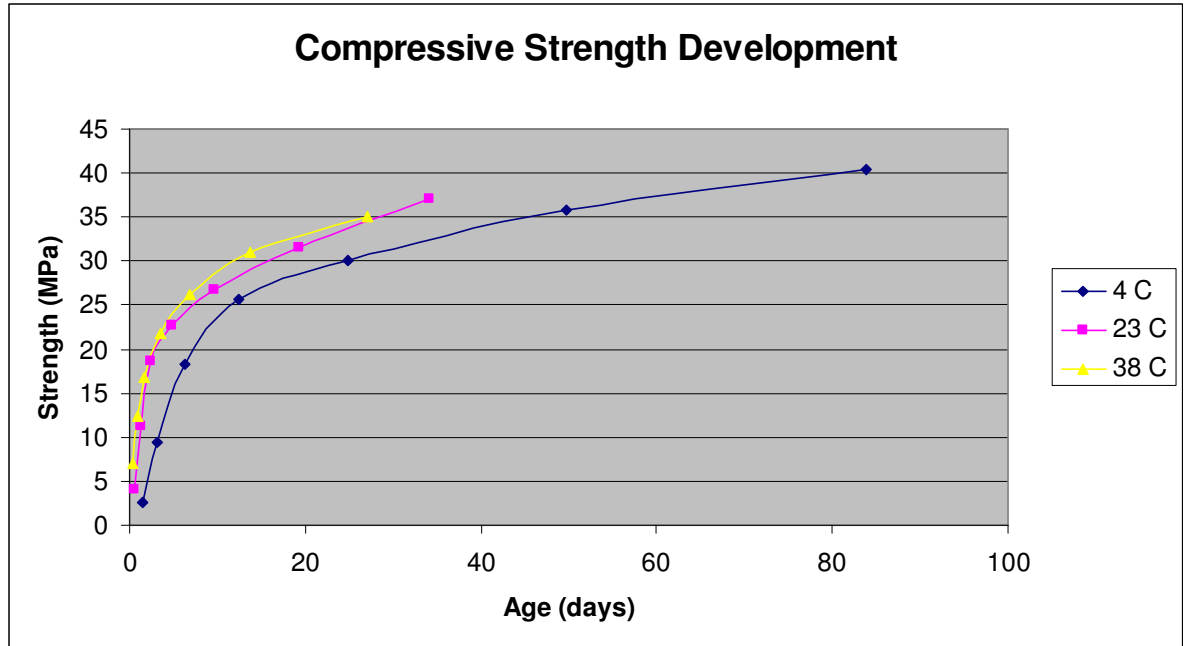


Figure 4.2: Compressive strength results for activation energy testing for 4 °C, 23 °C, and 38 °C

4.4 Monitoring of Temperatures

The effectiveness of maintaining isothermal temperature conditions was monitored using “i-buttons”. I-buttons are data logging temperature measuring devices that can be imbedded within the concrete. The measured temperatures at early ages are shown below in Figure 4.3. Each temperature profile is expected to develop an increase in temperature at early ages, in accord with the rate of concrete hydration, followed by a consistent temperature that demonstrates the isothermal curing conditions.

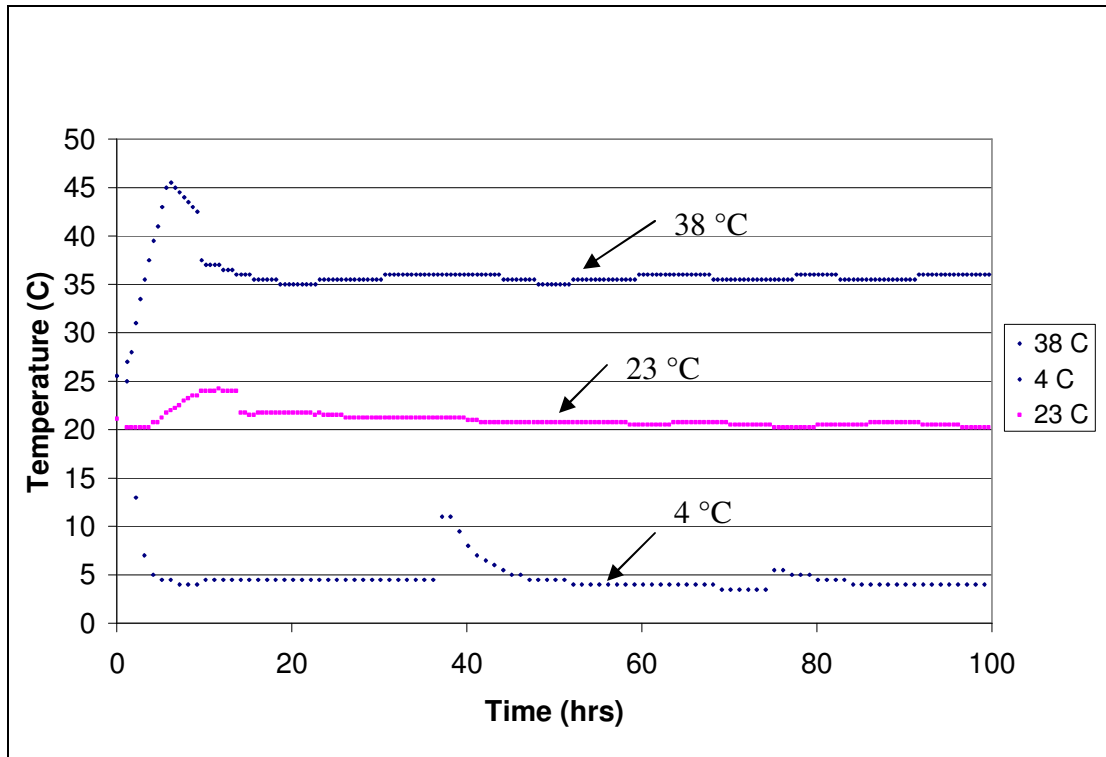


Figure 4.3: Monitoring of Isothermal Conditions at 4 °C, 23 °C, and 38 °C

4.5 Shrinkage Testing

Shrinkage measurements were collected for length change specimens at regular intervals of 1, 2, 4, 7, 14, 21, and 28 days. The initial shrinkage measurement was taken at the final setting time for each set of samples. Four sets of samples were prepared and kept at two temperatures, 23 °C and 38 °C, and two relative humidities of 50% and 90%. Early age shrinkage measurements did not have enough strength to withstand mold extrusion. In order to minimize variation, measurements at 4, 7, 14, 21, and 28 days were used. Table 4.6 contains the measured shrinkage data for all of the curing conditions.

Table 4.6: Shrinkage measurements

23 °C and 50% RH		38 °C and 50% RH	
Age Past T _o (Days)	Shrinkage (mm/mm)	Age Past T _o (Days)	Shrinkage (mm/mm)
0	0	0	0
3.71	0.0024	3.79	0.001
6.71	0.0122	6.79	0.0115
13.71	0.0198	13.79	0.0175
20.71	0.0218	20.79	0.0182
27.71	0.0212	27.79	0.0202
23 °C and 90% RH		38 °C and 90% RH	
Age Past T _o (Days)	Shrinkage (mm/mm)	Age Past T _o (Days)	Shrinkage (mm/mm)
0	0	0	0
3.71	0.0002	3.79	0.0002
6.71	0.0026	6.79	0.0028
13.71	0.0038	13.79	0.0048
20.71	0.006	20.79	0.005
27.71	0.0054	27.79	0.0052

Figure 4.4, shown below, shows the free shrinkage measurements for all of the temperature and humidity conditions for comparison. As expected, the samples exposed to higher relative humidity demonstrate less shrinkage than the samples exposed to lower relative humidity levels. More importantly, temperature appears to only have a slight effect on the shrinkage measurements found for samples cured at 50% relative humidity. It appears that temperature slightly reduces shrinkage for 50% relative humidity and has virtually no effect on the 90% relative humidity samples. In an article on accelerated curing, researchers found that exposing shrinkage samples to high early age temperatures caused more macropores to form in place of micropores (Myers, 2006). In turn, less shrinkage occurs because less capillary pressures can be developed in the micropores. The variation in shrinkage measurements is much more pronounced at 50% relative humidity than at 90% relative humidity because the drier conditions cause a greater amount of shrinkage.

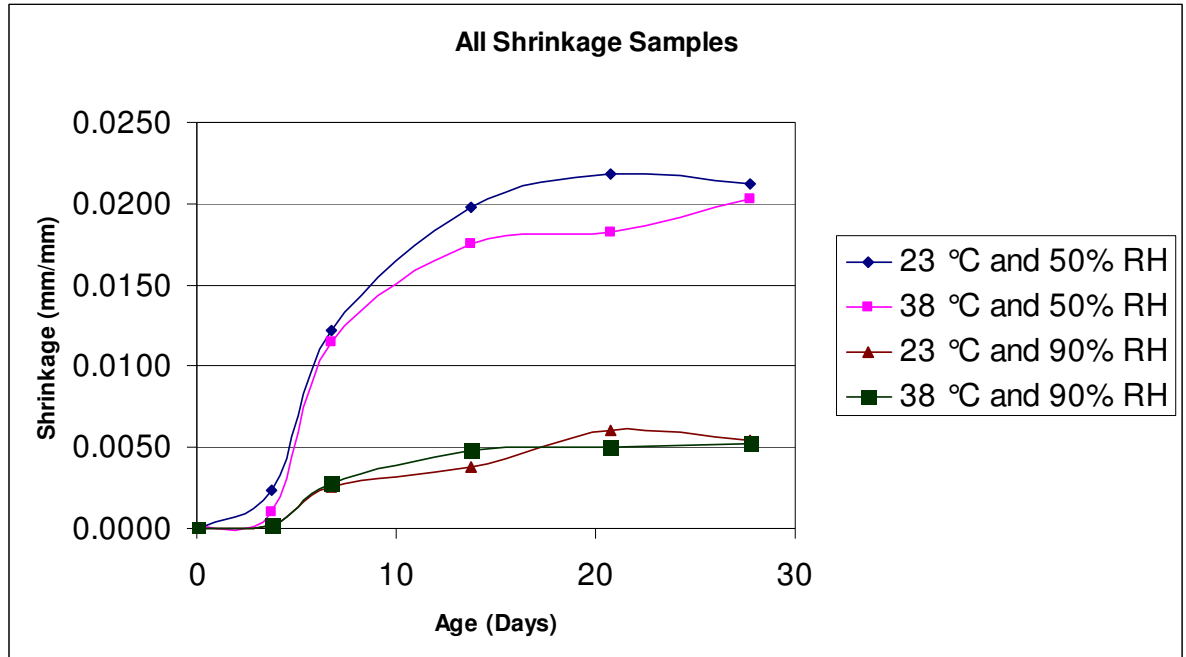


Figure 4.4: Shrinkage results for all temperature and humidity conditions

4.6 Compressive Strength Results at Isothermal Conditions

The strength development with age for the isothermal conditions was monitored by exposing concrete samples to the same curing conditions as the shrinkage samples, and measuring their compressive strength at 1, 2, 4, 7, 14, and 28 day age intervals. The results of the compressive strength testing are shown in Table 4.7 and the results are plotted versus time in Figure 4.5. Figure 4.6 demonstrates the strength development at early ages in better detail.

Table 4.7: Compressive Strength Results for Shrinkage Conditioned Samples

Age (days)	Strength (MPa)			
	23 °C at 50% RH	23 °C at 90% RH	38 °C at 50% RH	38 °C at 90% RH
1	9.10	8.75	10.73	12.34
2	13.37	13.81	13.70	16.55
4	18.10	18.93	16.74	18.49
7	20.19	20.52	17.19	21.53
14	22.18	24.86	17.99	25.11
28	22.56	26.97	17.97	27.07

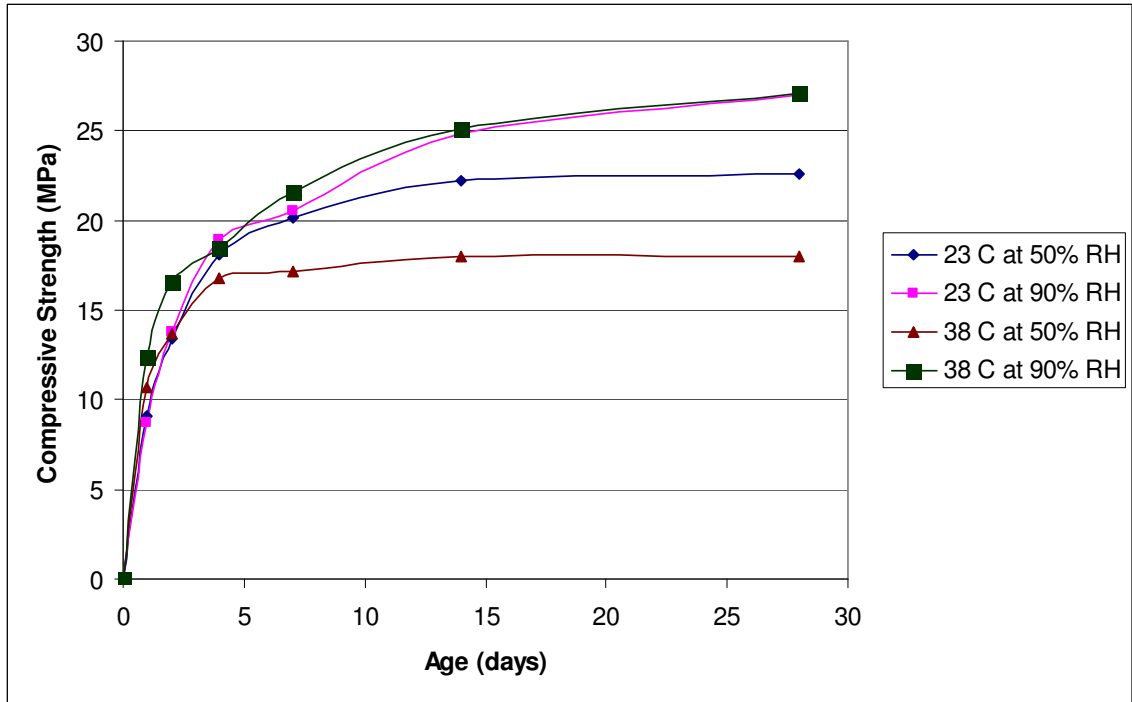


Figure 4.5: Compressive Strength Results for Shrinkage Conditioned Samples

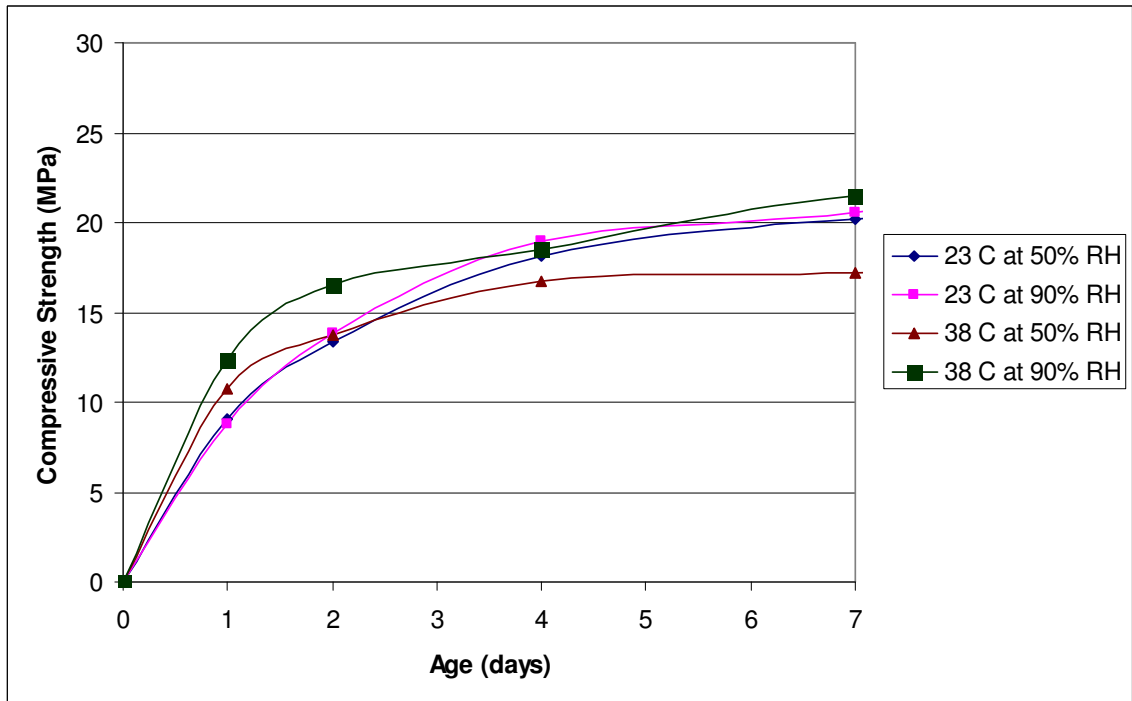


Figure 4.6: Compressive Strength Results for Shrinkage Conditioned Samples at early ages.

Based upon the compressive strength results several observations can be made. It appears that the temperature crossover effect occurred for both humidity conditions; also, for both instances of relative humidity, the higher temperature samples develop strength at a faster rate at earlier ages than the lower temperature strength samples. This is in agreement with established maturity principles. This leads to less ultimate strength for concrete samples cured at higher temperatures than for samples cured at lower temperatures despite faster rate of strength development at early ages.

Figures 4.5 and 4.6 also show that relative humidity can have a significant impact on the development of compressive strength. It appears after only 3 days the compressive strengths samples start to diverge from one another. The high temperature-low relative humidity samples develop the least strength, while both high humidity samples appear to develop approximately the same strength. The reduced relative humidity causes the samples to dry out and lose free moisture. This free moisture is necessary for the hydration reaction to continue efficiently. The higher humidity samples experienced less drying than the lower humidity samples, and therefore their strength development continued less impeded.

Chapter 5: Discussion of Results

5.1 Determination of Activation Energy

5.1.1 Penetration Data and Activation Energy Determination

Activation energies were calculated based upon the penetration testing results conducted at 4 °C, 23 °C, and 38 °C. In a study by Pinto and Hoover it was shown that the rate of strength development of penetration samples cured under various temperature conditions can be used to predict early age activation energy values using the penetration resistance results (Hoover and Pinto, 1999). Penetration resistance testing followed the procedures outlined in ASTM 403, where mortar mixtures are prepared and strength measurements based upon penetration are taken at various time intervals until 27.6 MPa (4000 psi) of strength has been measured. Mortar mixtures were prepared with a fine aggregate-to-cement ratio that matched the coarse aggregate-to-cement ratio from the concrete mixture used in this study. The fine aggregate percentage was altered to ensure that the amount of cement paste and the aggregate skeleton used during penetration testing of the mortar mixture closely represented the paste and skeleton structure that would be found in the concrete mixture.

For this study, the time intervals between mixing and initial set, initial set and final set, and mixing and final set were calculated and the natural log of the inverse of those time intervals were determined. The natural log of the inverse of the time intervals is comparable to the rate of reaction, “k value”, used to calculate activation energy from compressive strength testing. This natural log of the inverse of the time

intervals, therefore, demonstrates the rate at which the mortar specimens achieved a certain level of strength. For this study, these time intervals were analyzed to attempt to isolate ages in strength development where the chemical hydration reaction was occurring at different rates. The activation energy based upon penetration resistance data was determined by finding the best-fit slope between the independent variable, which was the inverse of temperature in Kelvin, and the dependent variable which was the natural log of the inverse of each time interval. Three activation energies were thus determined-- $E_{a\text{-initial}}=23,181.72$ J/mol, $E_{a\text{-final}}=27,591.89$ J/mol, and $E_{a\text{-}(final\text{-}initial)}=33,374.47$ J/mol--and represent the slope of the rate of chemical hydration occurring at these time intervals. The plotted best fit lines of the data for each time interval are shown in Figures 5.1, 5.2, and 5.3.

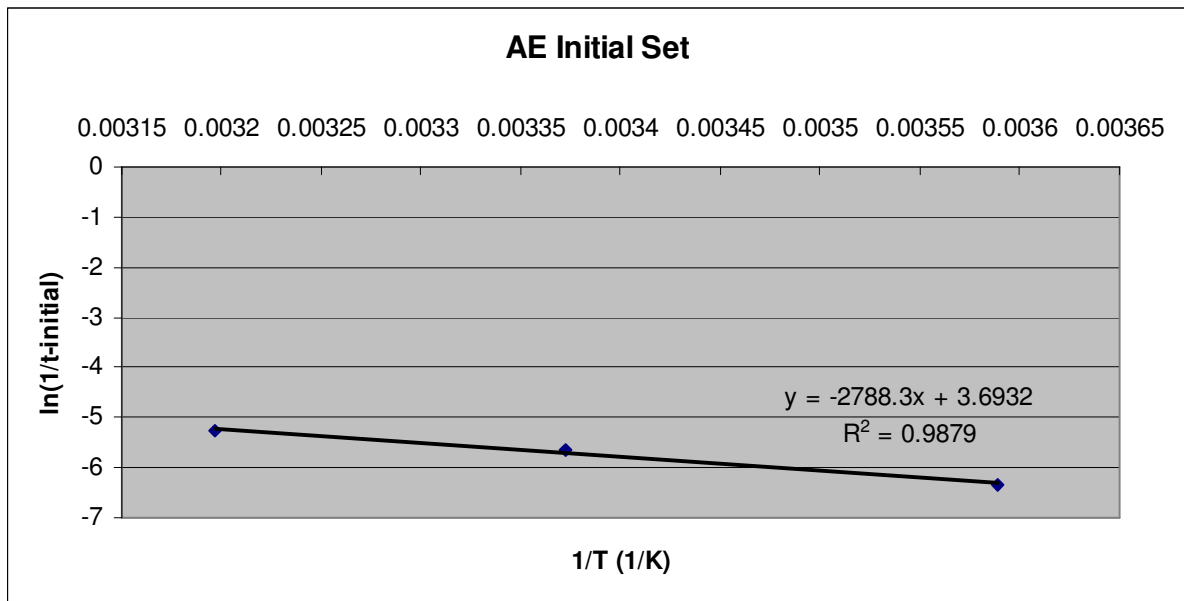


Figure 5.1: AE Determination Based Upon Penetration Data-Mixing to Initial Set

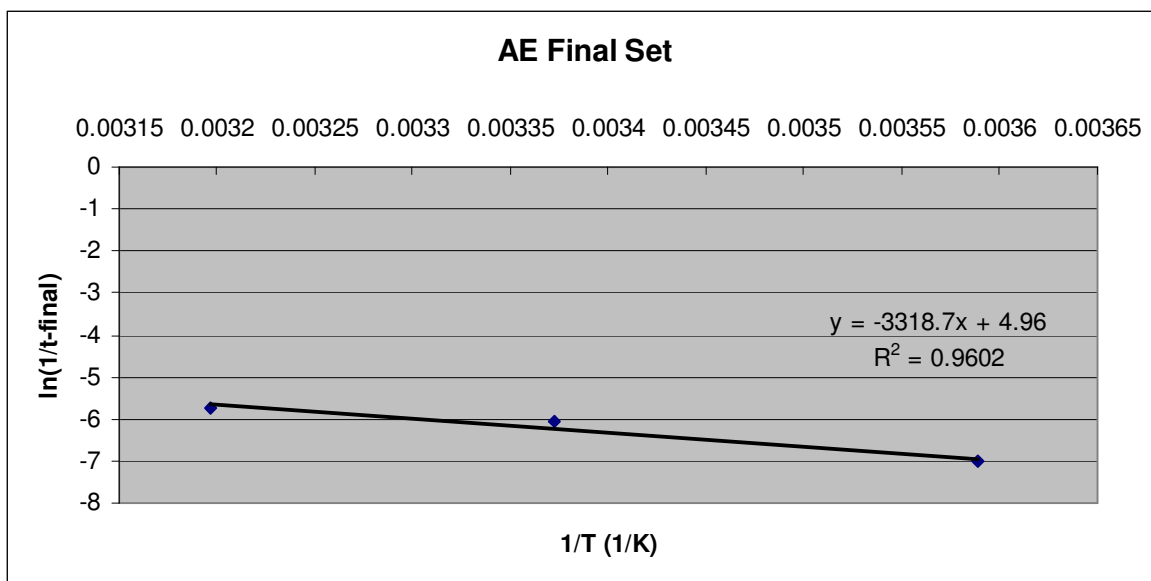


Figure 5.2 AE Determination Based Upon Penetration Data-Mixing to Final Set

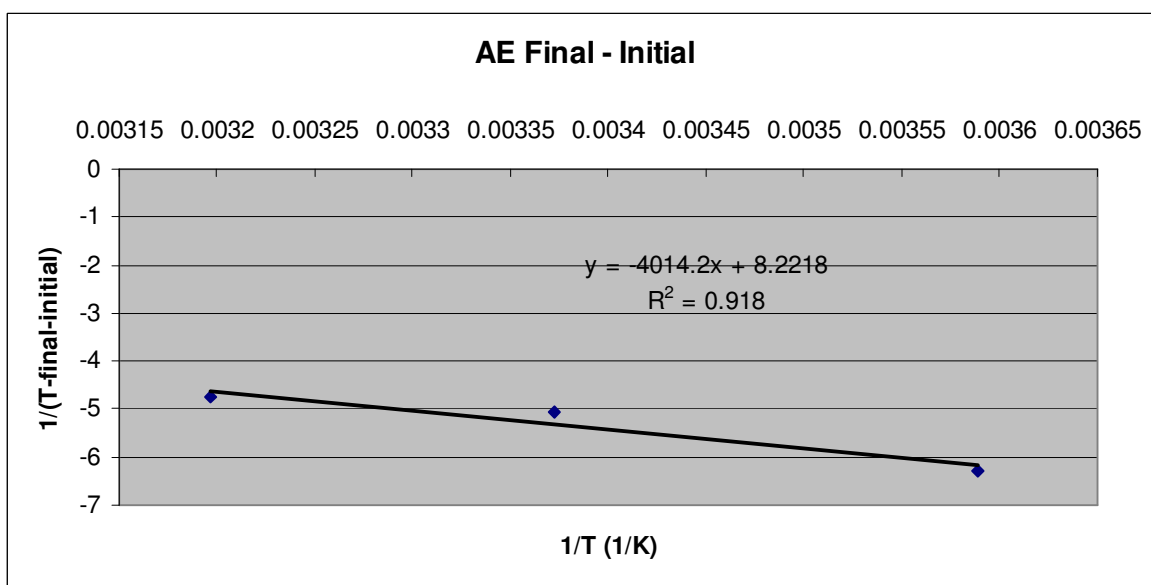


Figure 5.3: AE Determination Based Upon Penetration Data-Initial Set to Final Set

Activation energy is defined as the energy that must be overcome for a chemical reaction to occur. The value of activation energy is directly related to the rate at which a chemical reaction progresses based upon the Arrhenius equation. Equation 5.1, shows the Arrhenius equation. Notice that mathematically the rate of chemical reaction, k , must increase as the value of activation energy increases.

$$k = Ae^{-\frac{E_a}{RT}} \quad \text{Equation 5.1: Arrhenius's Equation}$$

Where:

A = Pre-Exponential Factor
 E_a = Activation Energy (J/mol)
 R = Universal Gas Constant (-8.314 J/K* mol)
 T = Temperature (K)
 k = rate of chemical reaction

The calculated activation energy values of $E_{a\text{-initial}}=23,181.72$ J/mol, $E_{a\text{-final}}=27,591.89$ J/mol, and $E_{a\text{-(final-initial)}}=33,374.47$ J/mol demonstrate an expected trend that the hydration reaction progresses slower at the very early phases of strength development (between mixing and initial set) and accelerates as the rate of strength development increases during penetration testing (between initial set and final set). Notice that the value of activation energy calculated from the penetration testing is higher between initial and final setting time than between mixing and initial setting time. The calculated value of activation energy between mixing and final set is less than the activation energy calculated for the time between initial set and final set, but more than the value of activation energy for time between mixing to initial set. This is because the value of activation energy between mixing and final set summarizes the rate of reaction for both time intervals (mixing to initial and initial to final). Therefore, the value of activation energy for mixing to final set should be between the two other activation energy values.

Past research has found activation energy values at early stages of hydration to be from 33.5 to 47 kJ/mol (Hoover and Pinto, 1999). This is in agreement with the calculated activation energy between initial and final set where $E_a=33,374.47$ J/mol.

However, the value of activation energy between mixing and initial set appears to be low.

During penetration testing, a higher volume of fine aggregate was used to more closely represent the aggregate proportioning found in a concrete mixture. In the Pinto and Hoover study, penetration testing was conducted using sieved concrete (Hoover and Pinto, 1999). Therefore, the mortar mixture tested by Pinto and Hoover did not have the same aggregate content as the mixture tested for this study. A higher aggregate content will cause strengths to be lower for mortar samples because the mortar structure would have more weak interfaces between the aggregate and cement paste. In turn, the time required to achieve the strength required for initial and final set would increase and would therefore represent a slower rate of reaction. This slower rate of reaction would lead to the calculation of lower values of activation energy.

5.1.2 Strength Data Activation Energy Determination

Activation Energies were determined using several analysis methods. Activation energies were first found using the three different procedures from ASTM 1074. The first analysis method, described in subsection A1.1.7, uses linear regression to find the best-fit line of the reciprocal of time beyond the final setting time and the reciprocal of strength values for each isothermal curing temperature (4 °C, 23 °C, and 38 °C). Based upon this method, t_0 is assumed to be equal to final setting time, where significant strength development begins. From each best-fit straight line, the intercept is divided by the slope to generate a k-value for each

temperature. To calculate activation energy, the slope of the best-fit line between the calculated k-values and each curing temperature is multiplied by the Universal Gas Constant, R. Using the method outlined in A1.1.7, the activation energy was found to be approximately 79,219 J/mol. ASTM 1074 states that activation energy values for normal strength concrete mixtures should be between 40,000 and 45,000 J/mol. Therefore, the value of activation energy using subsection A1.1.7 was considered unrealistic.

The next analysis method found within ASTM 1074 as detailed by subsection A1.1.8 states that activation energy can also be determined two additional ways. First, activation energy can be found either by fitting the strength versus time data using a computer program to equation 5.2, shown below, to calculate k-values for each isothermal curing temperature. To calculate activation energy, the slope of the best-fit line between the calculated k-values and each curing temperature is multiplied by the Universal Gas Constant, R. Using the best fit equation the activation energy was found to be equal to approximately 27,135 J/mol.

$$S = S_u \frac{k(t-t_0)}{1+k(t-t_0)} \quad \text{Equation 5.2}$$

Where:

S = average compressive strength at age t

t = test age

S_u = limiting strength

t₀ = age when strength development is assumed to begin

k = the rate constant

The second method outlined by ASTM 1074 subsection A.1.1.8 uses several analysis steps to approximate the best fit results to Equation 5.2 without using

computer software. Using the last four test ages, the reciprocal of strength versus the reciprocal of age is plotted and the y-axis intercept is found for each curing temperature. The inverse of these intercepts is assumed to be equal to the limiting strength S_u for each temperature. Next, for each curing temperature, the value of A was computed using equation 5.3, for the strength values from the first four test ages. The slope of the A values plotted versus age is equal to the k-values. To calculate activation energy, the slope of the best-fit line between the calculated k-values and each curing temperature was multiplied by the Universal Gas Constant, R. Using this analysis method, the activation energy was found to be approximately 25,944 J/mol, which is very close to the activation energy found by fitting equation 5.2 with computer software.

$$A = \frac{S}{S_u - S} \qquad \text{Equation 5.3}$$

In addition to the methods outlined by ASTM 1074, modifications to the curve fitting procedure found in subsection A1.1.8 were used to determine activation energy. Based upon research by Carrino and the analysis methods found in ASTM 1074, the time when significant strength development begins can be assumed to be the final setting time (Carrino 2003). Therefore, part of the analysis in this study used final setting time as t_0 for calculation of activation energy. Furthermore, the maturity concept and activation energy has been found to be more applicable for early ages of concrete hydration. Therefore, activation energy was also determined by limiting the test data from seven strength measurements to the first six early age strength

measurements. For example, to isolate the early ages of strength development at 38 °C the first six compressive strength results were analyzed at 0.43, 0.86, 1.72, 3.43, 6.87, 13.73 days, but not the seventh measurement at 27.02 days. Curve fitting was used with the following scenarios:

- All data points are used and t_0 =final set
- Six data points are used and t_0 =final set
- All data points are used but t_0 =final set only for the 38 °C sample sets
- Six data points are used and t_0 =final set only for the 38 °C data sets

Based upon the different methods of analysis, Table 5.1 presents the calculated activation energy values.

Table 5.1: Activation energy calculated by various analysis techniques.

Method	Activation Energy (J/mol)
ASTM 1074 A1.1.7	79218.84
ASTM 1074 A1.1.8 Curve Fit	27135.18
ASTM 1074 A1.1.8 Step based Method	25944.35
All Data and t_0 =Final Set	40287.96
6 Data Points and t_0 =Final Set	43182.17
All Data and t_0 =final Set 38 °C	38594.71
6 Data Points and t_0 =Final Set 38 °C	39840.37

5.1.3 Analysis of Calculated Activation Energies

Based upon the research conducted by Carrino in the area of concrete maturity, activation energy should show both a convergence of strength data when plotted against its equivalent age, as well as very close convergence into a single curve when the ratio of Strength/Limiting Strength is plotted versus equivalent age (Carrino 2003). A “control set” of activation energy data from a past University of Maryland study has previously assessed the activation energy for this concrete

mixture and used the results to incorporate the concrete maturity method (Upadhyaya 2008). Shown in Figures 5.4 and 5.5 are the results of a control set of concrete maturity data. Notice that at early ages the strength data plotted versus equivalent age is fairly consistent for the first four days and then diverges as age increases in Figure 5.4. Furthermore, Figure 5.5 demonstrates a good agreement between data points for equivalent age versus the degree of strength development S/S_u . Thus, it is expected that the data from this study should also exhibit the same age characteristics.

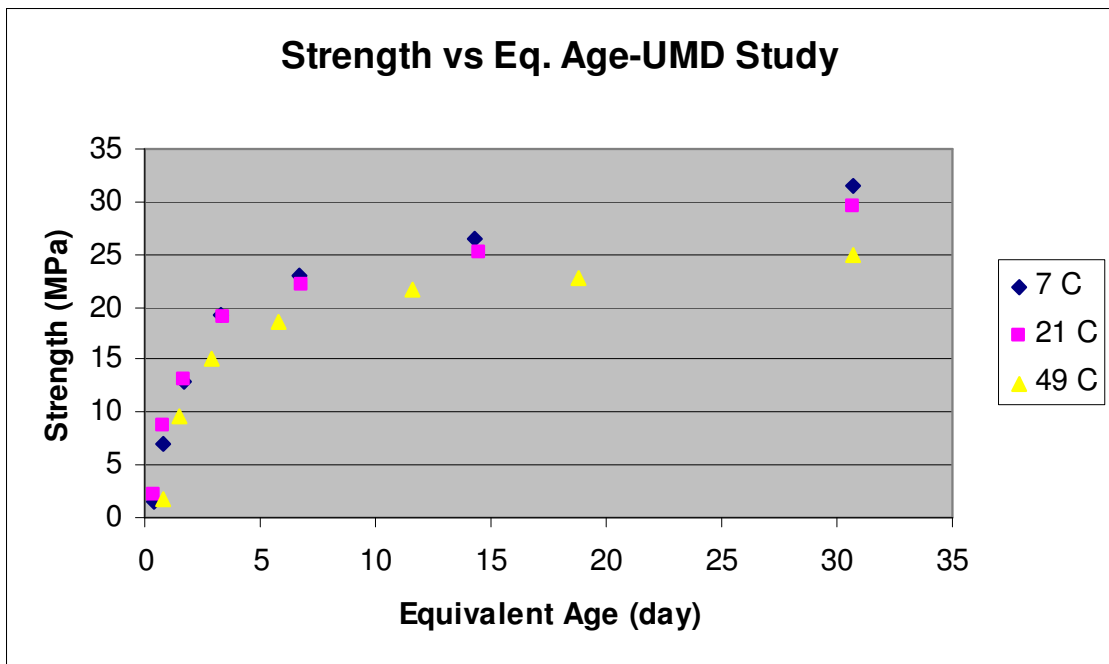


Figure 5.4: Strength values plotted versus equivalent age (Upadhyaya 2008).

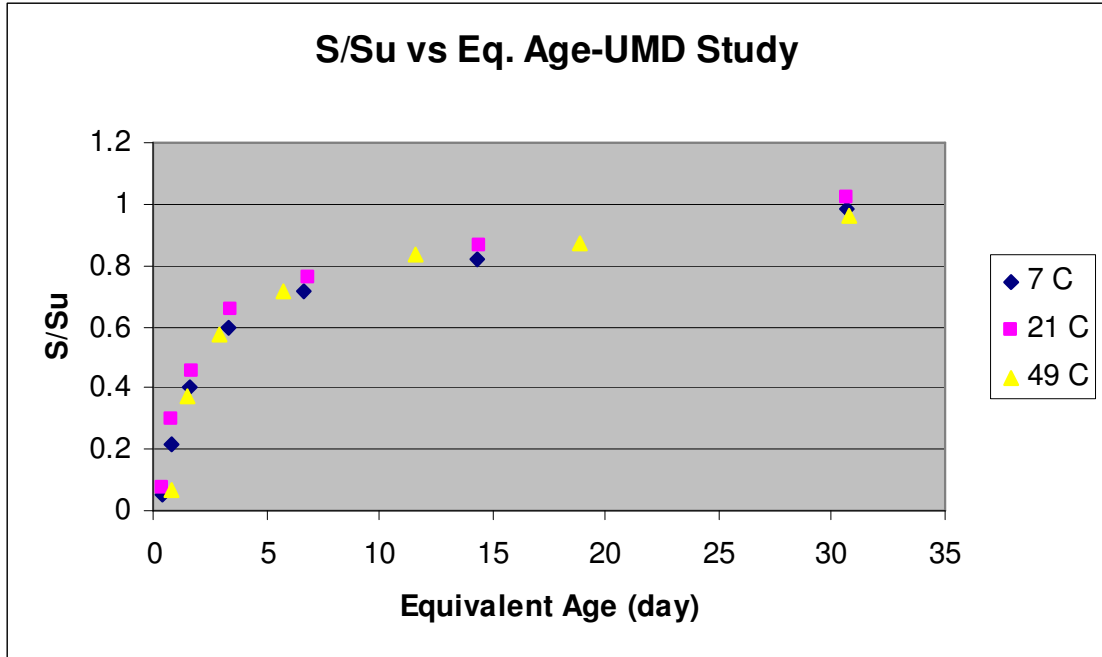


Figure 5.5: Control strength/limiting strength versus equivalent age (Upadhyaya 2008).

As previously mentioned, the activation energy found using the method outlined by ASTM 1074 subsection A1.1.7 was found to be 79,218.84 J/mol, which is unreasonable for the concrete mixture of this study. Similarly, ASTM 1074 subsection A1.1.8 recommended using the curve fitting method to Equation 5.2 with computer software. Therefore, the activation energy from A1.1.8 of 27,135 J/mol was analyzed based upon its summary of strength relationships versus equivalent age. Clearly, for activation energy to be representative of the concrete mixture in this study it must show a convergence of both strength data versus equivalent age, in addition to the ratio of strength divided by limiting strength plotted versus equivalent age. These plots for various analyses are shown below in Figures 5.6 through 5.15.

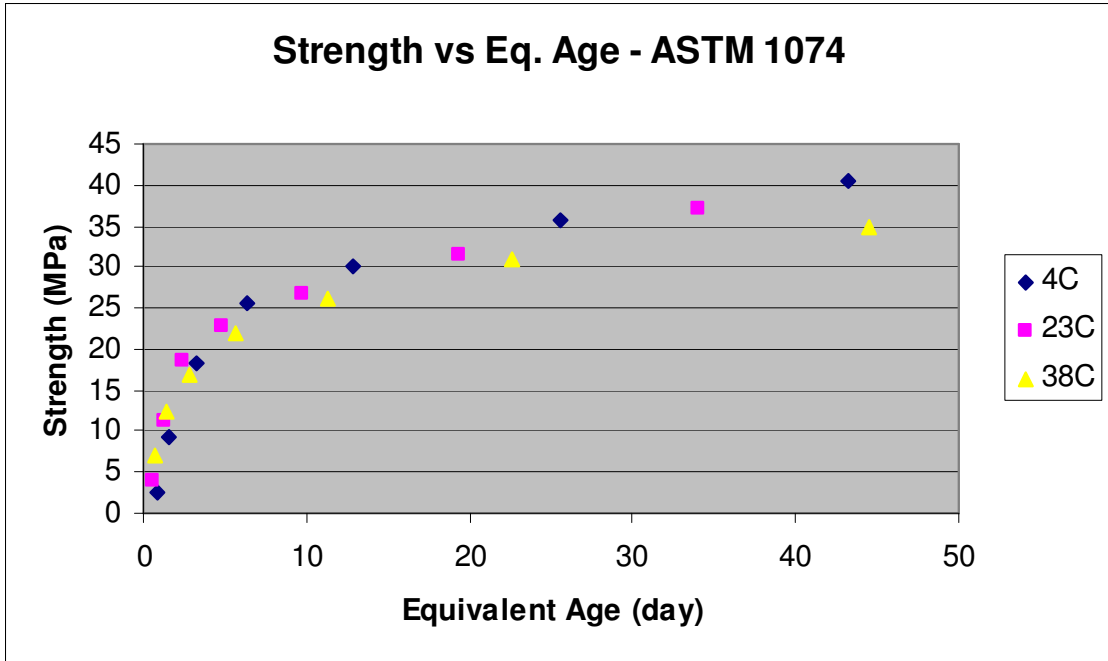


Figure 5.6: AE from ASTM 1074-A1.1.8. Activation Energy = 27,135.18 J/mol.

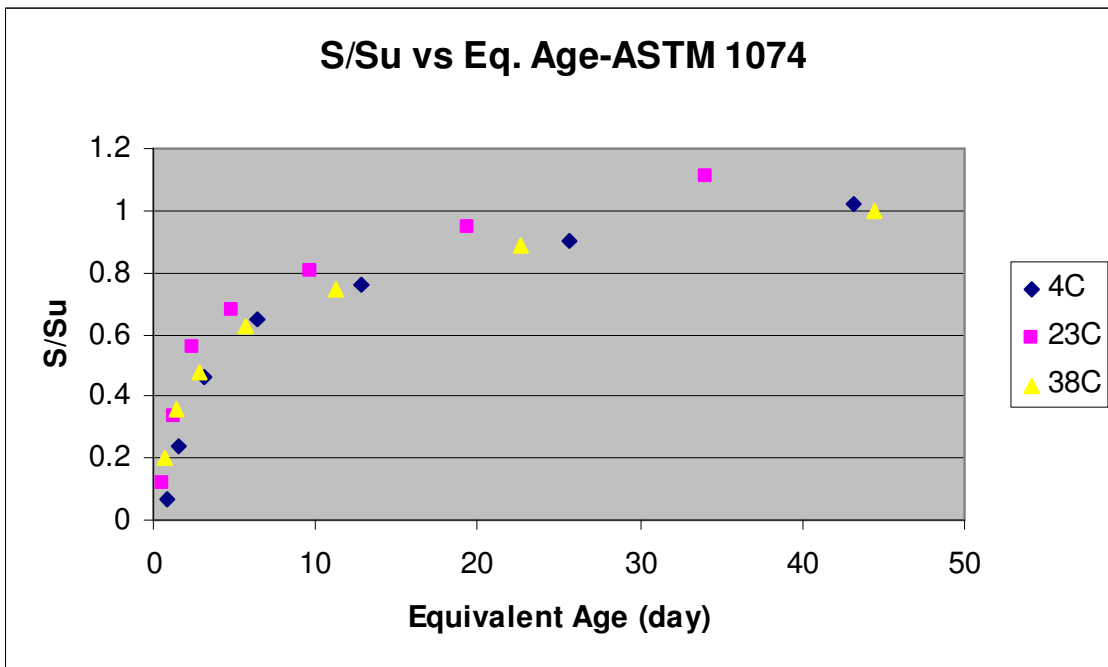


Figure 5.7: AE from ASTM 1074-A1.1.8. Activation Energy = 27,135.18 J/mol.

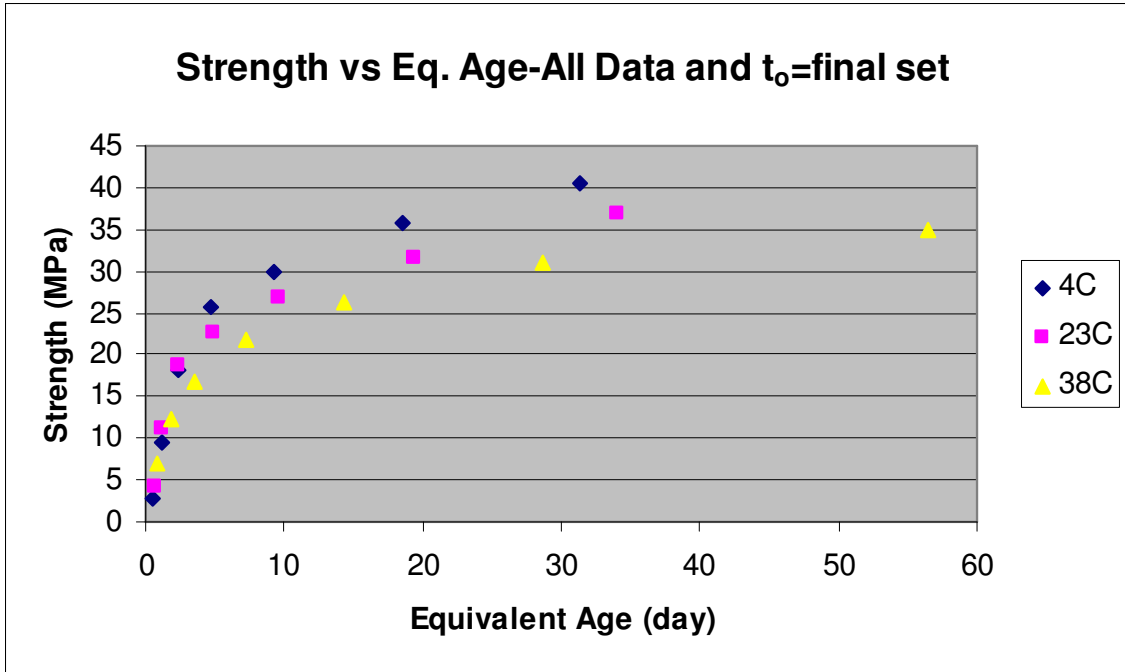


Figure 5.8: All Data with t_0 = final setting time. Activation Energy = 40287.96 J/mol.

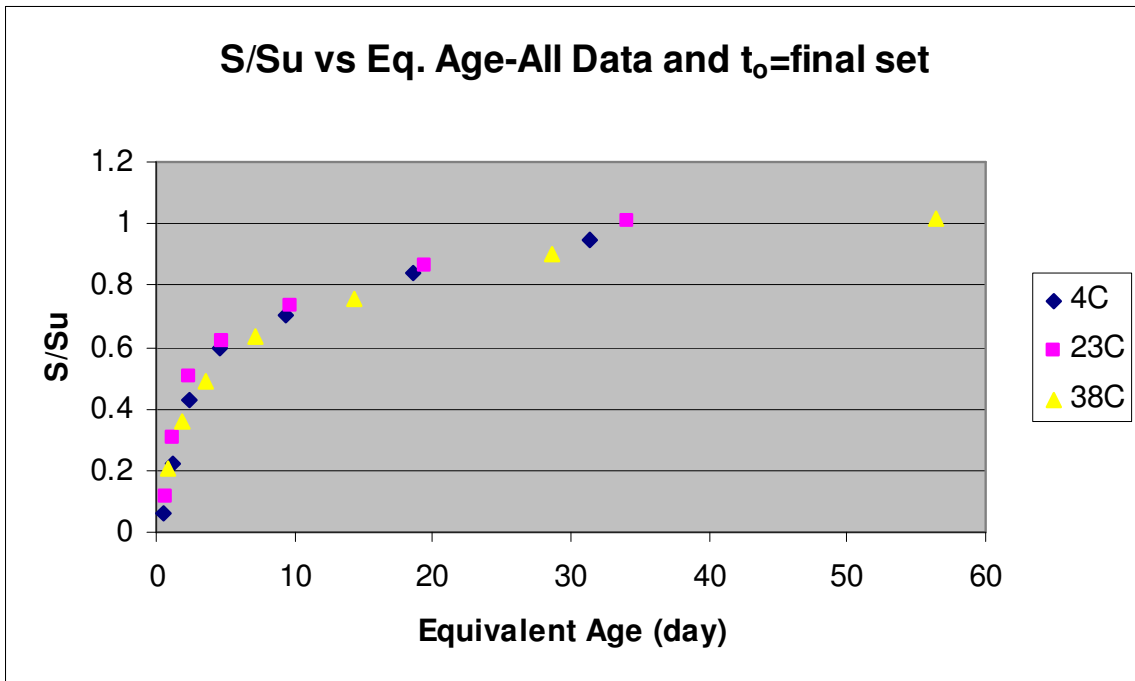


Figure 5.9: All Data with t_0 = final setting time. Activation Energy = 40287.96 J/mol.

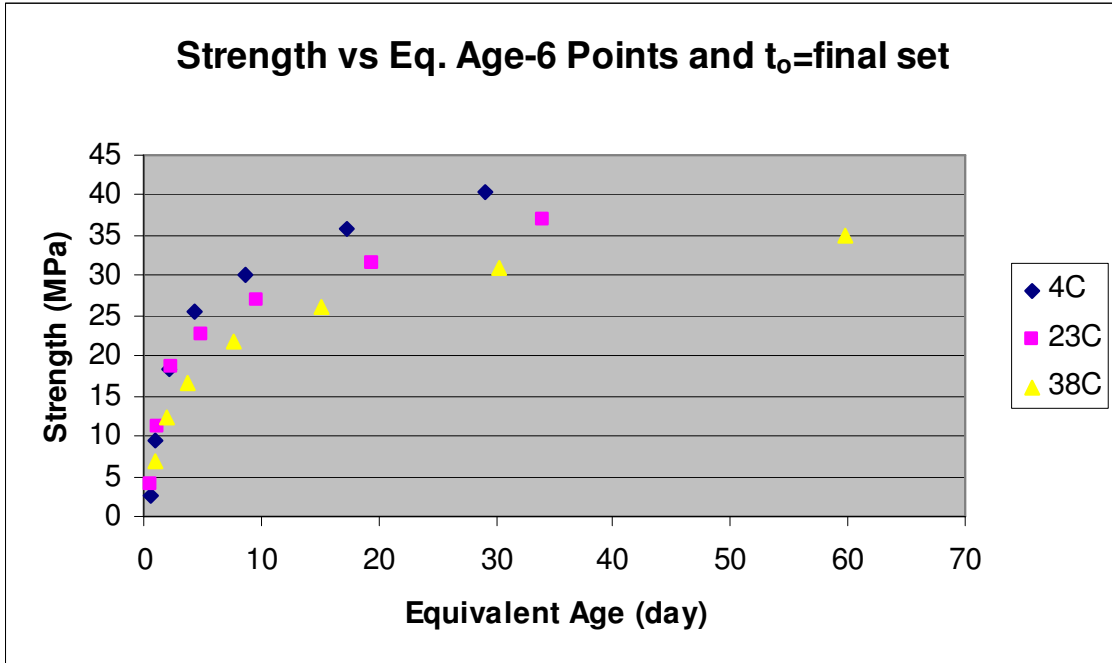


Figure 5.10: Six data points and t_0 = final setting time. Activation Energy = 43182.17 J/mol.

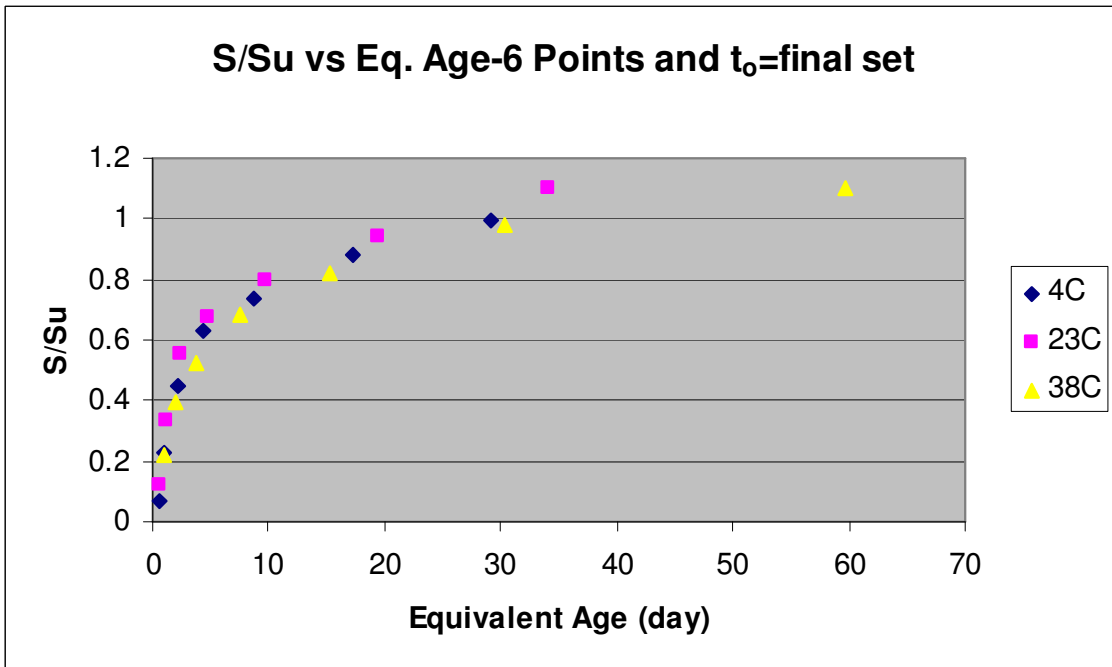


Figure 5.11: Six data points and t_0 = final setting time. Activation Energy = 43182.17 J/mol.

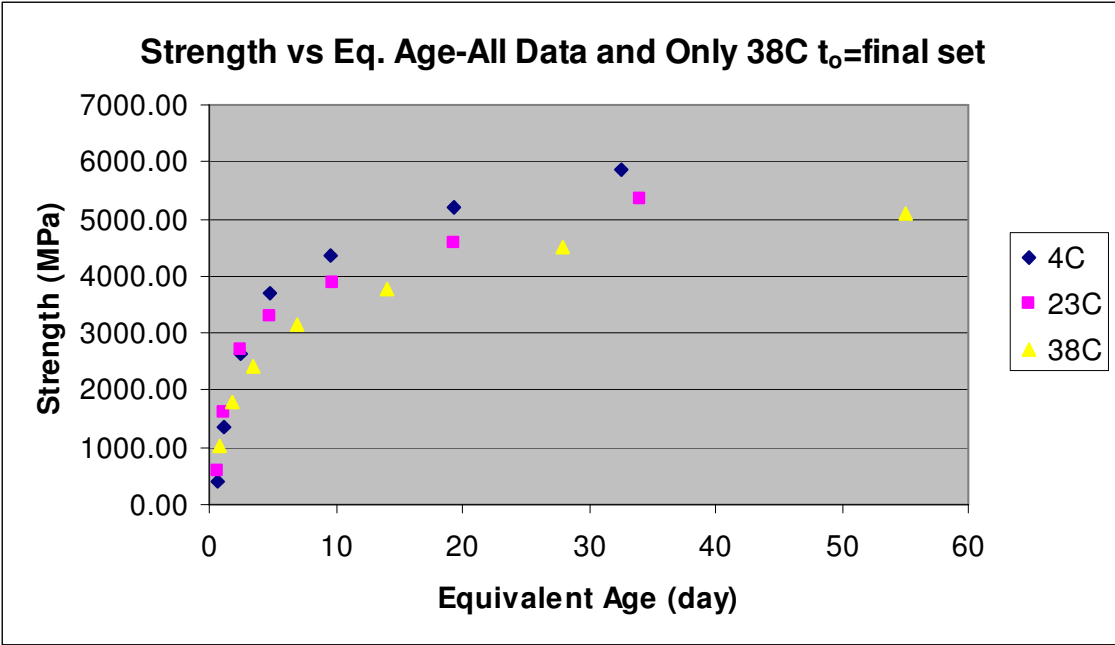


Figure 5.12: All data with t_0 = final setting for 38 °C data. Activation Energy = 38594.71 J/mol.

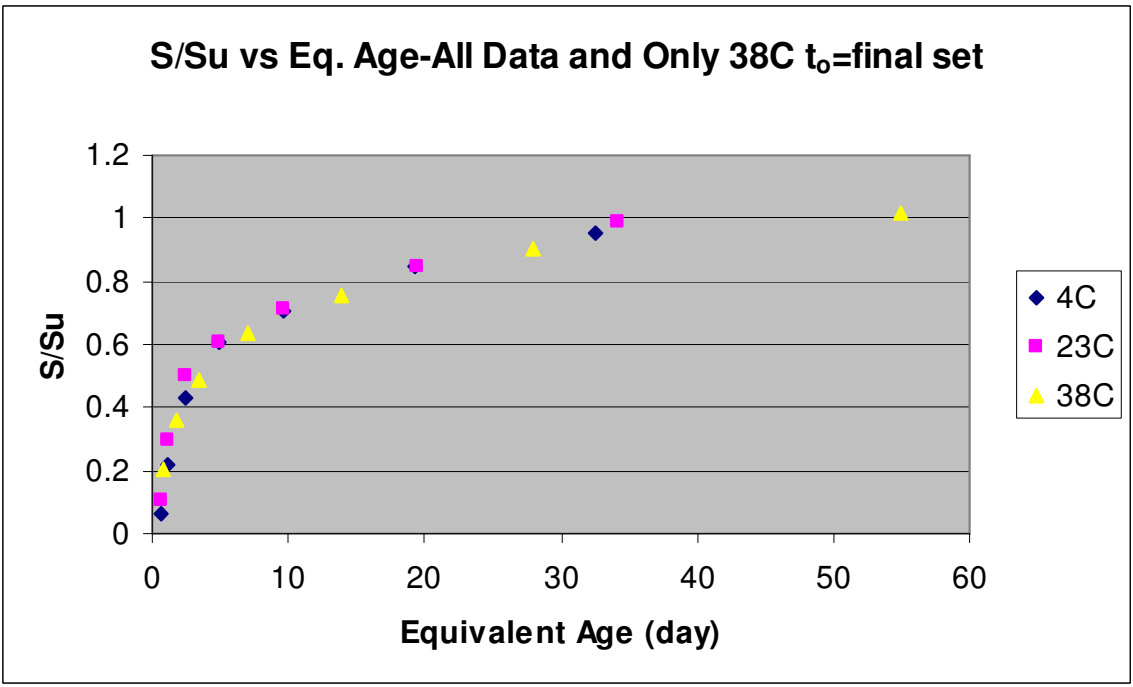


Figure 5.13: All data with t_0 = final setting for 38 °C data. Activation Energy = 38594.71 J/mol.

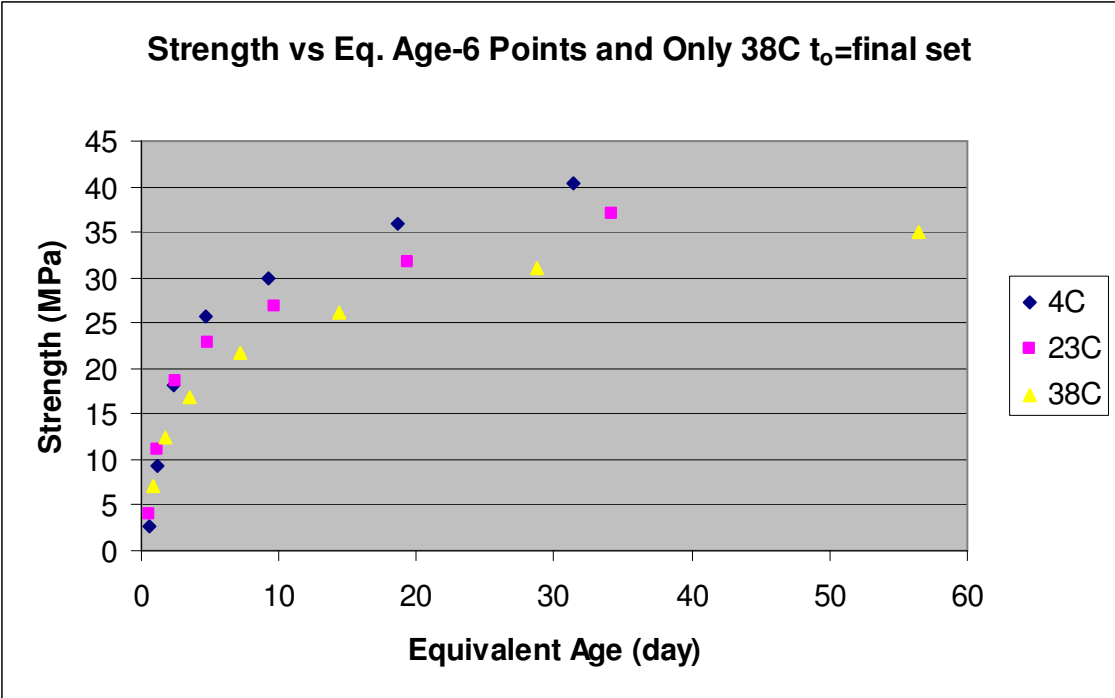


Figure 5.14: Six data points and t_o =final setting time for 38 °C data. Activation Energy = 39840.37 J/mol.

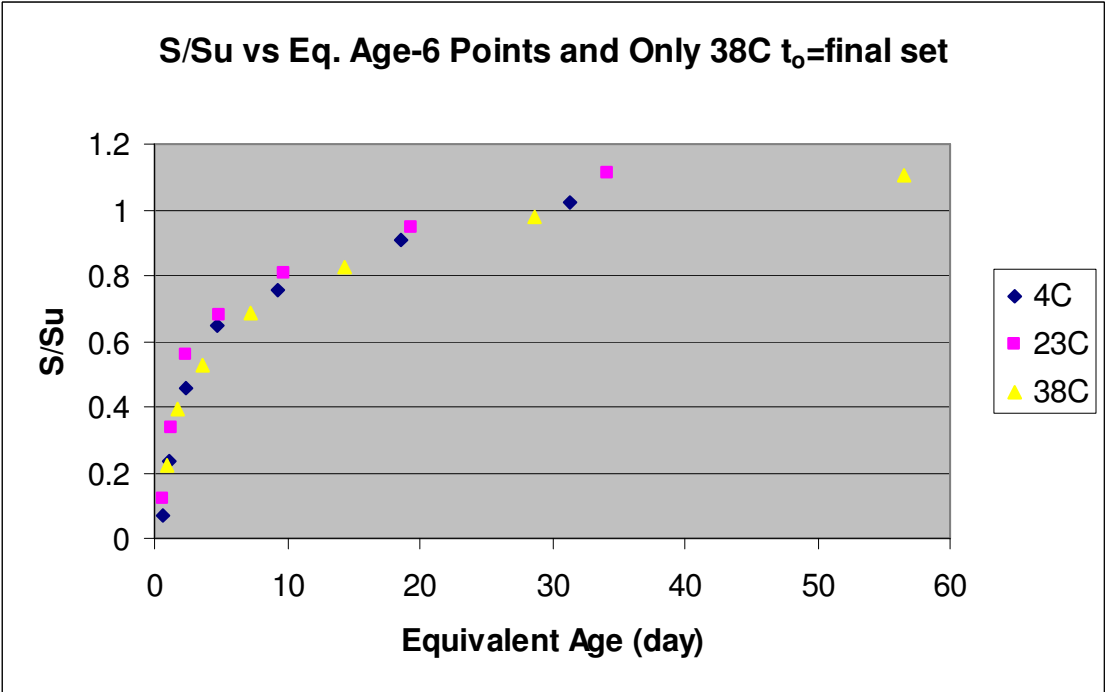


Figure 5.15: Six data points and t_o =final setting time for 38 °C data. Activation Energy = 39840.37 J/mol.

From the plotted data of Strength versus Equivalent Age and S/S_u versus Equivalent Age it appeared that the activation energy for this concrete mixture was equal to 40,000 J/mol. This value was found twice using various assumptions and gave the lowest measured error to the experimental data for both strength versus equivalent age and the ratio of strength divided by limiting strength versus equivalent age. This is shown above in Figures 5.8, 5.9, 5.14 and 5.15 and was statistically assessed by comparing the magnitude of errors between measured and predicted S/S_u values using the Chi-Squared statistic. Equation 5.4 shows the calculation of chi-squared error.

$$X^2 = \sum \frac{(\text{predicted} - \text{experimental})^2}{\text{experimental}} \quad \text{Equation 5.4}$$

The chi-squared error was analyzed for two time periods--at equivalent ages of less than 10 days and for all equivalent ages. Early ages were selected because past research has shown that the maturity method is the most applicable to early ages of strength development (Carrino 2003 and Upadhyaya 2008). Results showed that the value of activation energy calculated using ASTM 1074 subsection A1.1.8 was the least reasonable value because it had the greatest error between measured and predicted results. Furthermore, except for the error found using ASTM 1074, the error between the calculated activation energies was virtually the same when all of the equivalent age data was used. However, for the equivalent ages less than 10 days the activation energy calculated using all the results of the first six strength tests and a

t_0 value equal to final setting time for the 38 °C provided much lower error. Table 5.1 shows the results of the chi-squared error analysis.

Table 5.2: Chi-squared error analysis from activation energy data.

Analysis Method	All Ages	Equivalent Age < 10 days
ASTM 1074 A1.1.8 Curve Fit	0.3371	0.2874
All Data and t_0 =Final Set	0.1091	0.0919
6 Data Points and t_0 =Final Set	0.1064	0.0600
All Data and t_0 =final Set 38 °C	0.1113	0.0969
6 Data Points and t_0 =Final Set 38 °C	0.1191	0.0114

Based on the analysis, 40,000 J/mol was selected as the correct activation energy, which will be further used during this study. This is the same value of activation energy that was found from past University of Maryland research using the same concrete mixture design (Upadhyaya 2008).

Moreover, the past study by the University of Maryland also showed that the strength versus equivalent age data is tightly grouped during the first 10 days of equivalent age; see Figure 5.4 (Upadhyaya 2008). Past ten days of equivalent age, the rate of strength development begins to slow down significantly and a cross-over effect occurs where strength controlled by lower temperatures should develop to a higher ultimate strength value. This crossover effect can be shown throughout the plots (Figures 5.4, 5.6, 5.8, 5.10, 5.12, and 5.14). Notice that for all the measured data a crossover has occurred and that the 38 °C sample ultimately has the lowest strength value, while the 4 °C sample has the highest.

Table 5.3, shown below, summarizes the analyzed activation energies from both penetration testing and strength testing. The highlighted cells are the activation energy values which were selected to represent this mixture based on the analyses.

Table 5.3: Summary of Analyzed Activation Energy Values.

	Penetration Data	ASTM 1074 Fit	All Data to=Final Set	6 Data Points to=Final Set	All Data to=final Set 38 C	6 Data Points to=Final Set 38 C
Activation Energy (Mixing-Initial Set)	23000	-	-	-	-	-
Activation Energy (Initial Set-Final Set)	33000	-	-	-	-	-
Activation Energy (Mixing - Final Set)	27500	-	-	-	-	-
Activation Energy (Beyond Final Set)	-	27,000	40,000	43,000	38,500	40,000
UMD Control	-	-	40,000	-	-	-

5.1.4 Conclusions

From the analysis of activation energies as outlined in ASTM 1074, an activation energy value of 40,000 J/mol was determined for concrete ages past final setting time. The Arrhenius Equation, Equation 5.1, demonstrates that as activation energy increases the rate of chemical reaction or k-value must also increase. Furthermore, by applying the Arrhenius Equation to the concrete maturity method, activation energy can be used to predict the rate at which the concrete hydration reaction progresses and concrete develops strength. The following steps of analysis are focused on identifying a relationship between the activation energy value used to

define equivalent age and concrete maturity, and the rate of shrinkage experienced by concrete under different conditions.

5.2 Maturity and Shrinkage

An attempt was made to correlate concrete maturity and concrete shrinkage. The maturity approach normalizes the rate of strength development at different temperatures to the rate of strength development for a datum temperature. Similarly, one of the critical factors affecting concrete shrinkage is the rate and amount of compressive strength developed. Therefore, it seemed to be a logical to presume that a relationship may exist between concrete maturity and shrinkage.

5.2.1 Direct Application of Maturity Concept

The maturity approach was initially applied directly to the shrinkage data. Knowing the activation energy from the strength data analyzed in the previous section, an age conversion factor for each temperature was calculated. The age conversion factor was then applied in different ways to the shrinkage data plotted versus time. If the concept is applicable to shrinkage, there would be convergence of the data points to a unified curve for each tested temperature. When compared to the shrinkage versus time graph that is not adjusted to equivalent age, the data should change from four distinct curves to two approximately equivalent curves.

Similarly, the data could show a convergence when plotted versus equivalent age for specific time intervals, such as the first 7 days. Then the application of the maturity concept could be applicable for certain time periods of shrinkage development. Figure 5.16 shows the shrinkage versus actual time for each different

temperature and humidity condition (50% RH at 23 °C, 50% RH at 38 °C, 90% RH at 23 °C, and 90% RH at 38 °C).

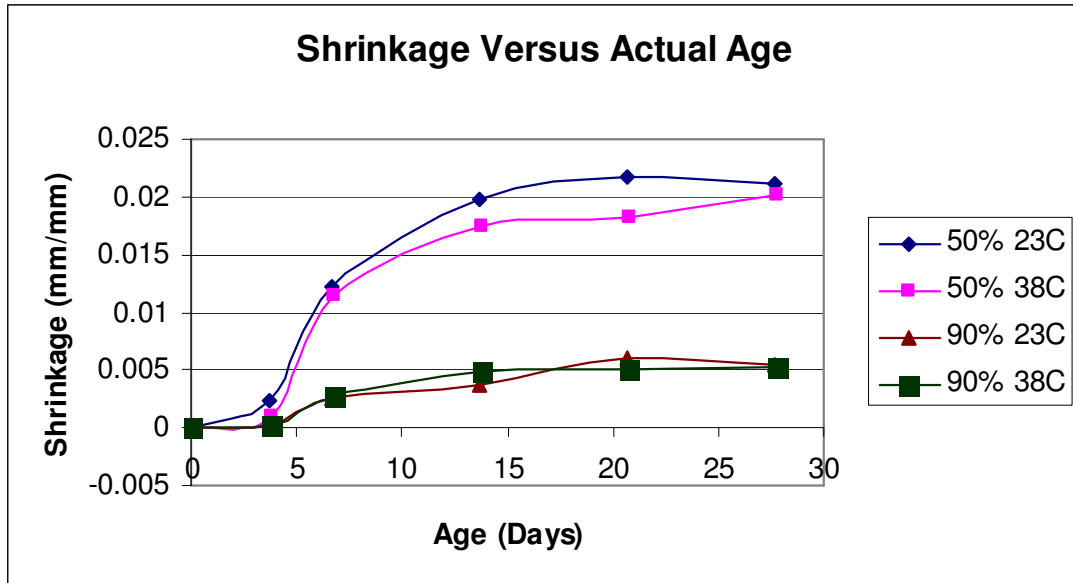


Figure 5.16: Shrinkage versus Actual Concrete Age

As can be seen from the shrinkage versus the actual age curves, the 38 °C samples appear to shrink less than the 23 °C samples. The difference between measured shrinkage values for samples cured at the same relative humidity is very small. For 50% relative humidity conditions the 23 °C samples experience shrinkage slightly more than then 38 °C samples. For 90% relative humidity conditions, the two temperate conditions results in approximately the same amount of shrinkage. The lack of a large variation in shrinkage due to temperature conditions leads to difficulties in a direct maturity relationship since the principle normally is applied to strength data, which has faster strength development for samples cured at higher temperatures. Figure 5.17 shows the equivalent age versus shrinkage relationships. Equivalent age was calculated using Equation 2.2 found in Chapter 2. Clearly, there

is no apparent convergence of the data into a single curve and no location appears to have a similar slope.

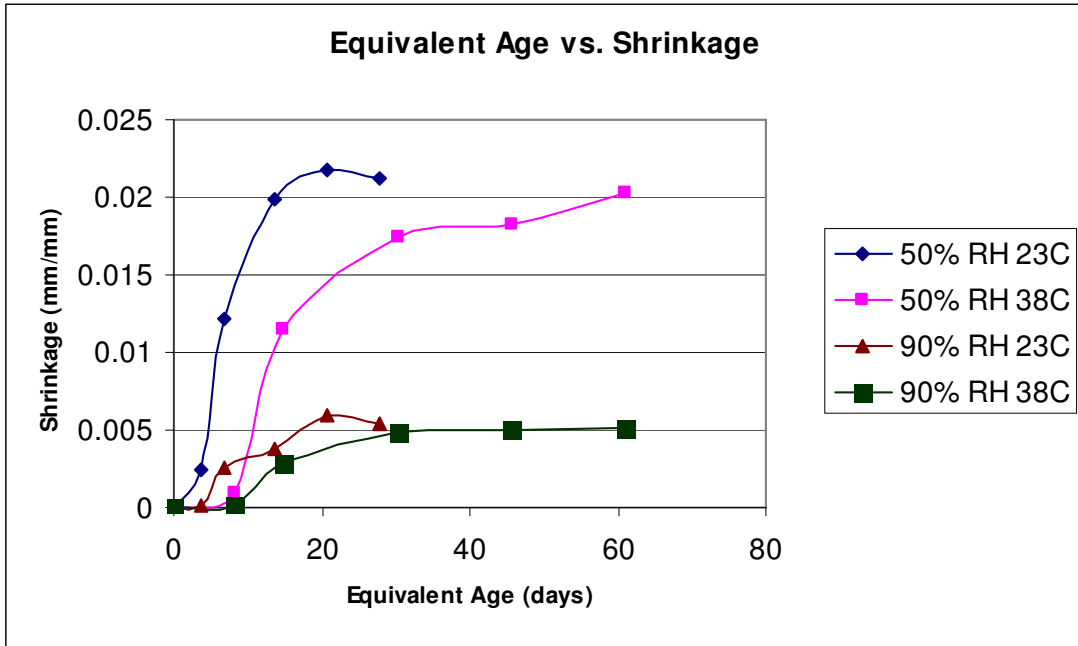


Figure 5.17: Shrinkage versus Equivalent age demonstrating no convergence.

Additionally, since shrinkage strains appeared to be lower at higher temperatures, possibly dividing the drying age of shrinkage samples by an age conversion factor would be a better application of the maturity concept to shrinkage. Equation 5.5 shows how the age conversion factor was calculated.

$$C_a = \sum_0^t e^{\frac{-E}{R} \left[\frac{1}{273+T} - \frac{1}{273+T_r} \right]} \quad \text{Equation 5.5}$$

Where:

C_a = age convergence factor

T = average temperature of concrete during the time interval Δt , °C

E = activation energy, J/mol

R = universal gas constant, 8.3144 J/(mol K)

Shrinkage modeling has shown that the rate of strength development is inversely related to the shrinkage of the concrete; therefore, it is possible to conclude that a sample hydrating and developing strength at a faster rate may have less total shrinkage. However, this relationship is related to drying shrinkage; which is traditionally the dominant shrinkage mechanism. Figure 5.18 shows the plot of shrinkage versus the concrete drying age divided by the age conversion factor. Notice again that there is no convergence of data nor is there any region that appears to have the same rate of shrinkage development with equivalent age.

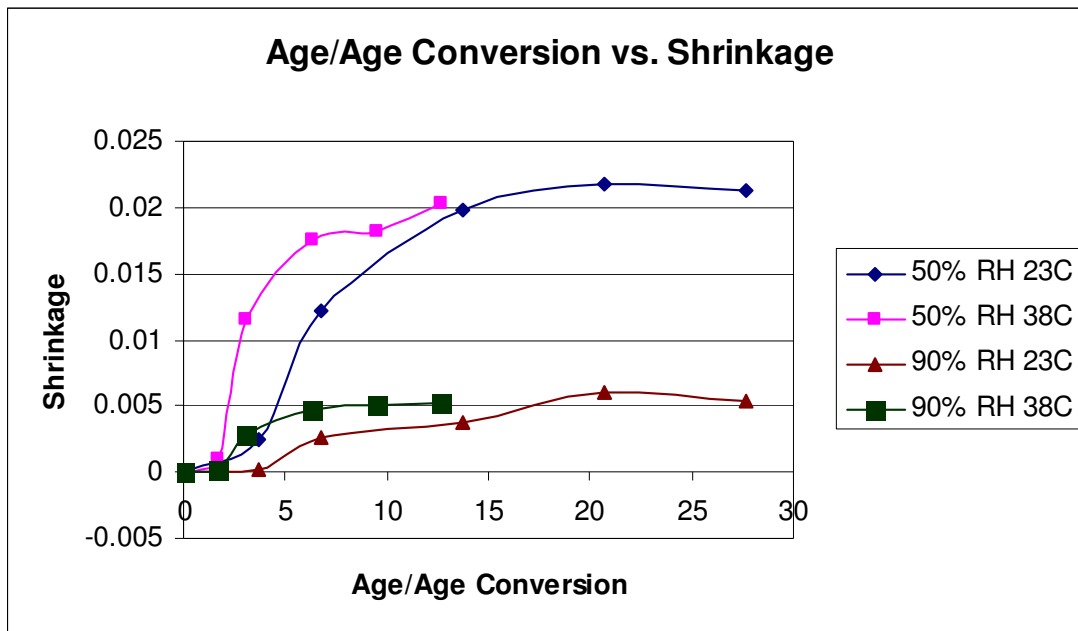


Figure 5.18: Shrinkage versus age divided by the age conversion factor.

Total shrinkage, as measured by this study, is a combination of several types of shrinkage including autogenous shrinkage, chemical shrinkage, and drying shrinkage. For autogenous shrinkage and chemical shrinkage, a faster rate of strength development is directly related to a faster rate of hydration. This causes shrinkage to increase more rapidly and to a greater magnitude. However, as previously stated,

drying shrinkage is reduced by a faster rate of strength development. Because of this complex interaction, it does not appear that concrete total shrinkage can be directly related to the maturity concept.

5.2.2 Maturity Approach as a Function of Ultimate Shrinkage

The next attempt to examine the relationship between maturity and shrinkage was to observe if the amount or percentage of the expected ultimate shrinkage versus time could be described by maturity. This has similarities to summarizing the rate at which concrete develops strength with a maturity concept by taking the ratio of the strength at any time over the limiting strength. The previous analysis described above has demonstrated that the shrinkage data could not be summarized directly by the application of a maturity concept. However, it may be possible to better summarize the rate of shrinkage development through the direct application of the maturity concept. This would lead to the conclusion that there is a proportional relationship between the rate of strength development and the rate of shrinkage development.

Using the 28 day shrinkage as a maximum and taking every preceding shrinkage value and dividing it by that 28 day shrinkage value, percentages of ultimate shrinkage were found. As shown by the plots of S/S_u in the activation energy section, activation energy based maturity should provide a good convergence for the rate of strength development at different temperatures. The desired goal of this analysis was to find a way of summarizing the temperature effects on concrete shrinkage to possibly develop a better shrinkage prediction model. Figure 5.19 shows the relationship between equivalent age and the function of shrinkage divided by the 28 day ultimate shrinkage (represented as e/e_u) for all of the various relative humidity

exposures. Notice that the points do not appear to show any convergence toward a single predictable curve. It appears that relative humidity has a significant effect on the rate of shrinkage development. Notice that the 90% relative humidity samples experience shrinkage at a slower rate than the 50% relative humidity.

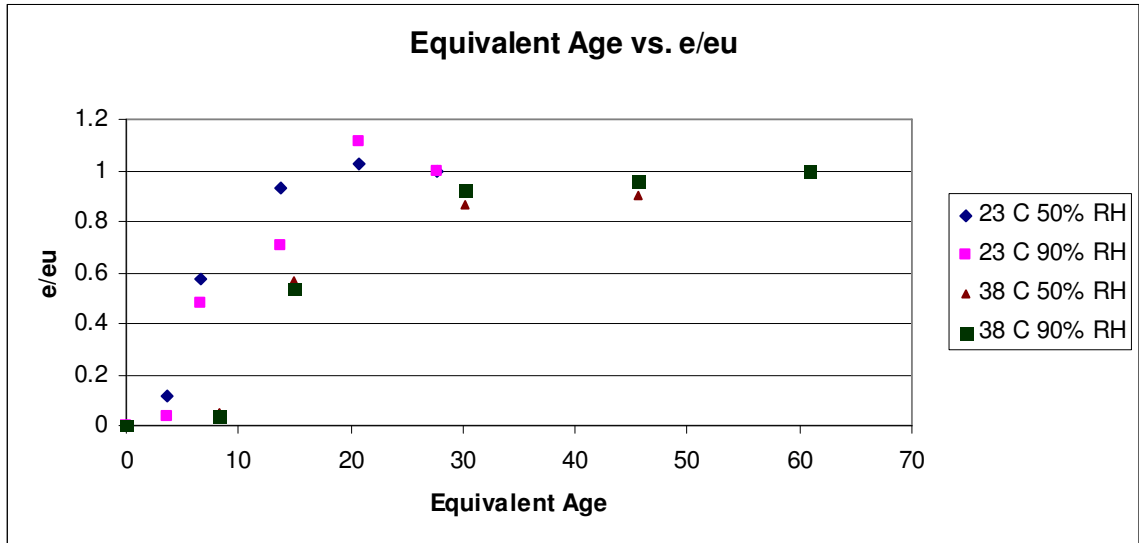


Figure 5.19: Equivalent age versus shrinkage normalized by the 28 day shrinkage.

Alternatively, the shrinkage versus the age divided by the age conversion factor, as shown in Equation 5.5, was again used to search for any additional relationship between concrete maturity based upon activation energy. Figure 5.20 shows the plot of the age divided by the age conversion factor and e/e_u for all of the exposure conditions. Notice that the graph also does not show any convergence of the data into a predictable curve. Furthermore, relative humidity appears to cause a divergence in the rate of concrete shrinkage between 50% RH and 90% RH samples.

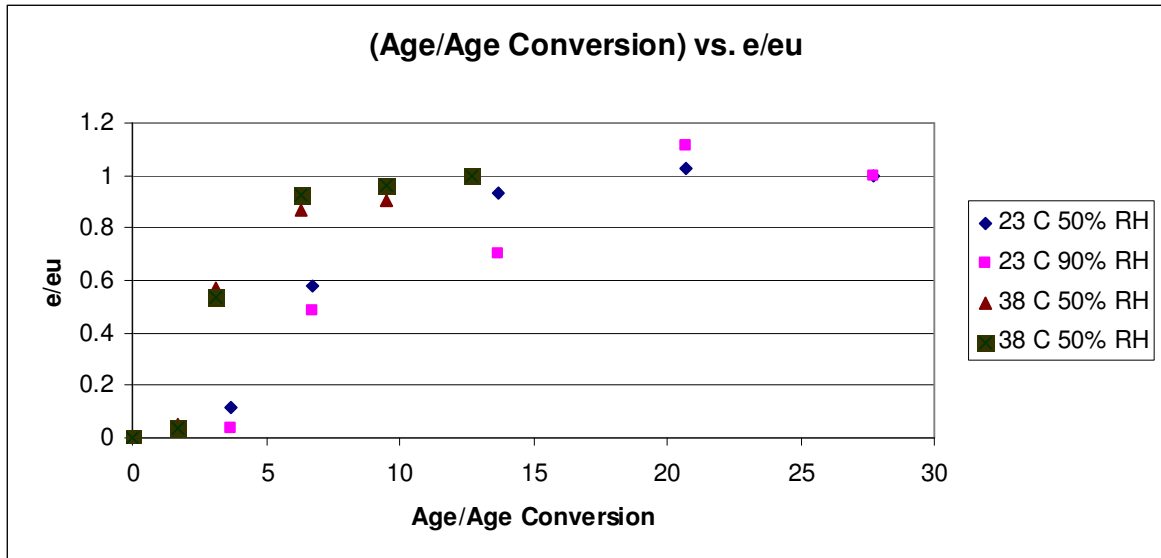


Figure 5.20: Age divided by age conversion factor versus shrinkage normalized by the 28 day shrinkage.

The relationship between shrinkage as a function of 28 day ultimate shrinkage was plotted versus the actual age of the concrete. Figure 5.21 demonstrates the plot of shrinkage divided by 28 day shrinkage versus drying age. Clearly, it can be shown from this diagram that there is a much tighter grouping of data when plotted in this manner than when the activation energy approach was applied. This leads to the conclusion that the rate of shrinkage can be best defined by a time function that is summarized by the actual age of the shrinkage samples and not the equivalent age used in concrete maturity. Based upon this conclusion, application of a maturity concept to a time function defining the rate of concrete shrinkage does not appear to be useful for shrinkage modeling.

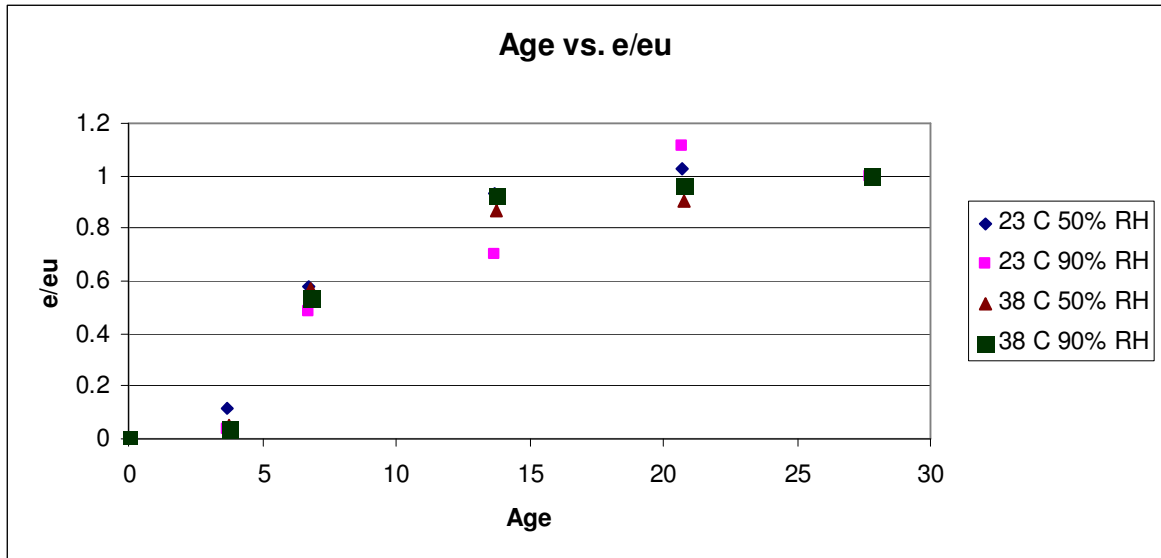


Figure 5.21: Age versus the shrinkage divided by the 28 day shrinkage.

5.2.3 Derivative Approach to Relate Shrinkage to Activation Energy

In a study by Mounanga et. al., which related chemical and autogenous shrinkage to activation energy based maturity, the researchers also attempted to define the shrinkage versus time relationship (Mounanaga et. al. 2006). In this study, Mounanga et. al. found that by taking the derivative of the polynomial equation that defined the amount of chemical shrinkage versus time, one could plot the rate of chemical shrinkage versus time. From the plotted curves a maximum or peak point where the rate of shrinkage was greatest could be determined for all various temperatures. This point was then used to calculate activation energies for cement pastes. The activation energy calculated by chemical shrinkage measurements was compared to the calculated activation energy values from strength data and were found to be equal (Mounanga et. al 2006). This study showed that for chemical shrinkage, a relationship between concrete maturity and the rate of concrete shrinkage

development exists. However, chemical shrinkage is only one component of total shrinkage and is directly caused by cement hydration.

Adopting a similar approach, polynomial curves were generated to the third order to model the shrinkage strain versus time for the shrinkage data from this study. Third order polynomial curves were used so that the derivatives of the shrinkage strain curves would become parabolic functions that show a peak where the maximum rate of shrinkage occurs. These derivative curves would represent the rate of shrinkage development over time. These maximum points would represent where concrete shrinkage is occurring most rapidly and could possibly be used to calculate activation energy. For concrete shrinkage to be related to maturity, the rate of concrete shrinkage development must be related to the rate of strength development through activation energy. However, from Figure 5.22--which is the plot of the derivative of the polynomial shrinkage curves versus time--there is no identifiable maximum shrinkage point.

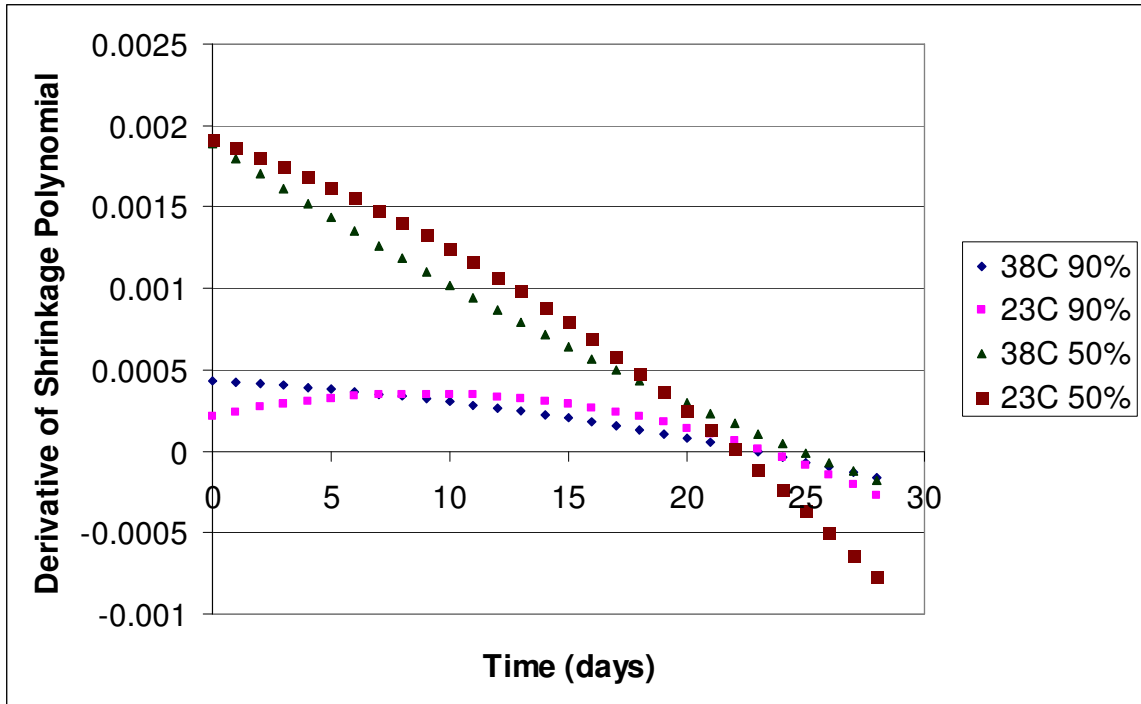


Figure 5.22: Derivative of the shrinkage polynomial versus time.
Note: only the 73F sample at 90% relative humidity reaches a location where the rate of shrinkage at later ages is greater than it was at zero time.

These curves show that rate of shrinkage strain is reducing over time. This would be expected if drying shrinkage was the dominate shrinkage mechanism. Drying shrinkage demonstrates that, during early ages, shrinkage occurs rapidly within the exterior volume of a concrete sample. As the exterior volume dries, air must permeate deeper into the concrete to begin to dry the interior volume of the concrete sample. Because of reduced permeability the rate of drying shrinkage will decelerate at later ages.

If shrinkage data from this study could be captured as a function of the rate of the hydration reaction, the maximum point would be shown in Figure 5.22. This maximum point of the derivative of shrinkage curve corresponds to the point where the rate of hydration was greatest. This point could have occurred at an earlier phase

of concrete shrinkage that was not measured by this study. Furthermore, the rate of concrete shrinkage should be greater for 38 °C than for 23 °C. Figure 5.22 appears to show approximately the same rate of shrinkage for samples cured at the same relative humidity. This further shows that relative humidity has a significant effect upon the rate of shrinkage development.

5.2.4 Compressive Strength under Shrinkage Curing Conditions

To further examine whether shrinkage can be related to a maturity approach, the strength versus age data was compared for each compressive strength sample that experienced the same environmental conditions as the shrinkage samples. By observing the strength data at earlier ages, it can be shown that there is an expected trend to the data; see Figure 5.23. The strength development appears to be developing faster at earlier ages for the higher temperatures than for the lower temperatures.

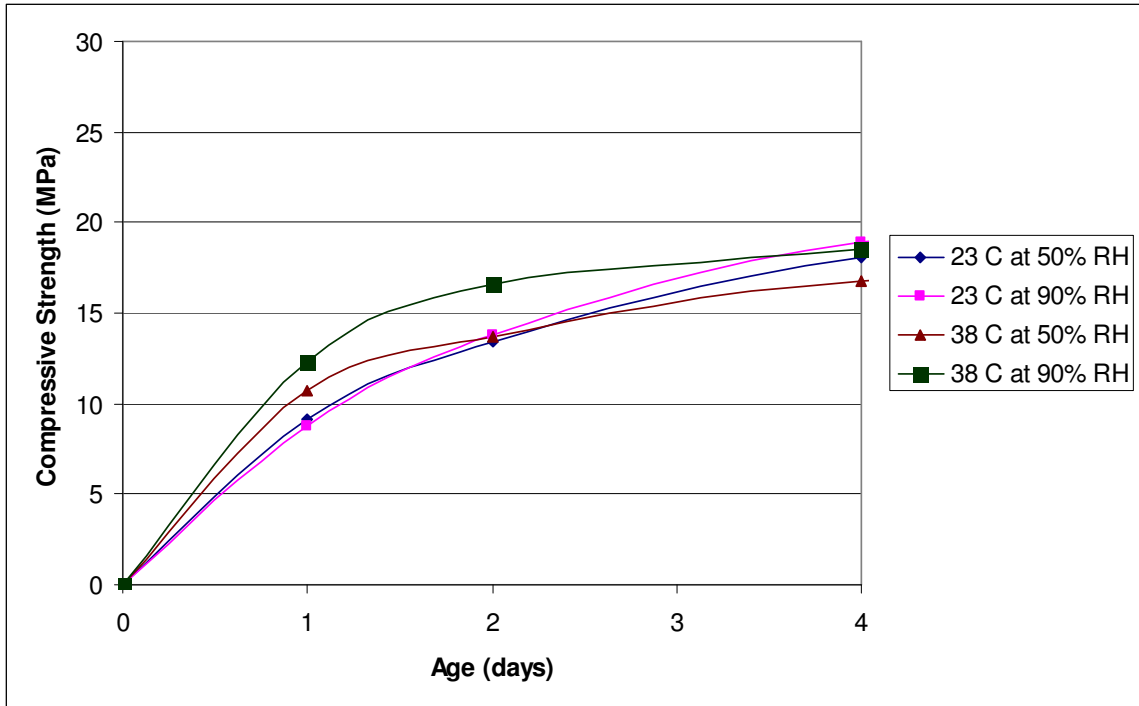


Figure 5.23: Earlier age Compressive Strength Development versus time.
Note: the dark red and dark green lines (38 °C) develop strength more rapidly than the blue and pink lines (23 °C).

When the strength values are plotted versus their equivalent ages, the maturity concept appears to only apply for the first 4 days, because the 38 °C samples generate strength faster and there appears to be a crossover when compared to the 23 °C samples. After the first 4 days the strengths diverges significantly because of different humidity and shrinkage conditions. Figure 5.24 shows the effects of the different curing conditions on strength development when plotted versus equivalent age. In addition, Figure 5.24 shows the strength development of moist cured samples plotted versus equivalent age. Notice that the samples kept at 90% relative humidity appear to develop more strength than the 50% humidity samples. This is expected since the lack of moisture would retard the rate of the hydration reaction. For all the

relative humidity conditions shown, there is a reduction of strength development when compared to moist cured samples.

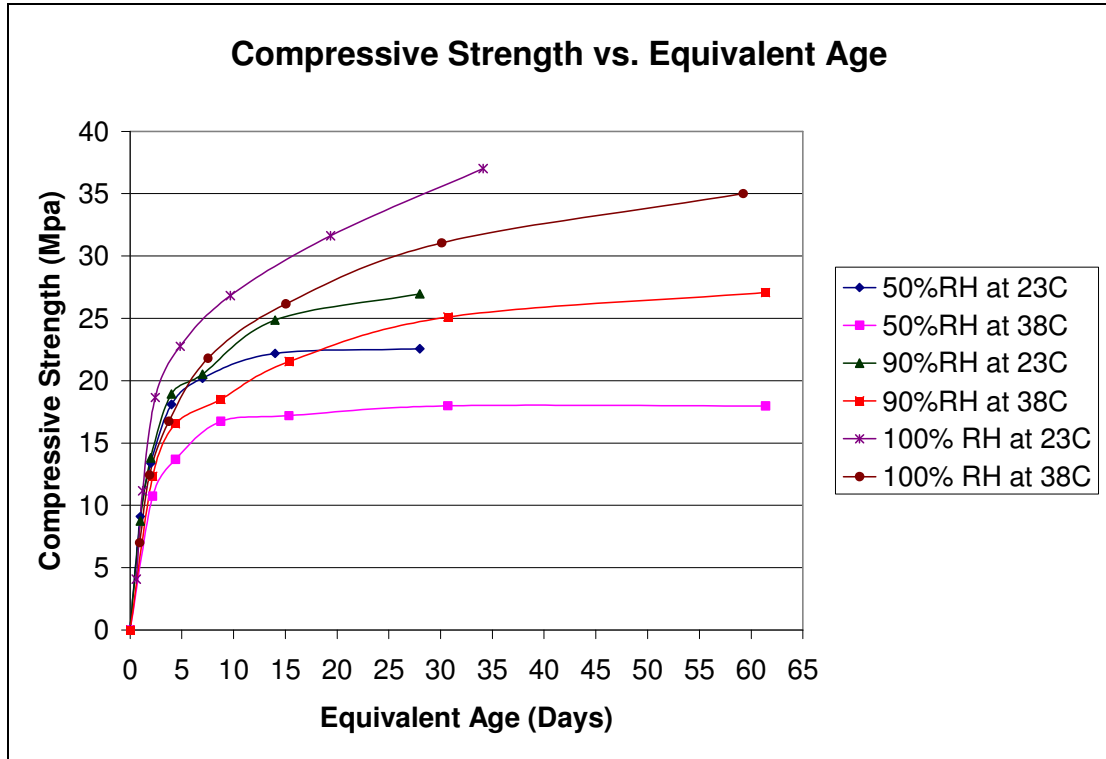


Figure 5.24: Compressive Strength of conditioned samples versus Equivalent Age.

Figures 5.25 and 5.26 compare the amount of shrinkage experienced versus the compressive strength for both 50% and 90% relative humidity, respectively. It is difficult to draw conclusions from these figures due to limited data. However, for the 50% relative humidity samples there is markedly less strength gain with age for the higher temperatures (38°C) than for the lower temperatures (23°C). Furthermore, the change in shrinkage for 90% relative humidity samples does not appear to be equivalent based upon a change in compressive strength. The change in shrinkage of the 23 °C samples at 90% is greater at later ages of strength development than at the

intermediate ages. As has been previously shown, relative humidity has a significant effect on strength development and shrinkage development. This is likely the reason that there is not a predictable change in shrinkage as concrete strength increases.

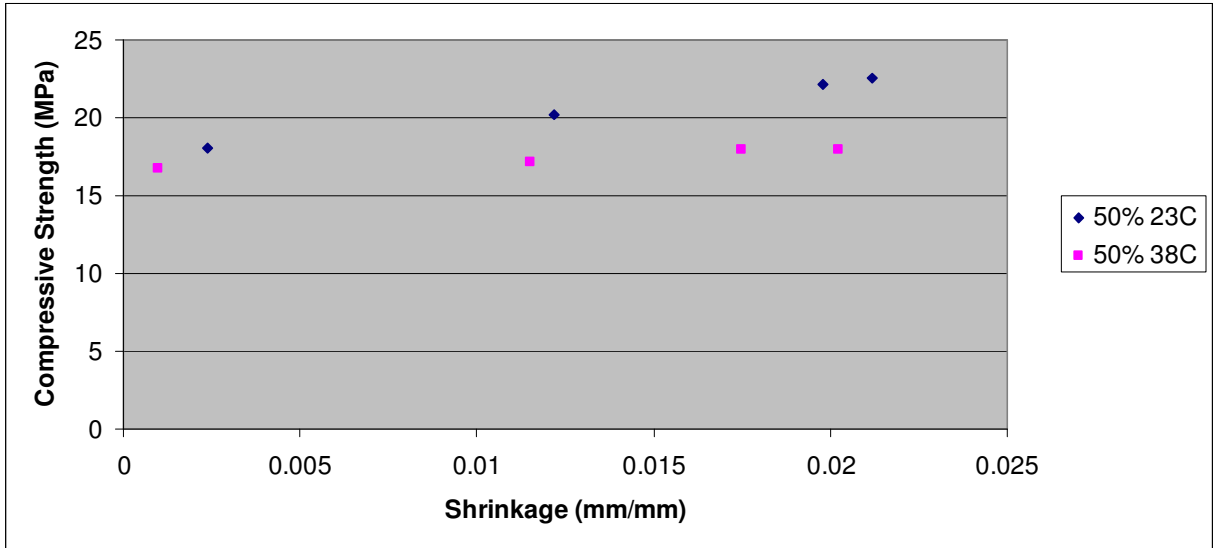


Figure 5.25: Shrinkage versus compressive strength for the 50% relative humidity samples.

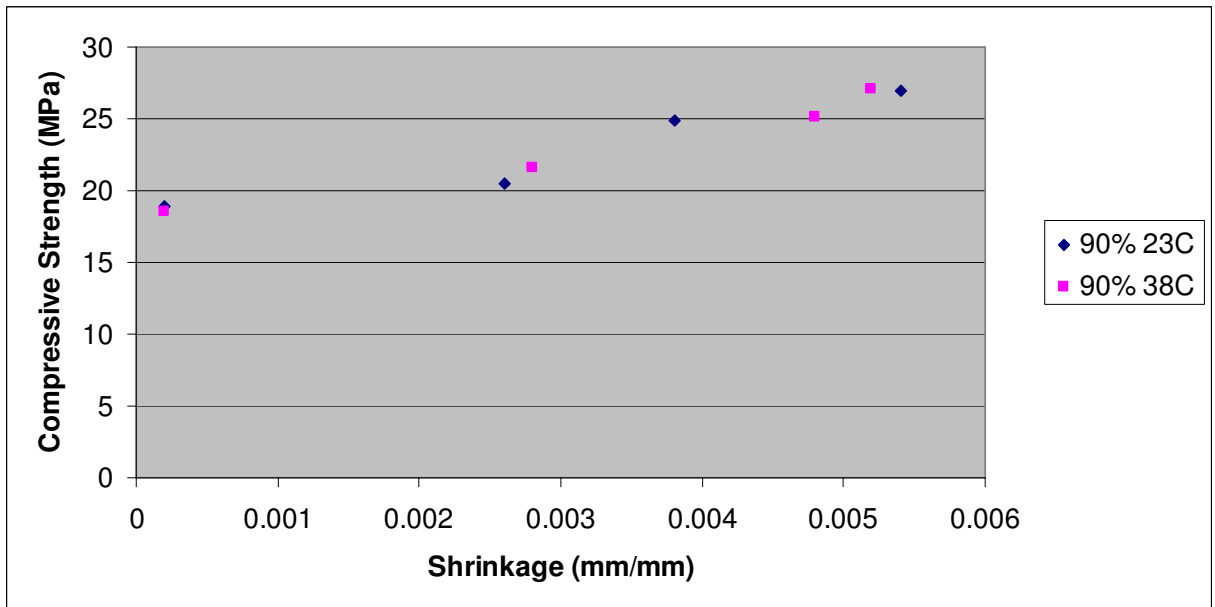


Figure 5.26: Shrinkage versus compressive strength for the 90% relative humidity samples.

In a study conducted by Myers on accelerated curing, it is suggested that curing at higher temperatures causes a larger pore structure to be formed. These larger pores can not develop the same stresses within the concrete as a network of micro-pores can (Myers 2006). This could explain why the concrete at a higher temperature, in this research study, experienced less shrinkage over time than concrete at a lower temperature. It is well known that the rate of evaporation is increased with increased temperature. It is highly plausible that a combination of faster strength development during the early ages, as well as a larger pore size distribution, may have led to less shrinkage at higher temperatures. This is not as pronounced for the 90% relative humidity samples as it is for the 50% relative humidity samples. This is due to the limited drying that occurred because there were higher humidity conditions; however, both higher temperature samples did experience less shrinkage during the same amount of drying time. Similar to what was conducted in Myer's study, the samples from this study were exposed to drying conditions at very early ages, when concrete is still in its formative stages, which means the effects of evaporation could be unique between different temperature samples. Normally, shrinkage samples are allowed to cure for 28 days in a temperature controlled water bath before exposing the samples to drying conditions. However, the samples in this study were exposed to temperature and humidity conditions shortly after final setting time in order to measure the early age shrinkage that occurs when concrete is experiencing significant strength development.

5.2.5 Conclusions

From studying the rate of shrinkage development and how it relates to both equivalent age and the rate of strength development, no direct relationship between shrinkage and equivalent age could be found. Strength testing of the concrete samples cured under the same conditions as the shrinkage samples shows that there is a relationship between concrete maturity and the strength that was developed under the shrinkage curing conditions during the first 4 days, but beyond that the curves diverge significantly due to humidity effects and varying temperatures. This leads to the conclusion that a maturity approach would be very difficult to apply to concrete shrinkage and that no unique relationship between shrinkage and maturity could be found by this study. The effect of humidity will significantly affect the rate of strength development and shrinkage development, causing difficulty in determining their relationship.

5.3 Shrinkage Modeling

The next objective of this study was to model shrinkage with both humidity and temperature effects.

5.3.1 Analysis of Existing Shrinkage Models

First, existing shrinkage models were analyzed to examine the significant parameters affecting shrinkage in order to develop a model representing the shrinkage data of this study. One commonality was that the shrinkage models were all similarly set up as product models. Product models are non-linear models where individual parameters, such as relative humidity or temperature, are multiplied along with other constants to represent the dependent variable. Another similarity between the models

was that they all tended to use a time function that was of hyperbolic form. The models also had corrections for humidity conditions, water-to-cement ratio, 28 day compressive strength, sizing effects, and others depending upon the model. The following equations 5.6, 5.7, and 5.8 summarize the time functions found within each model. The variables m_1 , m_2 , and m_3 summarize the constant terms found within each model that could be varied to better fit the experimental data.

ACI 209:

$$f(t) = \frac{x}{m_1 + x} \cdot m_3 \quad \text{Equation 5.6}$$

CEB-FIP 90 AND GL2000:

$$f(t) = \left(\frac{x}{m_1 + x} \right)^{m_2} \cdot m_3 \quad \text{Equation 5.7}$$

B3:

$$f(t) = \tanh\left(\frac{x}{m_1}\right)^{m_2} \cdot m_3 \quad \text{Equation 5.8}$$

Furthermore, besides the fact that these functions have hyperbolic time forms, the CEB-FIP 90 and B3 models express the humidity dependence function as $f(h) = (1 - h^3)$. This relationship is well defined in the literature and except for exceptionally low humidity levels the function typically defines the humidity relationship quite well.

There was no predefined temperature function found in the modeling, so one would need to be defined. Because the remainder of the conditions between the

tested samples, such as aggregate, water-to-cement ratio, 28 day moist compressive strength, etc., were the same for the samples tested their impact was not considered in the model.

5.3.2 Development of a Shrinkage Time Function

After analyzing the existing shrinkage prediction equations, an additional time function was proposed to forecast the shrinkage versus time dependency. Equation 5.9 shows the proposed alternative time function. The benefit of this time function is that it accelerates the hyperbolic relationship, allowing the shrinkage to reach its maximum at a shorter drying age. This is beneficial because the data from this study appears to have reached a limiting shrinkage level during drying.

ALTERNATE TIME FUNCTION:

$$f(t) = \frac{x^{m2}}{m1 + x^{m2}} \cdot m3 \quad \text{Equation 5.9}$$

The mean shrinkage data for the different humidity and temperature conditions were then analyzed versus time. A shrinkage model that is unique to this study was proposed using the time functions from Equations 5.6-5.9 and constants m_1 , m_2 , and m_3 , which were assumed to generate an initial predicted value. Then the squared error between predicted and actual shrinkage was calculated. Additionally, the square of the residuals (R^2) value was calculated for each of the four different humidity and temperature conditions. The equations were then optimized using the Microsoft Excel© solver function to reduce error by keeping the m_1 and m_2 values constant, but allowing the m_3 value to vary between conditions. This m_3 value is

used to summarize the effects of humidity and temperature on the shrinkage data. The R² values were also analyzed to judge the best time function. It was determined that the alternate time function was better than the existing code model functions for the conditions that were included in this research study. Equation 5.10 shows the time function that was obtained from the analysis.

$$f(t) = \frac{t^{2.573}}{131.385 + t^{2.573}} \quad \text{Equation 5.10}$$

The time function shown in Equation 5.10 fits well for the data tested for the four different exposure conditions. It should account well for exposure conditions that allow for drying at very early ages following final setting time, with no moist curing. Results of the analysis to determine the time function are shown in Table 5.4.

	Error Squared	R²
50% RH at 23 °C	4.401E-06	0.991727
90% RH at 23 °C	2.174E-06	0.943044
50% RH at 38 °C	1.048E-05	0.977929
90% RH at 38 °C	6.998E-07	0.982776
Combined	1.775E-05	0.988674

Table 5.4: Time function error measurements.

5.3.3 Development of Humidity and Temperature Functions

For the modeling to be correct, the varying values of m₃ calculated from the time function should be explained by a relationship that relates humidity, temperature, and a constant for all shrinkage curves. The constant would be the same

because the remainder of the mixture and strength characteristics for all four shrinkage conditions should be the same. Because the humidity relationship has been well defined by existing literature and models, the function of humidity followed the $1-h^3$ format, where h is equal to the relative humidity that concrete was exposed to, with an added constant term. Additionally, two different temperature and time functions were proposed. One model that defines the relationship between temperature and shrinkage is linear and one is non-linear. The proposed humidity and temperature functions were fit again using Microsoft Excel's solver function to the various m^3 values from the time function component. These values are summarized as either Model 1 for linear temperature effects, or Model 2 for non-linear temperature effects. Equations 5.11 and 5.12 present the humidity effects.

MODEL 1:

$$f(h) = (1 - 1.073821 \cdot h^3) \quad \text{Equation 5.11}$$

MODEL 2:

$$f(h) = (1 - 1.074569 \cdot h^3) \quad \text{Equation 5.12}$$

Furthermore, the temperature effects are summarized in Equations 5.13 and 5.14. For these models the temperature T is in degrees Celsius. Finally the constants multiplied to each model were determined to be equal to 0.025959 for Model 1 and .025966 for Model 2.

MODEL 1:

$$f(T) = \left[1 - \left(\frac{9T - 205}{365} \right) \cdot 0.278672 \right] \quad \text{Equation 5.13}$$

MODEL 2:

$$f(T) = \left[1 - \left(e^{-4811.16 \cdot \left(\frac{1}{273+T} - \frac{1}{273+22.78} \right)} - 1 \right) \cdot 0.086466 \right] \quad \text{Equation 5.14}$$

The final product models are shown below in Equations 5.15 and 5.16. It can be noticed that the time function, the humidity functions, and multiplicative constants are virtually equivalent. The only features that vary significantly are the temperature functions.

MODEL 1:

$$f(t, h, T) = \frac{t^{2.573}}{131.385 + t^{2.573}} \cdot (1 - 1.073821 \cdot h^3) \cdot \left[1 - \left(\frac{9T - 205}{365} \right) \cdot 0.278672 \right] \cdot 0.025959$$

Equation 5.15**MODEL 2:**

$$f(t, h, T) = \frac{t^{2.573}}{131.385 + t^{2.573}} \cdot (1 - 1.074569 \cdot h^3) \cdot \left[1 - \left(e^{-4811.16 \cdot \left(\frac{1}{273+T} - \frac{1}{273+22.78} \right)} - 1 \right) \cdot 0.086466 \right] \cdot 0.025966$$

Equation 5.16

5.3.4 Validation of the Shrinkage Models

The two models were then tested using the experimental data. From Figures 5.27 and 5.28, the accuracy of these models to represent the experimental data of this study can be observed.

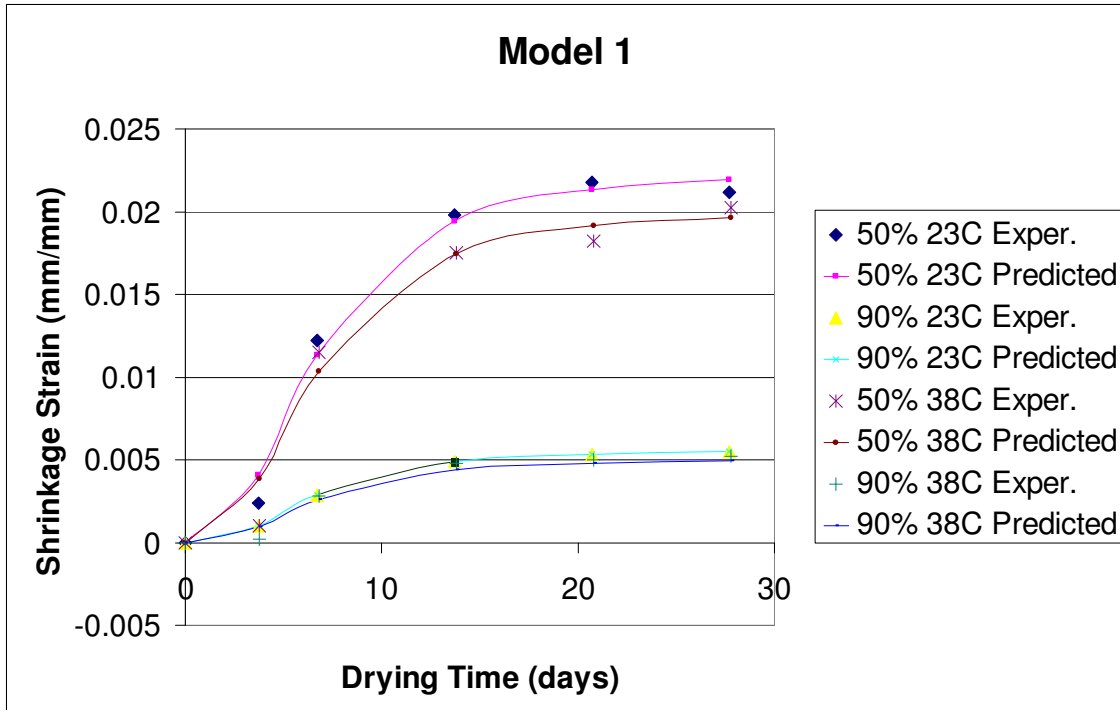


Figure 5.27: Model 1 predicted shrinkage plotted with the actual mean shrinkage data.

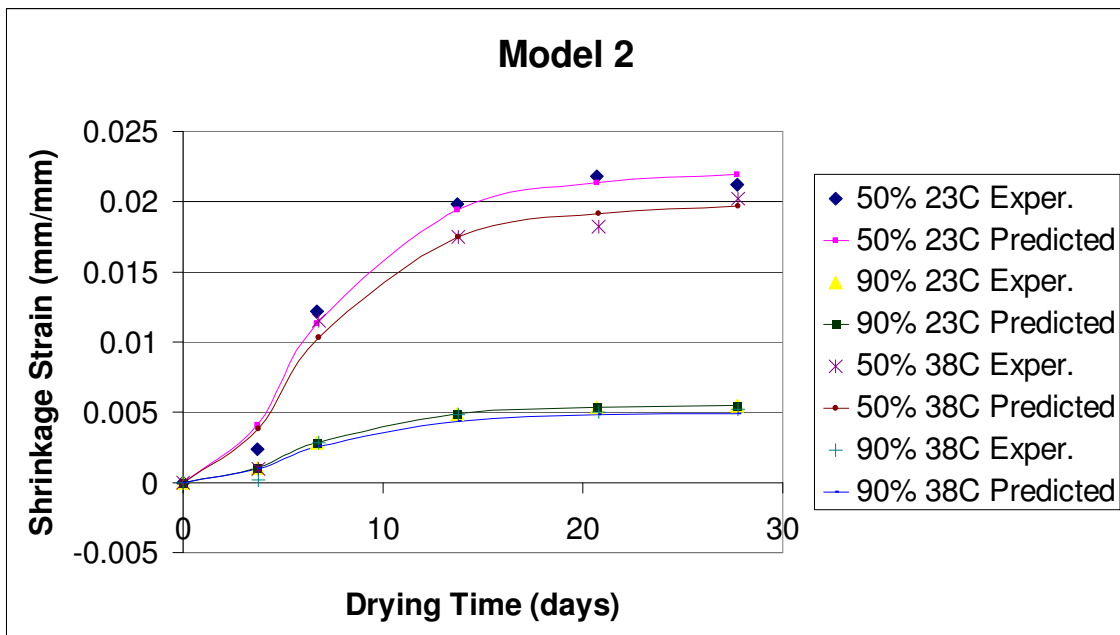


Figure 5.28: Model 2 predicted shrinkage plotted with the actual mean shrinkage data.

Additionally, the shrinkage models were compared using the Chi-Squared Goodness-of-Fit test. The benefit of this test is that it is a nonparametric method of

analysis that will indicate whether the predicted shrinkage is significantly far from the measured mean shrinkage values. The Chi-Squared statistical equation is shown in Equation 5.17

CHI-SQUARED EQUATION:

$$X^2 = \sum \frac{(\text{predicted} - \text{experimental})^2}{\text{experimental}} \quad \text{Equation 5.17}$$

Rejection Region: $X^2 \geq X^2_{\alpha, k-1}$
 Where:
 α =significance level
 k=degrees of freedom

The degrees of freedom were equal to 5 for each concrete shrinkage measurement; therefore k-1=4. The significance level (α) was set to be 0.1. It was found that all of the calculated chi-squared values at each humidity and temperature condition for both Model 1 and Model 2 were very low. All of the values fell below the rejection region of 7.77. The results of the Chi-Squared analyses for both models are shown in Table 5.5.

Table 5.5: Chi-Squared Analysis Results

	X^2 - Model 1	X^2 - Model 2
50% RH at 23 °C	1.28E-03	1.28E-03
90% RH at 23 °C	3.80E-03	3.78E-03
50% RH at 38 °C	8.18E-03	8.18E-03
90% RH at 38 °C	2.96E-03	2.95E-03

This means the models do not vary significantly from the tested data. Therefore, in terms of variation from the existing data, the two shrinkage models accurately predict the shrinkage versus time relationship.

5.3.5 Temperature and Humidity Response of Models

In addition to validating the two models for their convergence to the experimental data, the models were examined for their response to a wide range of humidity and temperature conditions. Figure 5.29 represents the effect humidity will have on Model 1 and Figure 5.30 represent the effect of temperature. The response of the model is as expected; as the relative humidity reduces, the shrinkage increases. Also, as temperature increases shrinkage reduces. Furthermore, Figure 5.31 represents the effect humidity will have on Model 2 and Figure 5.32 represents the effect of temperature. Similarly, the behavior shown is as expected; however, the temperature response of the model exhibits a non-linear change due to variations in temperature. It seems probable that this nonlinear behavior may be more characteristic of the temperature effects because the degree of formation of macro-pores at higher or lower temperatures will partially define the amount of shrinkage experienced. Similar to the Myer's study, increased temperature will lead to the formation of more macro-pores which will lead to less desiccation stress development (Myer's 2006). However, because this explanation is based on limited temperature data, this response needs to be further investigated.

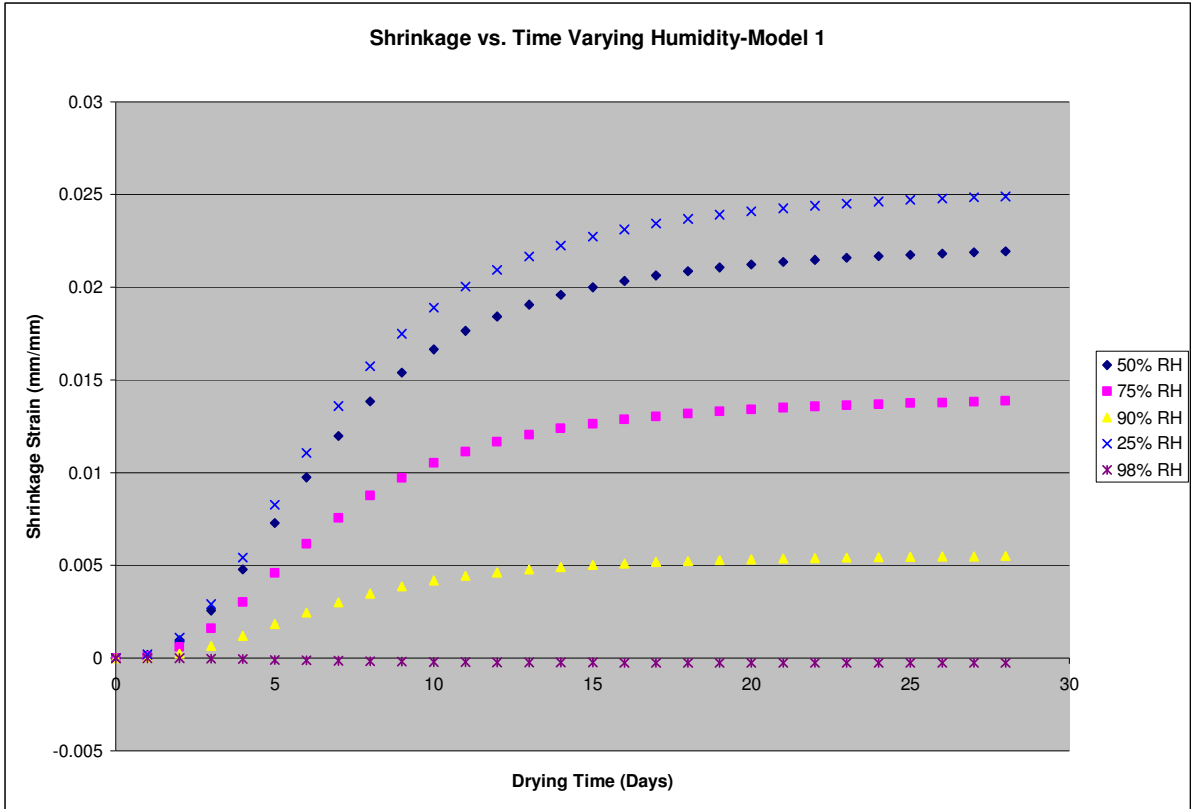


Figure 5.29: Humidity response of Model 1

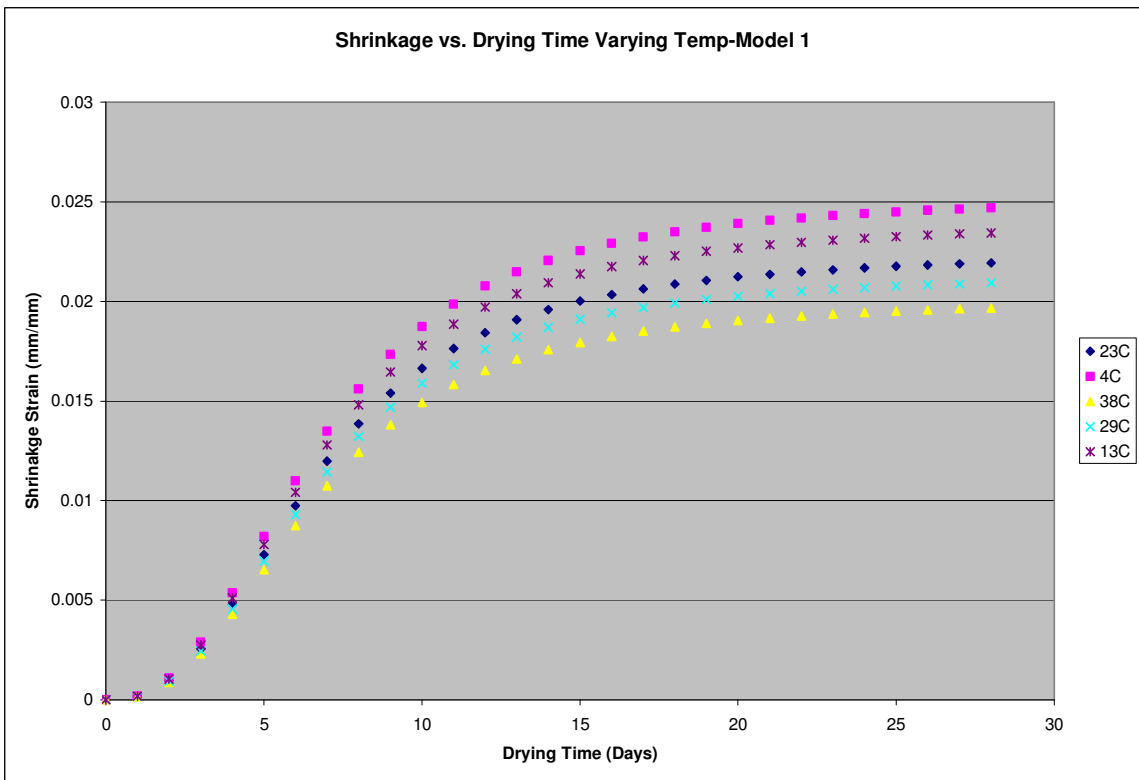


Figure 5.30: Temperature response of Model 1

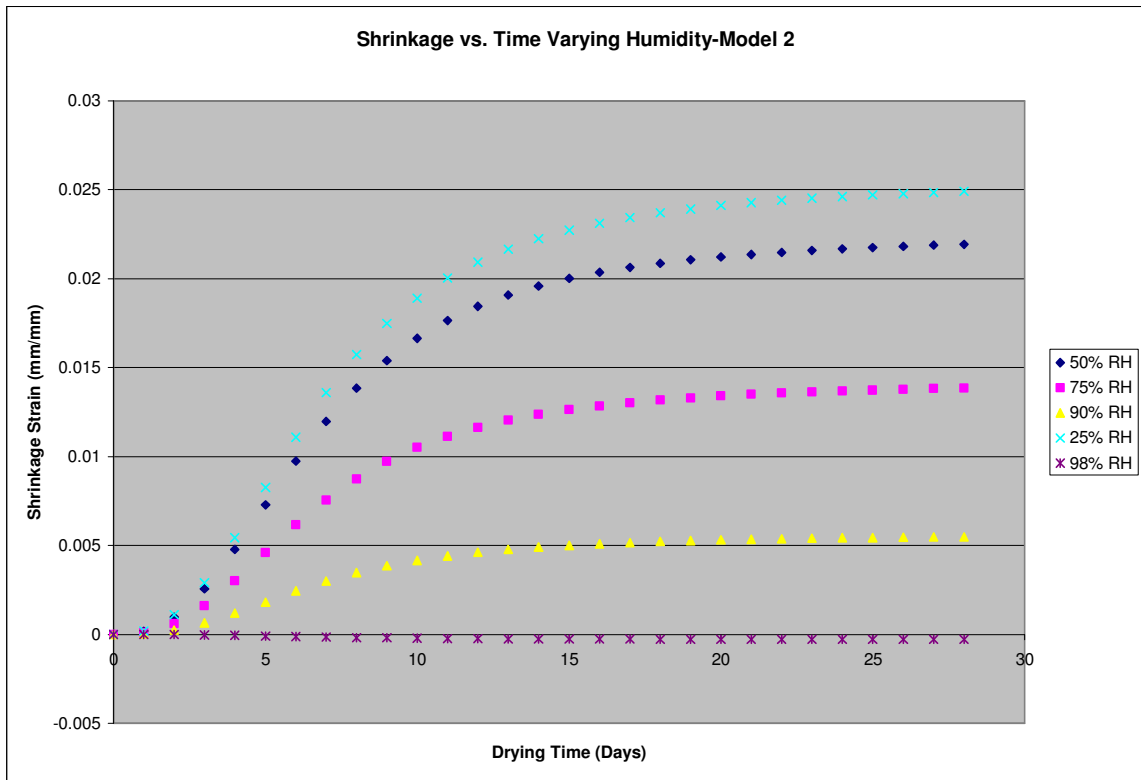


Figure 5.31: Humidity response of Model 2

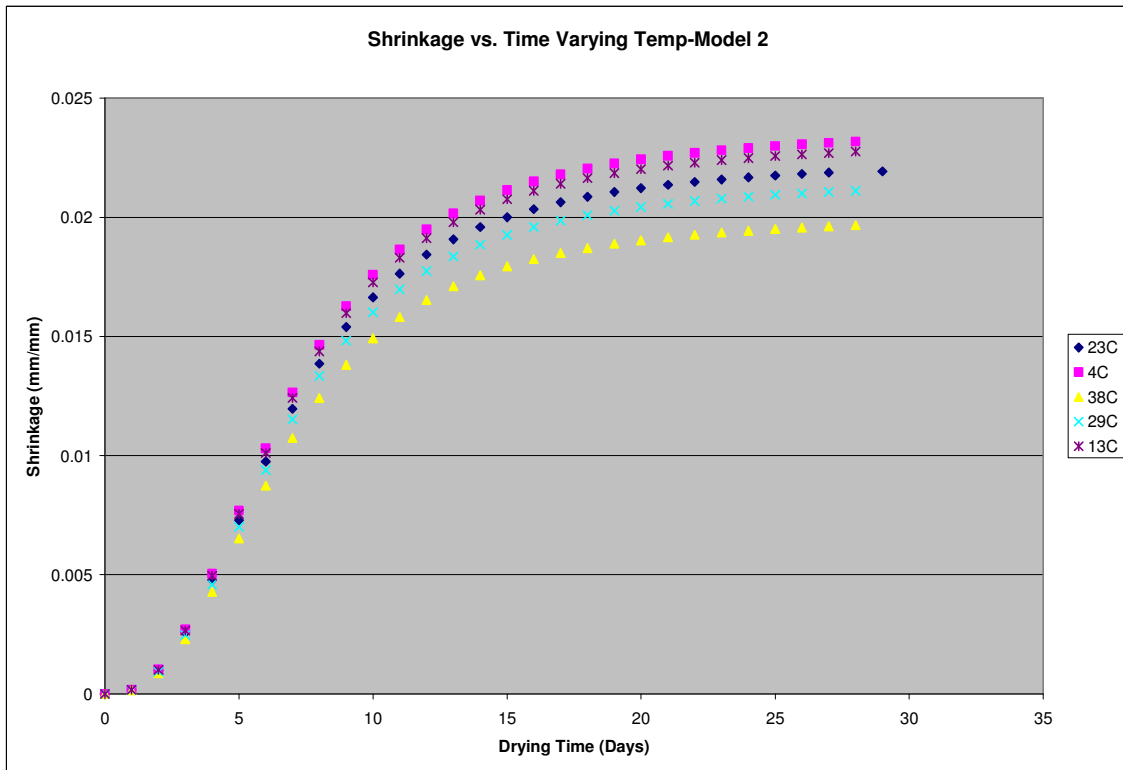


Figure 5.32 Temperature response of Model 2

5.3.6 Conclusions

Modeling of concrete shrinkage began by analyzing the existing models for similarities. Because it had been previously shown that the equivalent age approach would not cause a convergence of the shrinkage data, the drying time was used to model shrinkage through the use of a time function. Two models were developed, one which assumes that temperature will affect shrinkage linearly, and one which assumes temperature will affect shrinkage non-linearly. Both models appear to be a good representation of the experimental data and pass a Chi-Squared goodness-of-fit test. Furthermore, the response of both models to temperature and humidity exhibits expected trends.

5.4 Comparison of Model 1 and Model 2 to Existing Models

One very important variation between the models that were developed in this study and the already existing code models is that the developed models are based upon experimental data for shrinkage samples exposed very early to drying conditions. The code models predict shrinkage for concrete that has been assumed to have been moist cured to 28 days before being exposed to air. This means at 28 days the concrete is still at 100% saturation. Because the samples were allowed to dry at final setting time in this study, the rate of shrinkage is due to both chemical hydration as well as drying. The existing models from the literature only account for drying. The affects of hydration on shrinkage will not be as significant after 28 days of moist curing. Therefore, in the developed models, the time function and model formulation should differ from the existing models in the literature.

Figure 5.33 shows the actual mean shrinkage values for 50% relative humidity at 23 °C plotted with the predicted shrinkage from Model 1, Model 2, ACI 209, CEB-FIP 90, B3, and GL 2000. Similarly, Figure 5.34 shows the actual mean shrinkage data for 90% relative humidity at 23 °C plotted with the predicted shrinkage from the same models. The 38 °C samples were not plotted because the existing models do not have the ability to account for temperature effects and the variation between the experimental data from this study, and the predicted shrinkage calculated using the models from literature was found to be greater for 38 °C than for 23 °C.

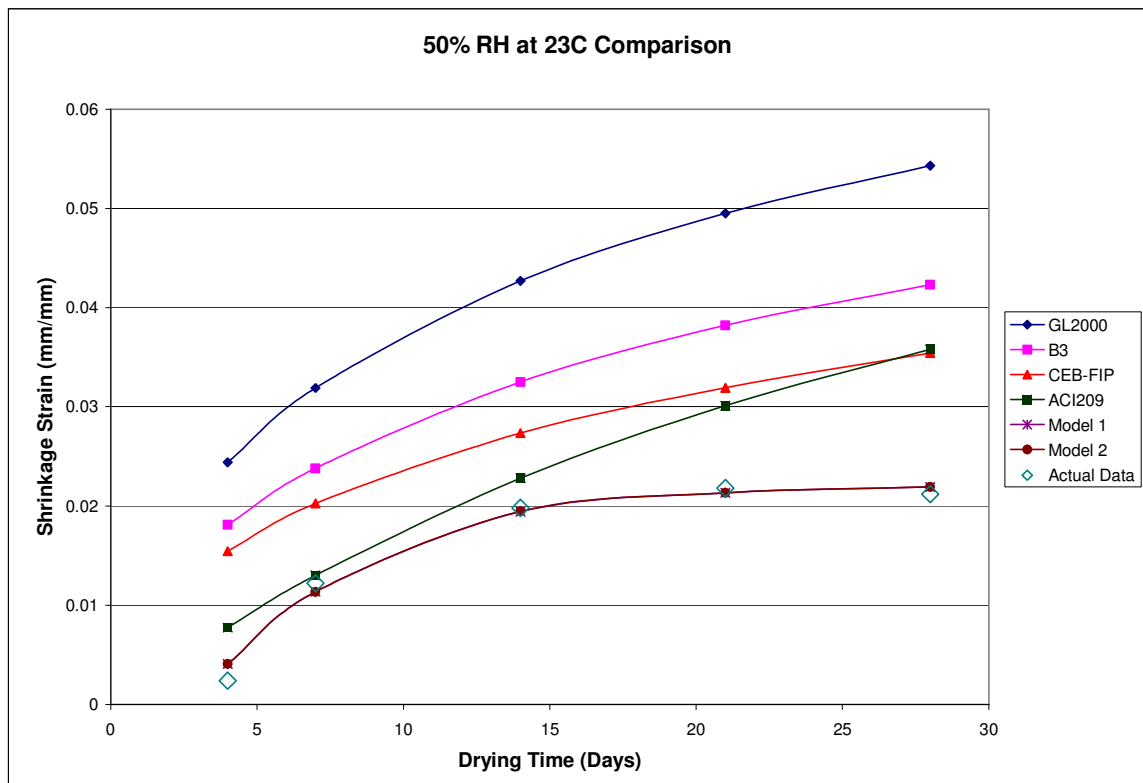


Figure 5.33: Shrinkage Data for 50% RH at 23°C versus existing and developed shrinkage models. Note: Model 1 and 2 are overlapping.

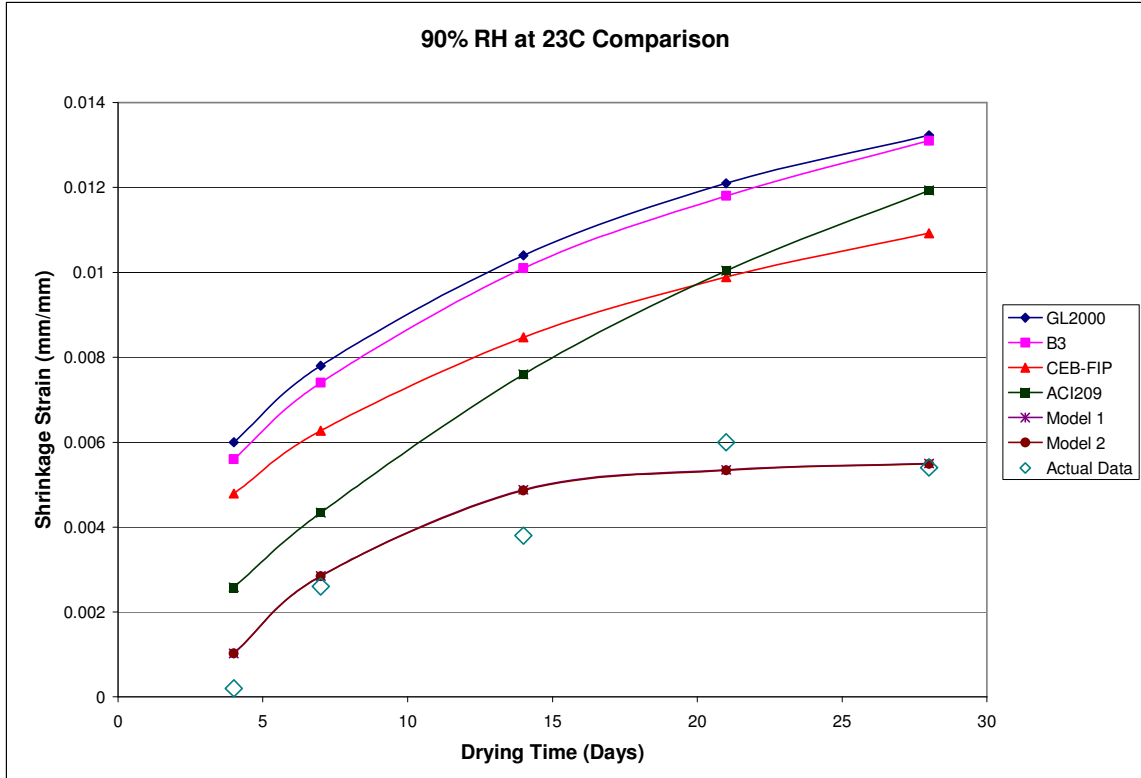


Figure 5.34: Shrinkage Data for 90% RH at 23°C versus existing and developed shrinkage models. Note: Model 1 and 2 are overlapping.

Furthermore, the predicted shrinkage from the existing models and the developed Model 1 and Model 2 were compared to the tested data by calculating the Chi-Squared error using Equation 5.17.

Table 5.6 summarizes the variation between the models and their response to various exposure conditions. For the existing models, the only method of distinguishing between 38°C and 23°C samples is by varying the time when the samples were exposed to drying conditions. These times were only slightly different because exposure began at the final setting time for each temperature. The data found in the table demonstrates that the closest existing model to the tested data was ACI 209, but that model is not as close as Model 1 and Model 2 which have even smaller Chi-Squared Error.

Table 5.6: Chi-Squared values for existing and developed models.

	GL2000	B3 Model	CEB-FIP	ACI 209	Model 1	Model 2
50% 23C	0.003259	0.001257	0.000597	0.00032	4.41E-06	4.41E-06
50% 38C	0.003762	0.001513	0.000805	0.000466	1.05E-05	1.05E-05
90% 23C	0.000203	0.000185	0.000102	8.21E-05	2.34E-06	2.32E-06
90% 38C	0.000205	0.000182	0.000104	8.77E-05	9.05E-07	9.23E-07

Additionally, the percentage residual error defined by Equation 5.18 was also calculated.

$$\% \text{ Residual Error} = \frac{\text{Predicted} - \text{Experimental}}{\text{Experimental}} \quad \text{Equation 5.18}$$

The calculated percentage residual error values were plotted for the 23 °C and 38 °C conditions. These are shown in Figure 5.35 for 50% relative humidity at 23°C, Figure 5.36 for 90% relative humidity at 23°C, Figure 5.37 for 50% relative humidity at 38°C, and Figure 5.38 for 90% relative humidity at 38°C. They were plotted for ages of 7, 14, 21, and 28 days to demonstrate the trend of error. The residual error plots show the same response as the Chi-Squared values; the ACI 209 model has the best response of the existing models. However, Model 1 and Model 2 are better at explaining the experimental results found in this study.

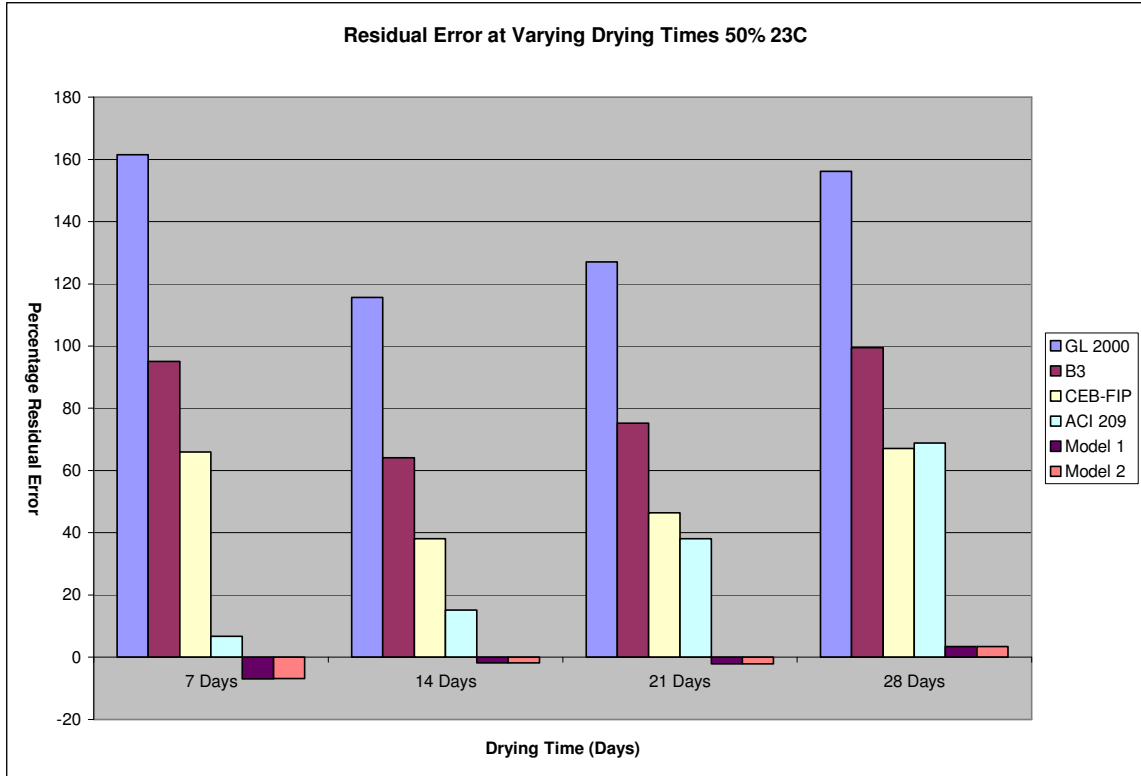


Figure 5.35: Percentage Residual Error of the models for 50% RH at 23°C.

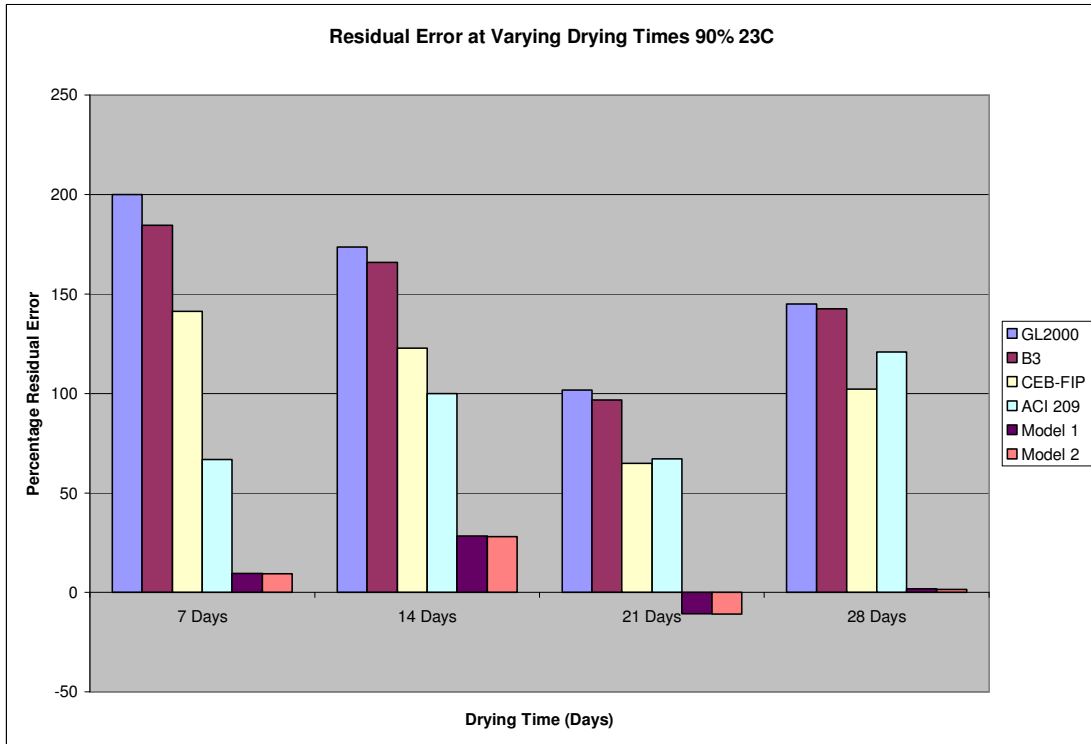


Figure 5.36: Percentage Residual Error of the models for 90% RH at 23 °C.

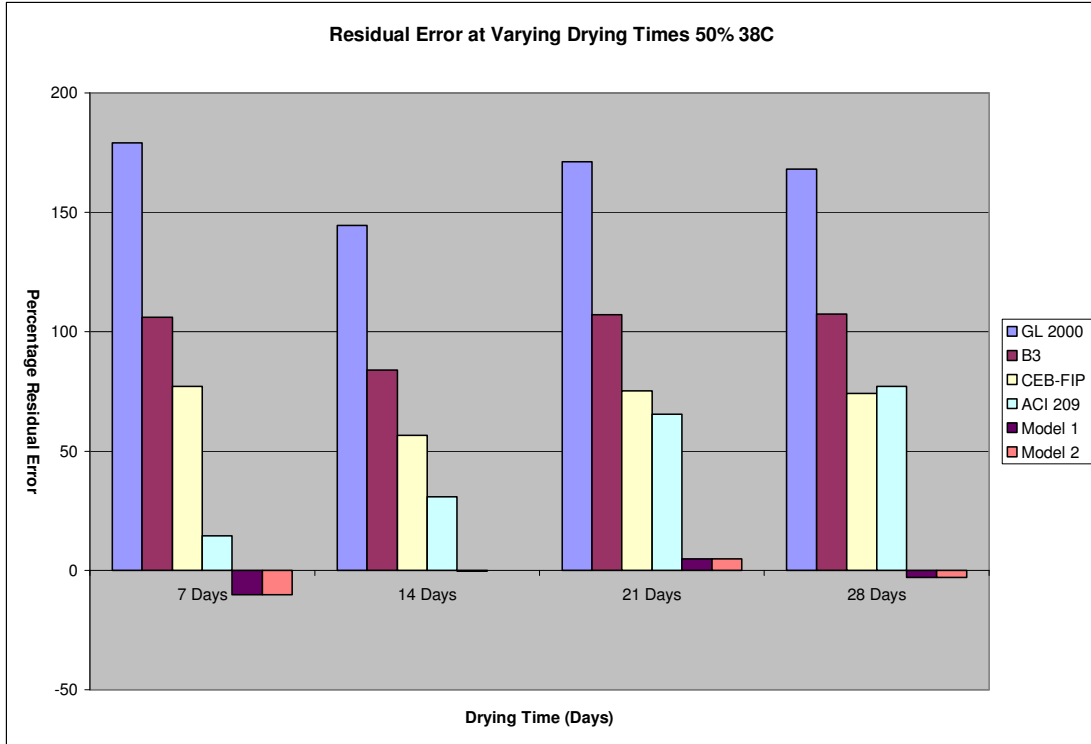


Figure 5.37: Percentage Residual Error of the models for 50% RH at 38 °C.

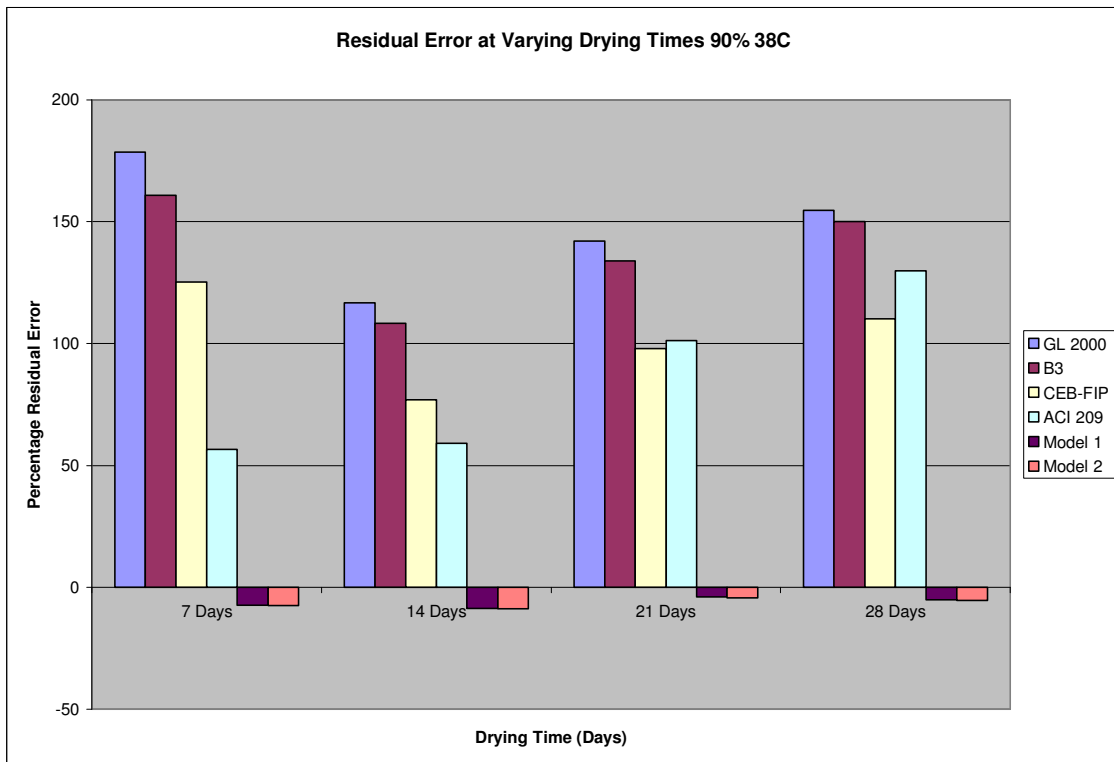


Figure 5.38: Percentage Residual Error of the models for 90% RH at 38 °C.

Chapter 6: Conclusions

This shrinkage study sought to investigate if there was a relationship between concrete shrinkage and maturity based on activation energy. Based upon the available literature, concrete shrinkage can be affected by multiple factors including compressive strength development, humidity, temperature, and drying time.

This study began by identifying activation energy values through penetration testing and through compressive strength testing. Next, this study monitored the free shrinkage for concrete samples exposed to controlled temperature and humidity conditions and coupled this analysis with compressive strength samples kept at the same conditions.

The humidity and temperature conditions produced results that showed expected trends. More concrete shrinkage was experienced with samples that were exposed to lower humidity levels. Furthermore, shrinkage samples that were cured at higher temperatures experienced less shrinkage, which can be attributed to the faster rate of strength development and the formation of a larger pore structure. The compressive strength samples exposed to shrinkage drying conditions showed that the concrete samples displayed characteristics of concrete maturity only for early ages of strength. The plots of equivalent age versus compressive strength diverged sharply at later ages; especially for the 50% relative humidity samples.

Shrinkage models that could accurately predict the concrete shrinkage found under various temperatures and relative humidities were developed. Model 1 and Model 2 use the same time functions to summarize the shape of the shrinkage curve.

Model 1 and Model 2 differ slightly because of the effect of temperature on concrete shrinkage; either linear (Model 1) or non-linear (Model 2). Due to a limited amount of data, prediction of the effects of temperature on concrete shrinkage should be further investigated.

6.1 Conclusions

Below are the main conclusions obtained from the results of this study:

1. An alternative method of calculation than what was recommended by ASTM 1074 provided the best calculation of activation energy. This method of calculation assumed the time at which the hydration reaction accelerated significantly (t_0) was equal to the final setting time. This was confirmed by comparing strength data normalized to an equivalent age.
2. The activation energy concept does not improve the time based prediction of shrinkage strains. The rate of shrinkage appears to be directly proportional to the amount of exposure to drying that concrete experiences.
3. The total shrinkage does not directly relate to the rate of concrete hydration; there are other effects involved, such as the formation of the micro and macro pore structure on the surface of the concrete.
4. The rate of strength development was affected greatly by humidity. The maturity approach using equivalent age was only applicable at very early ages of strength development. Long term strength development was significantly reduced at lower relative humidity.
5. A time dependent hyperbolic function was modified from the existing concrete shrinkage prediction models to fit the exposure conditions of this data set with

- excellent closeness of fit. This further suggests that the time dependent characteristics of concrete shrinkage are directly proportional to the amount of drying time a concrete sample experiences.
6. The effect of humidity on shrinkage appears to be quite close to what was found in the literature. This should be expected because the effect of humidity on concrete shrinkage has been well documented.
 7. Models for temperature effects were proposed for both linear and nonlinear phase shift relationships. Both models appear to accurately predict the measured data found in this study; however, because of the limited exposure conditions, the effect of temperature needs further validation.
 8. The best model from the literature explaining the experienced data was ACI 209. Clearly Model 1 and Model 2 are more capable to predict the shrinkage results for these exposure conditions. This leads to the conclusion that statistical shrinkage prediction models have limited accuracy because concrete can display a wide array of characteristics. It would be prudent to develop an individual concrete shrinkage prediction model for a mixture design when shrinkage prediction is important for design.

6.2 Recommendations

The following recommendations should be considered in future studies of concrete shrinkage:

1. Research should attempt to look at various exposure conditions, water-to-cement ratio, aggregate proportions, and other factors to create a relationship between the developed model and mixture properties.

2. The effect of temperature should be further examined to investigate if a nonlinear or linear response is more accurate for shrinkage modeling.
3. Future testing should single out and analyze the autogenous shrinkage as well as drying shrinkage to attempt to explain the total shrinkage of concrete as it may relate to Arrhenius based maturity.
4. The effect of activation energy on mixtures with different mixture design characteristics should be further investigated. Materials that have the same rate of strength development may display similar amounts of concrete shrinkage.

Appendix A

Testing Plan

Total Shrinkage of Concrete as a Function of Maturity

Task 1: Mixture Proportions

Objectives:

- To achieve a set of repeated mixtures that have consistent strength and consistency characteristics to the past UMD research.
- Only the “control” mixture will be used during the current testing.

Table A.1: Mixture Proportions

Item	Control
Type I cement (pcy)	510
Fly ash (pcy)	0
Total Cementitious	510
Fly Ash (%)	0%
Coarse Aggregate (pcy)	1940
Fine Aggregate (pcy)	1298
Water (pcy)	286
w/cm	0.56
w/c	0.56
Type F HRWR (oz/cwt)	2.1 oz

Table A.2: Consistency data for concrete

	Control
Slump (in)	6
Air (%)	1.4
Unit Weight (lb/ft ³)	149.80
Yield	1.93
Temp (°F)	55

1. Basic Concrete Mixture Properties
 - a. One mixture is selected that does not use fly ash, for which a maturity relationship has already been established.
 - b. The mixture will be checked after proportioning to ensure that slump, unit weight, and air content have been exacted to past UMD results.
2. Strength Characteristics
 - a. The target strength will be between 27.6 and 34.5 MPa
3. Material Characteristics-materials will be obtained to match past UMD materials. This includes cement, aggregate, fly ash, and HRWR.

Table A.3: Concrete Materials

	Source	Product Name	SG
Cement	Aggregate Industries	-	3.15
Fly Ash	STI Baltimore	-	2.18
Coarse Aggregate	Millville	-	2.84
Fine Aggregate	Accokeek Sand	-	2.59
HRWR	SIKA	Visocrete2100	Approx. 1.1

Task 2: Determine Activation Energy for Three Phases**Objective:**

- Establish reliable initial and final setting times under laboratory controlled temperatures to identify when specimens should be demolded and begin shrinkage measurements.
- Establish activation energies for concrete mixtures by relating penetration readings to concrete curing temperatures.
- Calculate activation energy for two of three phases using penetration readings--for times between placement and initial setting and time between initial setting and final setting.
- Calculate activation energy from cylinder testing past final set.
- Calculate equivalent ages for each concrete mixture and relate them to the degree of shrinkage achieved for each mixture.

Table A.4: Initial Activation Energy from Past UMD Research (Upadhyaya 2008)

Mixture	Initial Activation Energy
Control	43,233 J/mol

I. Phase I: Activation Energy Determination—Mixing to Initial Set

1. A total of nine 15.24x 15.24 centimeter (6x6 inch) cylinder specimens will be prepared.
2. 3 samples each will be cured at 4 °C, 23 °C, and 38 °C.
3. In accordance with ASTM C403, penetration readings will be taken at regular intervals to determine the time of initial set.
4. The natural log of the time period between two time periods (placement to initial set) will be plotted against the natural log of the control temperatures. From this linear relationship the rate constant K will be determined.

II. Phase II: Activation Energy Determination-Initial Set to Final Set

1. From phase I, the same nine 15.24x 15.24 centimeter (6x6 inch) cylinder specimens will be used.
2. 3 samples each will be cured at 4 °C, 23 °C, and 38 °C.
3. In accordance with ASTM C403, penetration readings will be taken at regular intervals to determine the time of final set.

4. The natural log of the time period between two time periods (initial set to final set) will be plotted against the natural log of the control temperatures. From this linear relationship the rate constant K will be determined.

Task 3: Free Shrinkage (C157)

Objectives:

- Develop measurements of the initial shrinkage occurring between placement and initial setting time.
- Develop shrinkage measurements under controlled conditions at two relative humidities and two temperatures; one moist and one moderately moist.
- Correlate shrinkage results to maturity concepts by relating the amount of shrinkage to the equivalent ages of the concrete. Shrinkage should be related to strength development of the paste matrix, which is related to the equivalent age of the concrete.
- Develop shrinkage results that can be compared to the B3 and GL2000 shrinkage prediction models.
- Establish a shrinkage model that incorporates a maturity concept and check the accuracy compared to existing models.
-

I. Phase I: Placement to Initial Set (Not Planned for Use)

1. A Total of 10, 10.16x20.32 centimeter (4x8 inch) cylinder specimens will be prepared
 - a. 5 samples for each temperature.
2. Samples be kept at the following ambient temperatures.
 - 23 °C
 - 38 °C
3. Each sample will be covered with some form of plastic membrane, and capped. A hole will be bored through each cap, where a LVDT will measure the change in height of the sealed specimen over time.

II. Phase II and Phase III: Initial Set to Final Set and Final Set to 28 days.

1. A total of 20, 7.62x7.62x28.575 centimeter (3x3x11.25 inch) shrinkage specimens will be made
 - a. 5 samples for each relative humidity and temperature will be needed.
 - b. There are a total of 2 relative humidities and 2 temperatures.
2. Each mixture will be demolded and begin curing at the beginning of initial setting. They will be kept at the following relative humidities and temperatures.
 - 90% RH at 23 °C -50% RH at 23 °C
 - 90% RH at 38 °C -50% RH at 38 °C

3. Shrinkage values will be measured at the following times:

	-Initial setting time (t_0)	-Halfway between Initial and Final Setting
time		
	-Final Setting time	-1 Day
	-2 Day	-4 Day
	-7 Day	-14 Day
	-21 Day	-28 Day

4. Equations for free shrinkage measurements:

$$\Delta L_x = \frac{CRD - initialCRD}{G} * 100$$

Where:

ΔL_x = length change of specimen at any age, %

CRD = difference between the comparator reading of the specimen and the reference bar at any age

G = the gage length (25.4 cm)

Task 4: Compressive Strength Testing for Activation Energy

Objectives:

- To measure the activation energy of concrete cylinders in order to get accurate activation energy measurements and confirm the findings of Sushant.

I. Phase III-Activation Energy Determination--Past Final Set.

1. Activation Energy values for the control mixture will be analyzed from the data that Sushant believes he already has.

Task 5: Compressive Strength Testing for Effect of RH and Temperature

- To develop the strength development of concrete mixtures under varied relative humidity and temperature conditions to the free shrinkage specimens kept at equal conditions.
 - Relate the strength development to the degree of shrinkage using the theory of equivalent age, which should prove to show a unique trend.
1. Seventy-two 10.16x20.32 centimeter (4x8 inch) compression samples will be prepared and tested for compressive strength.
 - a. 18 samples will be kept at either 50% RH and 38 °C, 50% RH and 23 °C, 90% RH and 38 °C, or 90% RH and 23 °C.
 - b. 3 of these specimens will be tested for compressive strength at 1, 2, 4, 7, 14, and 28 days.

Task 6: Strength-Maturity

Objectives:

- From pullout strength test data from past UMD research, equivalent age and strength will be estimated for each concrete mixture.
- Equivalent age will be plotted against total shrinkage. A linear relationship (at least at early ages) is expected as found from literature. This will show a relationship between maturity and shrinkage and prove that maturity can be included in a shrinkage model.
- Through regression analysis of the equivalent age and shrinkage characteristics, the maturity method will be incorporated into a shrinkage model.

References

- ACI 209R-92 “*Prediction of Creep, Shrinkage, and Temperature Effects in Concrete Structures.*” The American Concrete Institute. ACI Committee 209, 1997, pp. 1-47.
- ACI209.2R-08 “*Guide for Modeling and Calculating Shrinkage and Creep in Hardened concrete.*” The American Concrete Institute. ACI Committee 209, 2008, pp. 1-44.
- Aitcin, P. “*Demystifying Autogenous Shrinkage.*” Concrete International, November 1999, pp. 54-56.
- Aitcin, P., A. Neville, and P. Acker. “*Integrated View of Shrinkage Deformation.*” Concrete International, September 1997, pp. 35-41.
- Altoubat, Salah and David Lange. “*Creep, Shrinkage, and Cracking of Restrained Concrete at Early Age.*” ACI Materials Journal. July-August 2001, pp. 323-331.
- ASTM C39/C39M, 2005. “*Standard Test Method for Compressive Strength of Cylindrical Concrete Specimens,*” ASTM International, Volume 04.02.
- ASTM C157, 2003, “*Standard Test Method for Length Change of Hardened Hydraulic-Cement Mortar and Concrete,*” ASTM International, Volume 4.02.
- ASTM C403, 2006, “*Standard Test Method for Time of Setting of Concrete Mixtures by Penetration Resistance,*” ASTM International, Volume 04.02.
- ASTM C1074, 2004, “*Standard Practice for Estimating Concrete Strength by the Maturity Method,*” ASTM International, Volume 04.02.
- Bažant, Zdeněk. “*Creep and Shrinkage Prediction Model for Analysis and Design of Concrete Structures-Model B3.*” Materials and Structures, Volume 28, Issue 180, 1995, pp. 357-365.
- Bažant, Zdeněk. “*Prediction of Concrete Creep and Shrinkage: Past, Present, and Future.*” Nuclear Engineering and Design, Vol. 203, 2001, pp. 27-38.
- Carino, Nicholas J. “*The Maturity Method.*” The Handbook of Nondestructive Testing: Second Edition, 2003, Chapter 5, pp. 1-47.
- CEB-FIP 90. “*CEB-FIP Model Code 1990.*” Thomas Telford, London, 1994.

- Gardner, N. J. and M. J. Lockman. “*Design Provisions for Drying Shrinkage and Creep of Normal-Strength Concrete.*” ACI Materials Journal, Technical Paper 98-M18, 2001, pp. 159-167.
- Goel, Rajeev, Ram Kumar, and D. Paul. “*Comparative Study of Various Creep and Shrinkage Prediction Models for Concrete.*” ASCE. Journal of Materials in Civil Engineering, March 2007, pp. 249-260.
- Holt, Erika E. “*Early Age Autogenous Shrinkage of Concrete.*” ESPOO. Technical Research Centre of Finland. VTT Publication 446, 2001.
- Mokarem, David, Richard Weyers, and Stephen Lane. “*Development of Portland Cement Shrinkage Performance Specifications.*” Transportation Research Board, CD-ROM 2003, Washington, DC.
- Mounanga, Pierre et. al. “*Autogenous Deformations of Cement Pastes: Part I. Temperature Effects at Early Age and Micro-Macro Correlations.*” Cement and Concrete Research, Vol. 36, 2006, pp. 110-122.
- Myers, J. and I. Gurung. “*Shrinkage Behavior of High Strength Concrete (HSC) Subjected to Accelerated Curing.*” Structural Engineering and Public Safety, 17th Analysis and Computation Specialty Conference, 2006.
- Soroushian, P. and S. Ravanbkhsh. “*Control of Plastic Shrinkage Cracking with Specialty Cellulose Fibers.*” ACI Materials Journal, Technical Paper 95-M40, 1998, pp. 429-435.
- Upadhyaya, S., “*Early Age Strength Prediction for High Volume Fly Ash Concrete using Maturity Modeling,*” University of Maryland Dissertation, 2008.
- Videla, C. and C. Aguilar. “*An updated look at drying shrinkage of Portland and blended Portland cement concretes.*” Magazine of Concrete Research, Volume 58, Issue 7, September 2006, pp. 459-476.